MODELING STUDIES OF ACOUSTIC PROPAGATION THROUGH THE AGULHAS CURRENT REGION

J Courtney

Thesis submitted to the University of Cape Town in fulfillment of the requirements of the degree of Master of Science

Acknowledgements

At this stage I would like to thank:

- My supervisor, Geoff Brundrit and others in the Oceanography Department at the University of Cape Town who were willing to help and answer sometimes very remote questions, especially Frank Shillington and Henry Valentine.
- The authors of *HARPO* for their provision of a working model and their interest in this project.
- The authors of TEX and LATEX for designing such an excellent typesetter.
- My husband, Shaun Courtney, for believing that I would eventually finish this thesis, and for all the motivation and encouragement, not to mention chocolate that he gave me.

Contents

List of Figures

List of Tables

Glossary Of Symbols Used

Glossary Of Symbols Introduced In Section 3.1

ρ	density
T	temperature
S	salinity
p	pressure
η	potential temperature
c	sound speed (phase speed for acoustic waves in fluids)

Glossary Of Symbols Introduced In Section 3.2

ρ_o	density changes slow $\Rightarrow \rho \simeq$ constant i.e. ρ_o
$\underline{x} = (x, y, z)$	particle position
(u, v, w)	particle velocity

Glossary Of Symbols Introduced In Section 3.3

ω	radian frequency
k	wave number, $\frac{\omega}{c}$
c_o	reference sound speed
(x, y, z, t)	medium scale
$p(x, y, z, t)$	solution to the wave equation, in terms of pressure
A	wave amplitude
k_o	wave number (relative to reference sound speed), $\frac{\omega}{c_o}$
$\underline{\hat{n}} = (n_1, n_2, n_3)$	unit normal to the wave front
$\underline{k} = (k_1, k_2, k_3)$	wave number vector, $\underline{k} = k(n_1, n_2, n_3)$
$W(x, y, z)$	wavefront - defines a surface of constant phase, $W(x, y, z) = n_1 x + n_2 y + n_3 z$
$N(x, y, z)$	refractive index, $N(x, y, z) = \frac{c_o}{c(x,y,z)}$
$\psi(x, y, z, t)$	phase function
$\underline{U} = (U_1, U_2, U_3)$	vector group velocity, $\underline{U} = \frac{\partial \underline{x}}{\partial t}$

Glossary Of Symbols Introduced In Section 3.4

s	arclength - distance along the ray path
$\underline{n} = (\alpha, \beta, \gamma)$	- direction cosines (normal to the wave front), $(\alpha, \beta, \gamma) = (\frac{\partial x}{\partial s}, \frac{\partial y}{\partial s}, \frac{\partial z}{\partial s})$
θ	direction of propagation
g	sound speed gradient
R	radius of curvature
h	the maximum height reached by the ray above the initial position
l	the horizontal distance from the source to the point where the ray returns to the starting depth

Glossary Of Symbols Introduced In Section 3.5

H	Hamiltonian function
$p_1, p_2 \ldots p_3$	generalized momenta
$q_1, q_2 \ldots q_3$	generalized coordinates
$\underline{V} = (V_1, V_2, V_3)$	mean velocity field through which waves propagate
ω	absolute frequency, the frequency of oscillations occurring at a fixed point in space
ω_r	relative frequency, frequency of oscillations occurring at a point moving with velocity $\underline{V}$
ϕ	angle between $\underline{k}$ and $\underline{V}$

Chapter 1

INTRODUCTION

1.1 Historical Background And Motivation

The motivation for this thesis arises from the apparent global warming problem. It is common knowledge that the ocean is an important heat sink and that to predict global warming trends it is important to measure changes in the ocean temperature. Measurements of ocean temperature are subject to large local variability associated with mesoscale features. In order to measure global warming trends a method is required to determine large scale averages, over large oceanic ranges, in order to remove the inherent variability associated with mesoscale features, such as currents and mesoscale eddies. This requirement can be met by acoustic thermometry (Munk et al, in press).

Sound speed in the ocean is related to water temperature and an increase in water temperature results in an increase in sound speed. Sound speed increases by $4-5\ m.s^{-1} per\ ^{o}C$, which means that the travel time between the source

and receiver is shorter for a warmer ocean, in fact travel time fluctuations are a sensitive indicator of temperature variations (Baggeroer and Munk, 1992). By measuring the travel time from source to receiver during a series of successive tests it is possible to determine temperature fluctuations within the ocean. In this way the ocean can be used as a temperature gauge and therefore as a certain indicator of global warming.

ATOC - Acoustic Thermometry of Ocean Climate is an internationally supported project which intends to measure the rate of the anticipated warming of the world oceans using acoustic techniques. The plan for ATOC is to set up a global network of source and receiver stations throughout the oceans of the world. Then by measuring the travel time between stations over a number of years the worlds oceans can be used as an early warning signal of the apparent global warming problem.

The feasibility of long range sound transmission in the ocean has already been demonstrated in March 1960 (Munk, O'Reilly and Reid 1988). One hundred and fifty kilograms of TNT were detonated in the sound channel off Perth, Australia. The explosion was recorded on hydrophones at Bermuda, almost half way around the world. This demonstrated the remarkable long range transmission characteristics of sound within the ocean. After reconsidering the 1960 experiment it was Walter Munk's suggestion that these transmission properties could be used as an indicator of global temperature change (Gibbons, 1990).

In early 1991 the Heard Island Feasibility Test (HIFT) took place, with Walter Munk and Andrew Forbes at the helm. A source ship was stationed off Heard

Island, in the Southern Indian Ocean, and transmitted a low frequency sound signal over a period of five days. One of the objectives of the HIFT experiment was to determine the efficiency of the deep sound channel, also called the SOFAR channel. This channel is a function of the sound speed minimum, which is typically at a depth of $1\ km$ below the sea surface. The SOFAR channel behaves as a waveguide and directs acoustic energy through the world oceans. HIFT was a great success in that the transmitted signal, which propagated through the SOFAR channel, was received through out the oceans of the world (Forbes, 1991). Figure 1.1 contains a map showing the source and receiver stations involved in the experiment. Munk et al (in press) have written a full report on HIFT, which includes the background to the experiment, details pertaining to the results of the experiment and future objectives for ATOC.

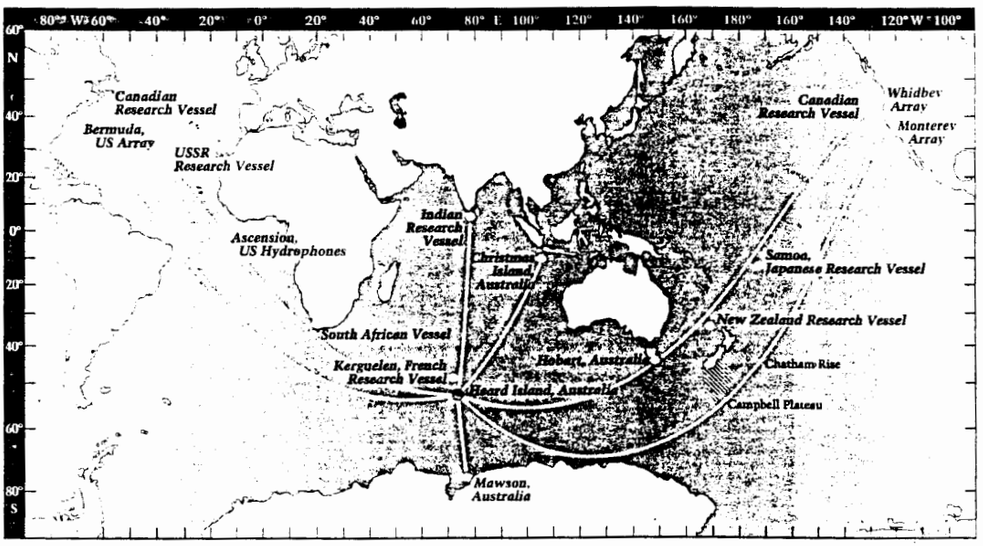

Figure 1.1: Map Showing The Source At Heard Island And The Fourteen Receiver Stations (Forbes, 1991)

Baggeroer and Munk (1992) suggest that ten years of observations with a reasonable global network of sources and receivers could lead to an estimate of ocean warming as a result of the greenhouse effect. A warming of $0.005^{o}C.year^{-1}$ produces a decrease in travel time of about $0.02\ sec.year^{-1}$ over a $10000\ km$ path. In acoustic tomography a precision of $0.001\ sec$ in measuring travel times over $10000\ km$ has been achieved, over long ranges a precision of $0.01\ sec$ is expected and is adequate for detecting the predicted global warming trends.

A problem with the proposed ATOC experiment is that the very large distances involved in global sound propagation implies a certain amount of dependency on the horizontal sound speed structure. The effects oceanographic features such as bottom topography, ocean fronts, currents and mesoscale eddies have on the sound speed structure, and hence on sound propagation through them, can not be ignored. These features do cause a disturbance to the ray path and do effect the travel time, a small deflection to a ray on a scale of $10000\ km$ will have a significant effect on the ray path and hence travel time.This means that a better understanding of these features in terms of ocean acoustics is necessary. Clearly physical experiments and monitoring are not practical either logistically or financially, for these reasons numerical modeling has been suggested as an exploratory tool.

The southern tip of Africa provides an excellent position for a source-receiver station, since it forms a link between three major oceans of the world: the Atlantic Ocean, the Indian Ocean and the Southern Ocean. Krige and Brundrit (in press) describe the South African participation in HIFT, they emphasize that the propagation paths through this region are highly variable as a result of

the extremely complex oceanographic environment associated with the region. Munk et al (in press) ascribes the relatively poor reception in this region not only to the extreme sea conditions at the time of the experiment but also to the highly variable oceanographic conditions associated with the region.

A number of semipermanent features have been observed within this area, for example the Agulhas Current, the Agulhas Return Current and the Retroflection. Apart from these semipermanent features this region is characterized by a large number of dynamic mesoscale eddies. These eddies may be formed by a variety of processes: they may be sheer eddies, formed at the edges of large currents; they may be formed by the occlusion of large meanders within the currents; or they may be topographically induced eddies. Clearly the complicated oceanic environment in the region south of Africa results in highly variable propagation paths for sound passing through the area.

Fundamental to South Africa's continued participation in the ATOC experiment is a better understanding of the oceanic features in terms of their acoustic properties, within the region south of Africa. The purpose of this thesis was to address this problem by determining the effects individual oceanographic features have on long range sound transmission south of Africa. In order to achieve this two requirements were needed: firstly a detailed understanding of the oceanography of the region including real data; secondly a computer model that was capable of modeling sound propagation through oceanographic features typical to this region. The first requirement was achieved by a study of oceanographic research papers and data reports pertaining to the area south of Africa. The second requirement, that of a range dependent computer model

was achieved by $\mathcal{HARPO}$ (Georges, Jones and Lawrence, 1990; Jones, Riley and Georges, 1986)a recently developed Hamiltonian Acoustic Ray tracing Program for the Ocean.

The objectives of this thesis were threefold:

- Firstly, using $\mathcal{HARPO}$ a numerical experiment was performed in order to determine the effects of a warm core feature, with either a zonal current or an anticlockwise vortex current, on long range sound propagation through it.
- Secondly the results for the numerical experiment were be applied to the area south of Africa, specifically sound propagation through the Agulhas Current, the Agulhas Return Current and an anticlockwise warm core eddy typical to the region.
- Finally the usefulness of $\mathcal{HARPO}$ as a predictive modeling tool was assessed, in order to achieve this the model results from the numerical experiment were compared with results obtained using mathematical methods.

1.2 Overview

This thesis is divided into two distinct sections. Chapters Two, Three and Four provide the necessary background to the numerical experiment which is described in Chapters Five and Six. A summary of the results and the conclusions are included in the final chapter, Chapter Seven. The subject content of the chapters are independent and diverse, for this reason a bibliography is included

at the end of each chapter. This method of referencing is useful because it furnishes a series of relevant references which are categorized according to their subject matter.

Chapter Two contains a discussion on the numerical experimentation philosophy used for this experiment. The philosophy is this: starting with a very simple model environment more complex features are added to it, tending to a more realistic model environment, through which sound rays are transmitted. This philosophy allows for a general understanding of individual features within the model. Also, the reasons for selecting *HARPO* to be the ray tracing program used throughout the experiment are given in Chapter Two, as well as a detailed description of the structure and features of *HARPO* .

The mathematical background to acoustic propagation modeling is described in Chapter Three. The Chapter begins with a characterization of the ocean as an acoustic medium. This is followed by an account of the mathematical theory which underlies acoustic propagation modeling. The theory begins with a derivation of the acoustic wave equation from fundamental physical principles. By applying a plane wave solution to the wave equation the eikonal equation is derived and the theory of ray tracing introduced. An application of ray tracing, refraction of sound in a variable medium, is demonstrated. By including a moving environment into the system the ray tracing equations are shown to parallel the characteristic form of Hamilton's equations in a dynamical system, and thus Hamiltonian ray tracing is introduced and described.

In Chapter Four a description of the Agulhas Current Region is given. It includes

an outline of the Agulhas Current System, which itself includes the Agulhas Current, the Agulhas Return Current and the Retroflection. This chapter provides a detailed description, in terms of their acoustic properties, of the semipermanent features found within the region, as well as the more variable and dynamic mesoscale eddie features.

In Chapter Five descriptions of the simulated model environments, through which sound rays were propagated for this research, are described in detail. Firstly a horizontally stratified environment is described, upon this a current and an eddy feature were positioned in order to consider the effects of each feature. Both the current and the eddy feature are divided into two components, the velocity and the temperature structure. Sound Propagation through the velocity and the temperature structure of each feature were modeled both separately and together in order to determine the individual and combined effects of the components of each feature on sound propagating through them. The last section of Chapter Five is included for completeness, it contains the precise mathematical descriptions of each of the $\mathcal{HARPO}$ submodels used to define the model environments which are used in the numerical experiment.

Chapter Six describes the numerical sound propagation experiments which were performed. The results are given in sequence, starting with the results of sound propagating through a horizontally stratified ocean, followed by sound propagating through a current environment and finally sound propagating through a warm core anticyclonic eddy feature. In order to make the results easier to interpret, the ray tracing experiment results are separated into vertical and horizontal components. A full set of the experiment results is included in the appendices

for completeness and to aid the discussion in Chapter's Six and Seven.

The final chapter, Chapter Seven, includes a summary of the results and the conclusions. The results correspond to those of previous physical and theoretical long-range sound propagation experiments. For a warm core feature the sound channel is depressed by the warmer surface waters. The results indicate that for a ray propagating through through a warm feature such as the Agulhas Current, Agulhas Return Current and a warm core eddy, the rays follows the SOFAR channel and dive beneath the feature. Propagation through the velocity structures associated with the features mentioned resulted in significant amounts of refraction in the direction of the current flow for the zonal current and away from the vortex center for the anticyclonic vortex. When the temperature and velocity structures associated with the features were combined together, to emulate a realistic environment, the ray was forced downwards by the temperature structure and less horizontal refraction occurred to the ray as it was propagating below the current core. The results indicate that *HARPO* is a useful predictive tool in terms of determining the effects of oceanic features on sound propagation through them.

Bibliography

[1] Baggeroer A.B. and Munk W.H. (1992).
The Heard Island Feasibility Test.
Physics Today, 45, September, pp22-30.

[2] Forbes A.M.G. (1991).
Acoustic Monitoring of Global Ocean Temperature?
In Scripps 1991 Annual Report, Scripps Institution of Oceanography, University of California, San Diego.

[3] Gibbons A. (1990).
What's the sound of the ocean warming?
Science, vol 248, April 6, pp33-34.

[4] Georges T.M., Jones R.M. and Lawrence R.S. (1990).
A PC version of the HARPO ocean acoustic ray tracing program.
NOAA Report, Wave propagation Laboratory, Boulder CO., pp18.

[5] Jones R.M., Riley J.P. and Georges T.M. (1986).
HARPO - A versatile three dimensional Hamiltonian ray tracing program for acoustic waves in an ocean with irregular bottom.
NOAA Report, Environmental Research Laboratories, Boulder CO., pp455.

[6] Krige L. and Brundrit G.B. (in press)
Heard Island signals through the Agulhas Retroflection Region.
Journal of the Acoustical Society of America, Special Edition.

[7] Munk W.H. (1989).
Global Ocean Warming: detection by long-path acoustic travel times.
Oceanography, vol 2, no 2, pp40-41.

[8] Munk W.H. and Forbes A. (1989).
Global Ocean Warming: an acoustic measure?
Journal of Physical Oceanography, vol 19, Nov, pp1765-1778.

[9] Munk W.H., O'Reilly W. and Reid J. (1988).
Australia-Bermuda Sound Transmission Experiment (1960) Revisited.
Journal of Physical Oceanography, vol 18, Dec, pp1876-1898.

[10] Munk W.H., Spindel R.C., Baggeroer A.B., Birdsall T.G. (in press).
The Heard Island Feasibility Test.
Journal of the Acoustic Society of America, Special Edition.

the most idealized situations, sometimes resulting in large errors in predictions. For these reasons numerical techniques are more appropriate to the calculation of the acoustic field and associated oceanic environment (Etter, 1991).

The numerical experimentation philosophy that is used in this project was this: beginning with as simplified a model as possible, more complicated features are included into the system one at a time, with the system gradually approaching reality. This approach to the experiment allows for a better understanding of the effects of individual components within the system and provides insight into the role oceanic features have on acoustic propagation through them.

A valuable use of this type of exploratory numerical modeling is that it assists in the interpretation of observed propagation results given an accurate data base of the oceanic environment using modern data collection techniques.

2.2 Why Harpo Was Chosen

A recently developed three-dimensional Hamiltonian ray tracing program for the ocean, *HARPO* (Georges, Jones and Lawrence, 1990; Jones, Riley and Georges, 1986), was chosen as the software for this project. Propagation models can be classified on the basis of the variation permitted in the sound speed environment. A model where the variation in sound speed is with depth, $c(z)$, is called a range independent model. Range dependent models can be two dimensional with the introduction of variation along a ray direction, $c(x,z)$ or $c(\theta,z)$, or fully three dimensional where horizontal refraction of the ray is modeled, $c(x,y,z)$ or $c(\theta,\phi,z)$. *HARPO* is a fully three dimensional range

dependent propagation model where sound speed can vary with range, azimuth angle from the receiver and depth.

The fact that *HARPO* is 'range - dependent' is important to the numerical modeling that was performed for this thesis, since the horizontal variability found at ocean fronts and current and eddy boundaries are thought to have a significant effect on sound propagating through them (Newhall et al, 1990). The effect the oceanographic features considered for this thesis have on the path length and hence travel time on a ray passing through them could not be ignored and a 'range - independent' model would not have sufficed.

HARPO was selected primarily because it is a ray tracing program with a graphically useful acoustic ray diagram as output, which provides intuitive insight into the problem at hand. *HARPO* is community software, written in FORTRAN, and readily available from the designers. A functional manual was provided with the program, from the authors (Jones, Riley and Georges, 1986), the manual contains historical background to the program as well as the modeling procedures, the theoretical basis of the code and detailed user information.

HARPO is a popular package used by a number of acoustic propagation modelers, for example Chiu et al (in press) and Newhall et al (1990). It is understandable, versatile and provides the user with a selection of models with which to set up the ocean environment. The user also has the option to include their own routines if the routines provided are inadequate for their purposes. In the PC version of *HARPO* used for this thesis only a limited number of idealized modeled perturbations to the sound speed environment could be included

at one time. While the essence of oceanographic features can be included the incorporation of real hydrographic data into the model environment awaits further developments in $\mathcal{HARPO}$.

The method of including data into the program is straightforward, the user specifies the magnitude and the units of the elements, of an input data file, that correspond to physical or mathematical quantities that notify the program: which models to use; rays to trace and in what form to present the results.

Until now ray tracing computer programs have been automated versions of one or two dimensional ray tracing graphical techniques. These types of program were implemented over limited regions, for longer ranges the solutions were patched together. Apart from being difficult to extend to three dimensions these models encountered discontinuities at the interfaces between two regions which made the results awkward to interpret.

$\mathcal{HARPO}$ avoids these problems since it models the ocean as a three dimensional function, with continuous gradients. $\mathcal{HARPO}$ computes each ray path by numerically integrating Hamilton's equations with a different set of initial conditions. Since $\mathcal{HARPO}$ uses continuous models the problems of discontinuities at the boundaries between smaller regions are avoided.

2.3 The Structure Of Harpo

An ideal model would completely represent reality, however this defeats the purpose of a model, which is to generalize and abstract the problem at hand, providing insight and understanding to the situation. Because of this modeling in the physical sciences has most often been reduced to more manageable components (Etter, 1991).

HARPO was designed with a useful modular structure. Figure 2.1 graphically depicts the main components and structure of *HARPO* , which includes the input file; the main program which is divided into two subsections, the ray tracing core and the model environment; and the output file which is represented by a ray diagram.

The main program is divided into two major components. The ray path calculation is completely separate from the model of the medium (i.e. sound speed structure, current velocity and boundary conditions). While these two components are completely independent of each other they do interact throughout a run of the model.

The ray tracing core is based on mathematical representations of the governing physics. The user provides the initial ray tracing conditions, including: the source location (latitude, longitude and depth); wave frequency and intensity; as well as the direction of transmission (elevation and azimuth angles).

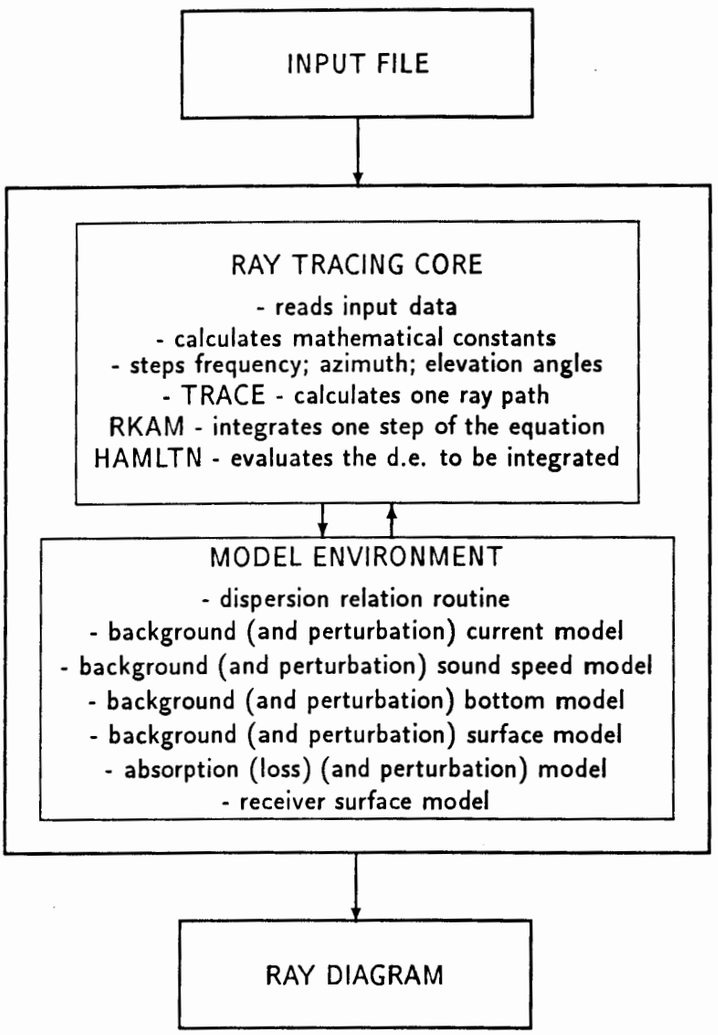

Figure 2.1: The Structure Of Harpo

The medium within which the ray tracing occurs is modeled separately from the ray tracing core, using a number of environmental model routines. Components that are included into this section are: the background sound speed; background current; bottom topography; ocean surface; as well as perturbations for each of these routines. A receiver surface model and an absorption loss model are also included here.

In conclusion, for a typical model run, the input file contains data pertaining to the initial ray conditions and a description of the model environment to be used. This file is used by the ray tracing core which reads the input data and calculates all mathematical constants to be used. With these initial ray conditions and the model environment parameters the ray propagation paths are calculated stepwise. The output of this procedure is described by a ray diagram which is fairly easy to interpret.

Bibliography

[1] Chiu C.S., Semtner A.J., Ort C.M., Miller J. and Ehret L.L. (in press).
A ray variability analysis of sound transmission from Heard Island to California.
Journal of the Acoustic Society of America, Special Edition.

[2] Etter P.C. (1991).
Underwater Acoustic Modeling: principles, techniques and applications.
Elsevier Science Publishers Ltd., New York, pp305.

[3] Georges T.M., Jones R.M. and Lawrence R.S. (1990).
A PC version of the HARPO ocean acoustic ray tracing program.
NOAA Report, Wave propagation Laboratory, Boulder CO., pp18.

[4] Jones R.M., Riley J.P. and Georges T.M. (1986).
HARPO - A versatile three dimensional Hamiltonian ray tracing program for acoustic waves in an ocean with irregular bottom.
NOAA Report, Environmental Research Laboratories, Boulder CO., pp455.

[5] Newhall A.E., Lynch J.F., Chiu C.S. and Daugherty J.R. (1990).
Improvements in Three Dimensional Ray Tracing Codes for Underwater Acoustics.

In Lee D., Cakmak A. and Vichnevetsky R. (editors).
Computational Acoustics Volume 1.
Elsevier Science Publisher, B.V., North Holland, pp169-185.

Chapter 3

MATHEMATICAL BACKGROUND TO ACOUSTIC PROPAGATION

Chapter Three is imperative to this thesis, it contains an introduction to the theory of acoustic propagation within the ocean. A glossary of symbols pertaining to this chapter can be found at the beginning of this thesis, on page x. The Chapter begins with a description of the fundamental physical properties of the ocean environment, the purpose of this is to provide insight into the ocean as an acoustic medium.

The background to the mathematical theory which underlies acoustic propagation modeling is introduced. The approach is this: Recognizing that sound travels through the ocean as a longitudinal wave, the wave equation is derived from fundamental physical principles. Any acoustic propagation model has to

make use of either the wave acoustic solution or the ray acoustic solution to the wave equation. Both solutions are discussed in this chapter and the reasons for selecting the ray solution are outlined.

A plane wave solution to the wave equation is considered and extended to three dimensions, the resulting expansion of the wave equation is then reduced to the eikonal equation. The advantage of the eikonal equation over the wave equation is that it is independent of time. However, there are sufficient conditions that must be satisfied before for the eikonal equation can be considered, these conditions are discussed. Solutions to the eikonal equation give rise to a set of ordinary differential equations, which describe ray paths of acoustic energy - where a ray is defined as the trajectory that is everywhere perpendicular to the wave front.

By considering the ordinary differential equations resulting from the eikonal equation the theory of ray tracing is introduced. Here the effects the environment has on a ray are investigated, the primary effect being that of refraction - which is the bending of a sound ray due to a variation within the oceanic medium. The ray tracing theory is then extended to a generalized theory of ray tracing. A parallel between the generalized ray tracing equations and Hamilton's equations for a conservative dynamical system is found and the generalized theory of Hamiltonian ray tracing is introduced. The effects a current has on sound propagating through it are considered and the generalized Hamiltonian ray tracing equations are extended to accommodate current features within the modeling environment.

3.1 The Acoustic Medium

To understand the physics of acoustic propagation in the ocean a fundamental understanding of the ocean as an acoustic medium is imperative. In this section the sound speed structure of the ocean is described.

The equation of state for sea water declares that every physical quantity can be related to three fundamental state variables. Typically for oceanographic studies the three state variables chosen are temperature, salinity and pressure.

$$\rho = \rho(T, S, p)$$

For acoustic oceanographic studies potential temperature (or entropy), salinity and pressure are preferred.

$$\rho = \rho(\eta, S, p)$$

Sound speed is a physical quantity in the ocean and is therefore, through the equation of a state, a function of potential temperature, salinity and pressure.

$$c = (\eta, S, p)$$

The relationship between sound speed, c , and density, ρ , (derived in section 3.2) is given by:

$$\frac{1}{c^2} = (\frac{\partial \rho}{\partial p})_{\eta,S}$$

Both the sound speed and density are determined at a particular point by the in situ temperature, salinity and pressure values and the relevant equation of state. Changes in temperature, salinity and pressure are reflected by relative variations in the sound speed. A positive (or negative) variation in the temperature, salinity or pressure results in an increase (or decrease) in the sound speed.

Temperature changes normally dominate salinity changes in their contribution to sound speed variations. In the region of the thermocline, which in temperate and tropical waters is the top $1000\ m$ of the ocean, temperature changes dominate pressure changes. However in deep waters, below the thermocline and in polar waters, pressure changes dominate temperature changes.

Variations in salinity are only important close to the ocean surface and at river mouths. Also changes in sound speed as a result of changes in depth are fairly small, for example the variation in sound speed over $100\ m$ due to hydrostatic pressure alone is about 0.1% (Kinsler et al, 1982). Nevertheless pressure variations become important in the deep isothermal waters.

In contrast variations in sound speed as a result of changes in the ocean temperature are large, especially near the ocean surface. Variations in temperature of more than $5°C$ are common near the ocean surface, resulting in changes of about 0.2% of the total sound speed (for temperatures in the region of $15°C$) (Kinsler et al, 1982).

It is important to observe that the actual variations in sound speed, compared to its magnitude, are small - for example in a vertical sound speed profile the total sound speed variation is typically about $30\ m.s^{-1}$, which is 2% of a typical sound speed value of $1500\ m.s^{-1}$. Even though this variation is relatively small it has a large effect on the propagation of sound in the ocean.

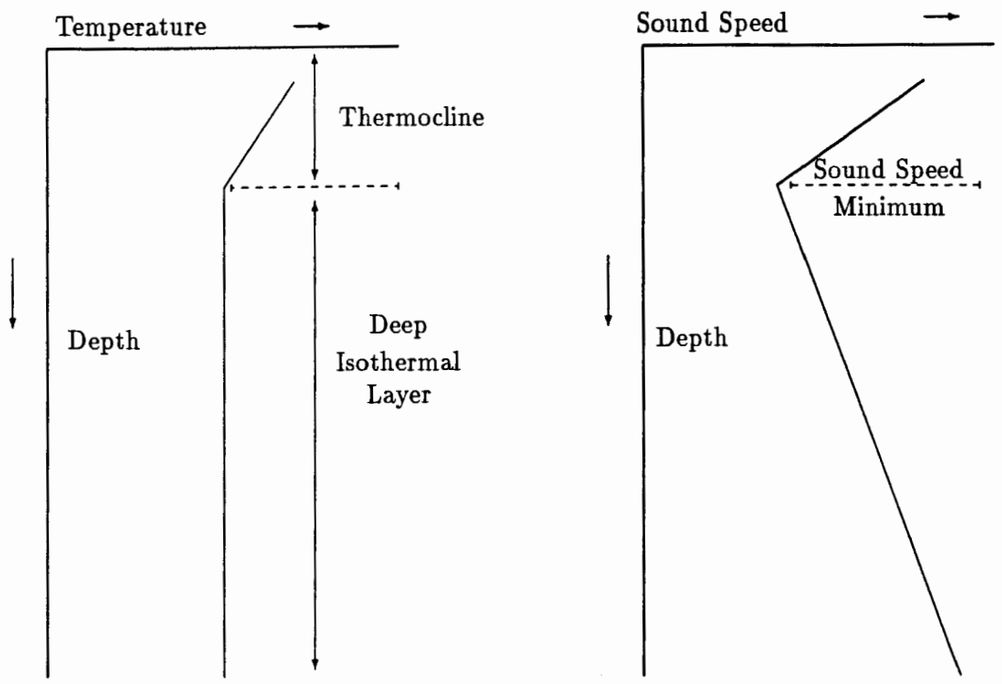

Figure 3.1: Schematic Relationship Between Temperature And Sound Speed Profiles In The Deep Ocean

The temperature field of the ocean displays a high degree of stratification with depth. Since the isotherms are virtually parallel to the horizontal plane, this structure has been referred to as horizontal stratification (Weinberg, 1978). The range of the vertical temperature profile, in the ocean consists of a number of recognizable layers. These sections are discussed here and then related to corresponding acoustic zones. Figure 3.1 is included in order to demonstrate the relationship between the thermal and acoustic structures within the ocean. Etter (1991) describes the relationship between temperature layers and their corresponding acoustic layers in more detail.

The surface layer is usually associated with a well mixed layer of isothermal water. Within this layer the sound speed structure is influenced by the local environmentally influenced temperature variations experienced at the sea surface. This thesis is only concerned with sound propagation through the deep ocean and so the sound speed structure at the surface is only mentioned briefly.

Below the well mixed surface layer lies the thermocline, a section of the water column in which the temperature decreases rapidly with depth. The decrease in temperature in the region of the thermocline results in a decrease in sound speed with depth. This means that there is a negative sound speed gradient within this zone.

Between the thermocline and the ocean floor is the deep isothermal layer, this layer has an almost constant temperature. But because of the increasing pressure with depth found in this region the sound speed increases with depth. The deep isothermal layer therefore exhibits a positive sound speed gradient.

At the interface between the thermocline and the deep isothermal layer a sound speed minimum is present. This minimum occurs at the boundary between the zone with the negative sound speed gradient and the deeper region with the positive sound speed gradient. The depth of the sound speed minimum is called the sound channel axis.

3.2 The Acoustic Wave Equation

Acoustic waves in fluids are longitudinal waves - this means that the molecules move back and forth in the direction of propagation of the wave, producing adjacent regions of compression and rarefaction. For this reason the theoretical basis underlying all mathematical models of acoustic propagation in the ocean is the wave equation. A good derivation of the wave equation in terms of ocean acoustics can be found in Kinsler et al (1982) and Urick (1982).

A number of physical assumptions are necessary to derive the acoustic wave equation, and the resulting ray tracing techniques. Ross (1976) lists the physical assumptions used in deriving the acoustic wave equation from fluid mechanics. The assumptions used in this particular derivation of the wave equation are presented here so as to ensure that the essence of the derivation which follows can be understood easily.

Firstly, the effects of gravitational forces are neglected, which means that the instantaneous density was constant throughout the medium, or $\rho \simeq \rho_o$ (Boussinesq approximation) (Lighthill, 1978).

Secondly, it has been found experimentally that acoustic processes are approximately adiabatic, this means that there is an insignificant exchange of thermal energy from one particle of fluid to another, under these conditions the potential temperature of the fluid is approximately constant and the temperature gradients are small.

Using the three acoustic oceanographic state variables: potential temperature, salinity and pressure means that density can be written:

$$\rho = \rho(\eta, S, p) \, .$$

In general: $\Delta\rho = (\frac{\partial\rho}{\partial\eta})_{S,p}\Delta\eta + (\frac{\partial\rho}{\partial S})_{\eta,p}\Delta S + (\frac{\partial\rho}{\partial p})_{\eta,S}\Delta p$

but: an adiabatic system $\Rightarrow$ mechanical processes only.

	$\Delta\eta = 0$	no heat exchange
	$\Delta S = 0$	no diffusion
hence	$\Delta\rho = (\frac{\partial\rho}{\partial p})_{\eta,S}\Delta p$	(adiabatic approximation).

($\frac{\partial\rho}{\partial p}$ has dimension $\frac{1}{velocity^2} \Leftrightarrow \frac{1}{c^2}$ i.e sound or compression)

In this approach basic equations from fluid mechanics are used to derive the wave equation. The fundamental equations used are: the continuity equation; the equations of motion and the equation of state for fluids.

The continuity equation expresses the conservation of mass, that is it relates the motion of the fluid to its compression or dilation. It is a functional relationship between particle velocity, (u, v, w) , and the instantaneous density:

$$\frac{1}{\rho_o}\frac{\partial\rho}{\partial t} = - (\frac{\partial u}{\partial x} + \frac{\partial v}{\partial y} + \frac{\partial w}{\partial z}) \qquad (1)$$

The equations of motion represent the law of conservation of momentum:

$$\frac{\partial u}{\partial t} = - \frac{1}{\rho_o}(\frac{\partial p}{\partial x}) \qquad (2)$$

$$\frac{\partial v}{\partial t} = - \frac{1}{\rho_o}(\frac{\partial p}{\partial y}) \qquad (3)$$

$$\frac{\partial w}{\partial t} = - \frac{1}{\rho_o}(\frac{\partial p}{\partial z}) \qquad (4)$$

Here the Boussinesq approximation in which only variations of the instantaneous density are retained, which means that the typical density, ρ_o is used. Need to eliminate (u, v, w) from the equations:

$$\frac{\partial(1)}{\partial t}: \quad \frac{1}{\rho_o}\frac{\partial^2 \rho}{\partial t^2} = -\left(\frac{\partial^2 u}{\partial t \partial x} + \frac{\partial^2 v}{\partial t \partial y} + \frac{\partial^2 w}{\partial t \partial z}\right)$$

$$\frac{\partial(2)}{\partial x}: \quad \frac{\partial^2 u}{\partial t \partial x} = -\frac{1}{\rho_o}\left(\frac{\partial^2 p}{\partial x^2}\right)$$

$$\frac{\partial(3)}{\partial y}: \quad \frac{\partial^2 v}{\partial t \partial y} = -\frac{1}{\rho_o}\left(\frac{\partial^2 p}{\partial y^2}\right)$$

$$\frac{\partial(4)}{\partial z}: \quad \frac{\partial^2 w}{\partial t \partial z} = -\frac{1}{\rho_o}\left(\frac{\partial^2 p}{\partial z^2}\right)$$

Giving:

$$\frac{1}{\rho_o}\frac{\partial^2 \rho}{\partial t^2} = +\frac{1}{\rho_o}\left(\frac{\partial^2 p}{\partial x^2} + \frac{\partial^2 p}{\partial y^2} + \frac{\partial^2 p}{\partial z^2}\right)$$

But: $\Delta\rho = \left(\frac{\partial \rho}{\partial p}\right)_{\eta,S}\Delta p$ **(adiabatic assumption)**

$$\Rightarrow \quad \left(\frac{\partial \rho}{\partial p}\right)_{\eta,S}\frac{\partial^2 p}{\partial t^2} = \nabla^2 p$$

$$\Rightarrow \quad \frac{\partial^2 p}{\partial t^2} = c^2\nabla^2 p \quad \textbf{(The Wave Equation)}$$

Previously it was mentioned that the wave equation has two categories of solution: the wave theory solution and the ray theory solution, and that all acoustic propagation studies make use of either the wave or the ray tracing solution to determine the acoustic propagation paths.

The wave theory solution numerically integrates the wave equation to describe the propagation of sound through water. Given both boundary and initial conditions wave theory provides a formally complete solution applicable under all conditions.

Alternatively in the ray theory solution sound waves are treated like particles that travel along geometric trajectories called rays. Where a ray is defined as that trajectory which is everywhere perpendicular to the wave front. Acoustic ray tracing is a technique used to mathematically describe the path traveled by an acoustic ray. In the past graphical techniques and more recently computer models have been used to display the results of ray tracing computations in an informative way.

Ray tracing does provide an easy to interpret ray diagram as output, graphically showing the path of acoustic propagation. The primary reason a ray tracing program was used throughout the project is because of the useful graphical output of a ray tracing program, and the graphical insight this solution provides to the propagation problem being considered. Ray theory does not depict an exact solution, like wave theory, to the wave equation. For this reason there are distinct restrictions when using ray tracing, which are outlined in the conditions for the eikonal equation - further on in this chapter. Despite these restrictions ray tracing is an extremely useful method for the graphical representation of the acoustic situation corresponding to the ocean.

Not only can ray tracing give accurate information about the geometrical paths followed by acoustic rays, but further information about shadow boundaries, reflections from surfaces, phase, intensity, pulse travel time, absorption and Doppler shift (for time varying media) can be determined along the ray path.

3.3 The Eikonal Equation And Dispersion Relationship

Here appropriate solutions to the wave equation, which can lead to the derivation of the eikonal equation are considered. The dispersion relation, which provides a relationship between the local frequency, ω , and the local wavenumber, k , is also introduced in this section.

Consider the one dimensional wave equation, in a region where the speed of sound is constant, $c = c_o$.

$$\frac{\partial^2 p}{\partial t^2} = {c_o}^2 \frac{\partial^2 p}{\partial x^2}$$

Plane waves of the form $p = Ae^{i(\omega t - kx)}$ are exact solutions to the wave equation, where $k = \frac{\omega}{c}$ is defined as the wave number. The local frequency, ω , and the local wave number, k , are connected by a dispersion relationship, in this case the dispersion relationship is $\omega = kc_o$.

An analogous solution in three dimensions would be

$$p(x, y, z, t) = Ae^{i(\omega t - (k_1 x + k_2 y + k_3 z))}$$

with a dispersion relation:

$${k_1}^2 + {k_2}^2 + {k_3}^2 = \frac{\omega^2}{{c_o}^2} = {k_o}^2$$

and the normal to the wave front: $(n_1, n_2, n_3) = \frac{1}{k_o}(k_1, k_2, k_3)$

An equivalent solution would be:

$$p(x, y, z, t) = Ae^{i(\omega t - k_o W(x,y,z))}$$

where: $W(x,y,z) = n_1x + n_2y + n_3z$ with $\nabla W = (n_1, n_2, n_3)$

In a region where the sound speed varies slowly in all three spatial dimensions, $c = c(x,y,z)$, it is reasonable to look for solutions that closely approximate plane waves, these solutions are slightly distorted by the index of refraction:

$$N(x,y,z) \equiv \frac{c_o}{c(x,y,z)} = \frac{k(x,y,z)c_o}{\omega}$$

The local wave number $k(x,y,z)$ also varies slowly with position and is related to the local sound speed through the extended dispersion relation:

$$k(x,y,z) = \frac{\omega}{c(x,y,z)}$$

In a three dimensional region where the sound speed varies slowly with position, the wave equation can be written:

$$\frac{\partial^2 p}{\partial t^2} = [c(x,y,z)]^2 \nabla^2 p$$

The assumed quasiplanar wave solution can be written:

$$p(x,y,z,t) = A(x,y,z)e^{i(\omega t - k_o W(x,y,z))}$$

With the amplitude, A , and the phase function, W coping with the slow variability. Substituting this solution into the acoustic wave equation leads to:

$$-\frac{\omega^2}{c^2}A = (\nabla^2 A - k_o^2 A(\nabla W)^2) - ik_o(2\nabla W \nabla A + A\nabla^2 W)$$

separating this into real and imaginary parts gives:

$$\nabla^2 A - k_o^2 A(\nabla W)^2 + \frac{\omega^2}{c_o^2}\frac{c_o^2}{c^2}A = 0$$

and: $$2\nabla W \nabla A + A\nabla^2 W = 0$$

The first equation can be rewritten:

$$\frac{1}{Ak_o^2}\nabla^2 A - (\nabla W)^2 + N^2 = 0$$

Now $N = \frac{c_o}{c}$ varies slowly with position and its size is essentially 1 . The assumption of slow variation requires the assumption that the fractional curvature, $\frac{1}{Ak_o^2}\nabla^2 A$, is small over a wavelength. This means that the phase function, $W(x, y, z)$ must satisfy the eikonal equation:

$$\nabla^2 W \equiv (\frac{\partial W}{\partial x})^2 + (\frac{\partial W}{\partial y})^2 + (\frac{\partial W}{\partial z})^2 = N^2 = \frac{c_o^2}{c^2}$$

Once the detail of the phase function, $W(x, y, z)$, is established using the real part of the wave equation, the imaginary part of the equation can provide information on the (slow) variation in energy density.

Constant values of $W(x, y, z)$ represent surfaces of constant phase or wavefronts. The normals to the wavefronts, defined as rays, are the paths of energy flux away from the source. A bundle of adjacent rays is known as a pencil of rays, within it the acoustic energy is constant along the propagation path. This is an important concept, since within ray theory there is no place for the effects of diffraction and scattering, since there can be no leakage out of the pencil (Apel, 1987).

An advantage of the eikonal equation over the wave equation is that it does not depend on time (Apel, 1987). Also the propagation it describes is not dependent on frequency. There are certain limitations (mentioned previously) associated with the ray theory solution to the wave equations, these limitations present themselves in the form of sufficient conditions, which arise in the reduction from the wave equation to the eikonal equation. Kinsler et al (1982) describes

these conditions in detail, here they are outlined so as to provide insight and understanding.

The first condition is this: 'the amplitude of the wave must not change appreciably in a distance comparable to a wavelength'. This means that for a beam of sound traveling through a fluid the eikonal equation can be applied to the central portion of the beam where the wave amplitude, A , is not varying rapidly. However, at the edges of the beam, ' A may rapidly $\rightarrow 0$ ' over distances of a wavelength, in which case the eikonal equation would no longer be valid. Failure of the eikonal equation means that diffraction of sound at the edges of the beam would occur.

And the second condition: 'sound speed must not change appreciably in a distance comparable to a wavelength', means that the speed of sound must be slowly varying in space (one of the assumptions mentioned) so that the local direction of wave fronts does not significantly change over a distance of one wavelength, in other words the refraction of a sound beam must not be too rapid.

To summarize the sufficient conditions: it can be said that the eikonal equation is in general an accurate description of acoustic propagation in the limit of high frequencies (short wave length) - how high depends on the rapidity of spatial variations of sound speed and amplitude.

The following discussion regarding the dispersion relationship has been adapted from Lighthill (1978), which provides an in depth explanation of the dispersion

relationship. The assumption that the wavenumber vector, $\underline{k}$, is assumed to vary only gradually on a scale of one wavelength, has been maintained from here onwards.

Consider a three dimensional solution to the wave equation:

$$p(x,y,z,t) \;=\; A(x,y,z,t)e^{i\psi(x,y,z,t)}$$

where $A(x,y,z,t)$ is a positive slowly varying amplitude and $\psi(x,y,z,t)$ is a phase function. At a fixed point (x,y,z) the equation requires that the phase increases by 2π in one wave period, so that $\frac{\partial\psi}{\partial t}$ can be regarded as the local frequency, ω , in radians per second. Similarly, at a given time, t , ψ shows a decrease with x at a rate equal to k_1 , the x - component of the local wave number in radians per meter, with analogous results for y and z .

$$\frac{\partial\psi}{\partial x} = -k_1; \quad \frac{\partial\psi}{\partial y} = -k_2; \quad \frac{\partial\psi}{\partial z} = -k_3; \quad \frac{\partial\psi}{\partial t} = \omega$$

Whenever the derivatives of a phase function, ψ , satisfy a dispersion relationship:

$$\omega = \omega(\underline{k})$$

specifying the local frequency ω as a function of the magnitude and direction of the local wave number vector, the value and the main properties of the vector group velocity can be deduced.

The analysis that follows here is easier to follow and interpret if suffix notation and the summation convention are used.

The phase can be written: $\psi \;=\; \psi(x_1,x_2,x_3,t)$,

the phase equations: $\frac{\partial \psi}{\partial x_i} = -k_i$ and $\frac{\partial \psi}{\partial t} = \omega$

The dispersion relationship: $\omega = \omega(k_1, k_2, k_3)$

becomes: $\frac{\partial \psi}{\partial t} = \omega(-\frac{\partial \psi}{\partial x_1}, -\frac{\partial \psi}{\partial x_2}, -\frac{\partial \psi}{\partial x_3})$

Differentiating the function ω with respect to x_i gives:

$$\frac{\partial^2 \psi}{\partial x_i \partial t} = (\frac{\partial \omega}{\partial k_j})(\frac{-\partial^2 \psi}{\partial x_i \partial x_j})$$

using the phase equations gives:

$$\frac{\partial k_i}{\partial t} + U_j(\frac{\partial k_i}{\partial x_j}) = 0 \qquad \text{(The Three Dimensional Dispersion Rule)}$$

where: $U_j = \frac{\partial \omega}{\partial k_j}$ is defined as the vector group velocity. This means that the wavenumber vector, $\underline{k}$, is constant in changes satisfying $\frac{\partial x_j}{\partial t} = U_j$. For example, consider an observer watching a point (x_1, x_2, x_3) that is moving according to the group velocity, $\frac{\partial x_j}{\partial t} = U_j$. Then the three dimensional dispersion rule means that the observer will always observe waves of the same wavenumber, $\underline{k}$.

Also notice that when $\underline{k}$ is constant then the group velocity U_j is also constant. Thus the path: $\frac{\partial x_j}{\partial t} = U_j$ is necessarily a straight line, $x_j - U_j t = constant$, traversed at a constant velocity U_j.

This means that in a homogeneous system, waves of a given wavenumber vector k_i are found at points moving at constant velocity U_j, along such straight line paths $x_j - U_j t = constant$, and there is a different path for each wavenumber. These paths in three dimensional systems are called rays. Thus sound waves with constant sound speed c_o and wavenumber vector $\underline{k}$ have frequency:

$$\omega = c_o({k_1}^2 + {k_2}^2 + {k_3}^2)^{\frac{1}{2}}$$

so: $U_j = c_o k_j({k_1}^2 + {k_2}^2 + {k_3}^2)^{-\frac{1}{2}}$

This group velocity vector has constant magnitude c_o and is directed along the wavenumber.

3.4 Ray Tracing

At this stage it has been established that the eikonal equation is time and frequency independent. The purpose of introducing the eikonal equation was that it leads to a set of first order ordinary differential equations which describe the path of individual rays as they propagate through the ocean. These equations can be integrated, and given an initial sound speed or the index of refraction, the progress of an acoustic ray can easily be determined.

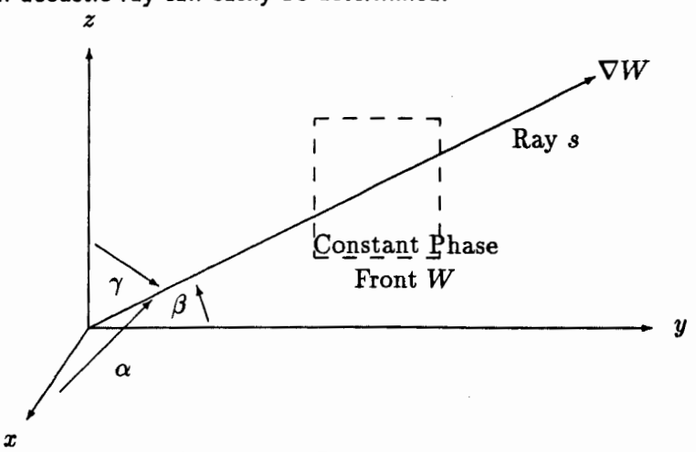

Figure 3.2: Direction Cosines, Giving The Direction To A Ray, s, And A Constant Phase Front, W (Apel, 1987)

Consider figure 3.2, by labeling the distance along a ray path by coordinate s the way ∇W changes along a ray path are determined by the vector differential $\frac{\partial \nabla W}{\partial s}$. ∇W determines the direction of the normal to the wave front, where:

$$\nabla W = N(\alpha, \beta, \gamma)$$

or: $\frac{\partial W}{\partial x} = \alpha N; \quad \frac{\partial W}{\partial y} = \beta N; \quad \frac{\partial W}{\partial z} = \gamma N$

(α, β, γ) are the direction cosines to the normal. Both N and α, β, γ vary slowly, but:

$$\alpha^2 + \beta^2 + \gamma^2 = 1 \qquad \text{is fixed.}$$

The ray equations arise from the variations of ∇W along the ray path, with distance s along the ray path in the direction of the normal.
Consider:

$$\frac{\partial}{\partial s} = [(\alpha, \beta, \gamma)\nabla] = (\alpha\frac{\partial}{\partial x} + \beta\frac{\partial}{\partial y} + \gamma\frac{\partial}{\partial z})$$

Applying this to each component of ∇W , starting with $\frac{\partial W}{\partial x} = \alpha N$

lhs: $\frac{\partial}{\partial s}(\frac{\partial W}{\partial x}) = (\alpha\frac{\partial}{\partial x} + \beta\frac{\partial}{\partial y} + \gamma\frac{\partial}{\partial z})(\frac{\partial W}{\partial x})$

$= \alpha\frac{\partial}{\partial x}(\frac{\partial W}{\partial x}) + \beta\frac{\partial}{\partial y}(\frac{\partial W}{\partial x}) + \gamma\frac{\partial}{\partial z}(\frac{\partial W}{\partial x})$

$= \alpha\frac{\partial}{\partial x}(\frac{\partial W}{\partial x}) + \beta\frac{\partial}{\partial x}(\frac{\partial W}{\partial y}) + \gamma\frac{\partial}{\partial x}(\frac{\partial W}{\partial z})$

rhs: $\frac{\partial}{\partial s}(\alpha N) = \alpha\frac{\partial}{\partial x}(\alpha N) + \beta\frac{\partial}{\partial y}(\alpha N) + \gamma\frac{\partial}{\partial z}(\alpha N)$

$= \alpha\frac{\partial}{\partial x}(\alpha N) + \beta\frac{\partial}{\partial x}(\beta N) + \gamma\frac{\partial}{\partial x}(\gamma N)$

$= \frac{\partial N}{\partial x}$

So: $\frac{\partial}{\partial s}(\alpha N) = \frac{\partial N}{\partial x}$

similarly: $\frac{\partial}{\partial s}(\beta N) = \frac{\partial N}{\partial y}$ (Ray Equations)

$\frac{\partial}{\partial s}(\gamma N) = \frac{\partial N}{\partial z}$

These equations are known as the ray equations and an important application of the ray equations is refraction. Refraction is the bending of sound waves as a result of velocity changes accompanying temperature and pressure changes

(Seto, 1977). Throughout the ocean, in both the vertical and the horizontal planes, there exists a high degree of variability, especially temperature variability and this implies a high degree of variability in the sound speed field. Understanding the mechanism of refraction through a varying ocean is a prerequisite to considering the effects of oceanic features, for instance ocean currents and eddies, on acoustic propagation through them.

Here the ordinary differential equations derived from the eikonal equation, known as the ray equations, are used to show how the path a ray takes when propagating through a variable medium can be determined. A useful consequence of the ray equations, is Snell's law.This is a powerful statement concerning the direction of propagation of a ray, it states that the direction of propagation, taken as θ, for a ray is uniquely determined.

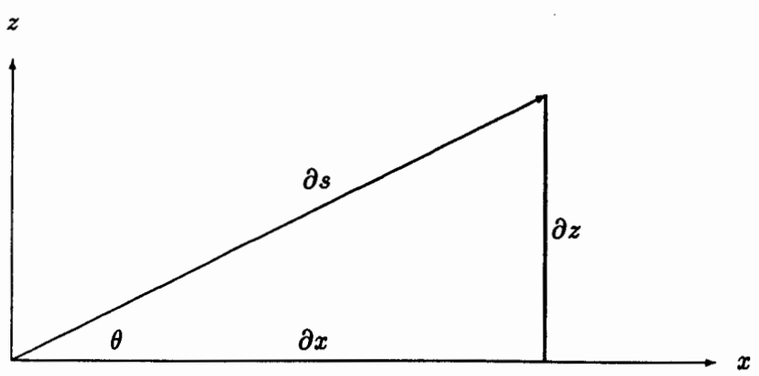

Figure 3.3: Diagram Used To Derive Snell's Law

Consider the two dimensional case: x and z, where x and z could be the vertical or horizontal plane (refer to figure 3.3), and using the ray equations:

Let: N be a function of z only: $\Rightarrow \frac{\partial N}{\partial x} = 0$.

And ignore the third equation in y.

Let: $\theta :=$ angle of ray with $x - axis$.

$\alpha := \frac{\partial x}{\partial s} = \cos\theta$

From the ray equation: $\frac{(\partial \alpha N)}{\partial s} = \frac{\partial N}{\partial x} \Leftrightarrow \frac{(\partial N \cos\theta)}{\partial s} = 0$

$\Rightarrow$ $N\cos\theta$ is constant along any ray.

But: $N = \frac{c_o}{c(z)}$

$\Rightarrow$ $\frac{c_o \cos\theta}{c(z)} =$ constant $= \cos\theta_o$ (say)

$\Rightarrow$ $\frac{c_o}{\cos\theta_o} = \frac{c(z)}{\cos\theta}$ (Snell's law)

The relationship, Snell's law, can be used to construct the path of a ray starting at an angle, θ_o, where the sound speed is c_o, and progressing through the medium, where the sound speed is $c(z)$. This corresponds to the theory used for range dependent models which were described in section 2.2.

Consider the vertical plane and choose c_o to coincide with the point at which the sound ray is horizontal. Then, by Snell's law: the angle associated with any other point along the ray is given by: $\frac{\cos\theta}{c} = \frac{\cos\theta_o}{c_o} = \frac{1}{c_o} \Rightarrow \cos\theta = \frac{c}{c_o}$ $(\cos 0 = 1)$.

This means that at any point in the medium the angle the ray makes with the horizontal is the arccos of: 'the ratio of the local sound speed to the speed at depth at depth where the ray is horizontal'. Also, the local sound speed on the acoustic ray is always less than the value of c_o (since $|\frac{c}{c_o}| \leq 1$). This is a far reaching result, it means that for any acoustic ray propagating through a

medium, the ray always bends towards the region of decreasing sound speed.

When performing ray tracing complicated sound speed profiles (in the vertical or horizontal plane) are usually separated into segments, each short enough that the sound speed gradient may be considered constant over its length. The advantage of this is that the path of a sound ray through a layer of water of constant speed gradient, g say, is the arc of a circle. To show this consider a medium in which sound speed is a linear function of depth. (This theory is equally applicable in the vertical and horizontal plane, and is described here in the vertical plane because of the way that the ray tracing method is demonstrated hereafter.)

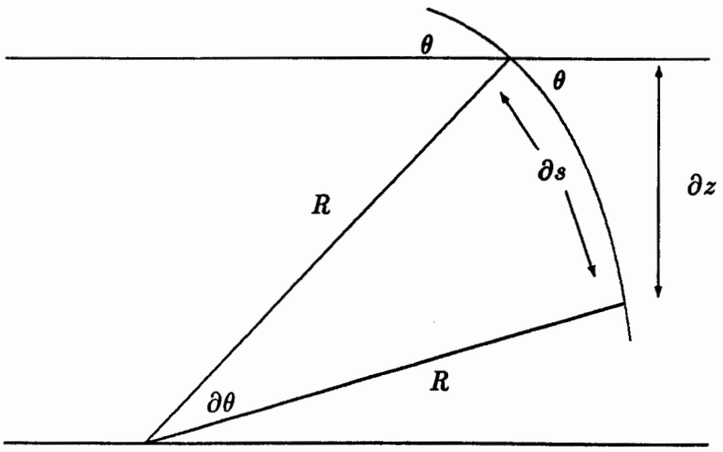

Figure 3.4: Diagram Used To Derive The Radius Of Curvature (Burdic, 1984)

So: $c(z) = c_o + g.z$

Differentiating this gives: $\partial c = g\partial z$

Where: c_o := speed at reference depth $(z = z_o)$

g := sound speed gradient

z := depth below the reference depth

Differentiating $\cos\theta = \frac{c}{c_o}$ gives a relationship between an incremental change in sound speed and the resulting incremental change in direction, that is:

$$\frac{\partial c}{c_o} = -\sin\theta\partial\theta$$

So: $$g\frac{\partial z}{c_o} = -\sin\theta\partial\theta$$

This equation describes the type of curve followed by an acoustic ray in a constant sound speed gradient medium.

Consider the vertical motion of a point moving on the arc of a circle of radius R (see figure 3.4). Then the relationship between: angle θ, arclength ∂s and vertical distance ∂z, is:

$$\partial z = \sin\theta\partial s$$

But: $$\partial s = R\partial\theta$$

$\Rightarrow$ $$\partial z = R\sin\theta\partial\theta$$

But previously: $$g\frac{\partial z}{c_o} = -\sin\theta\partial\theta$$

So $$R = -\frac{c_o}{g} = -\frac{c}{g\cos\theta}$$

For a region of ocean where the velocity variation is linear, which means that the sound speed gradient is constant,

$$R = -\frac{c}{g\cos\theta} \quad \text{is constant.}$$

Hence R describes a radius of a circle, and the path of a sound ray in a linearly varying sound speed profile is an arc of that circle. This means that an acoustic profile which decreases with depth results in a positive radius of curvature and the ray will bend downwards. Conversely a sound speed that increases with depth results in a negative radius of curvature and the ray will curve upwards. The result of this is that sound rays oscillate about the sound channel axis.

Above the sound channel axis the sound speed gradient is positive, which results in the ray path curving downwards towards the sound speed axis. Alternatively below the sound channel axis the sound speed gradient is negative and the rays are refracted upwards towards the sound channel axis. Thus the sound speed minimum causes the ocean to act as a lens, which has rays, above and below it, continuously refracting back towards the depth of the minimum sound speed. The region within which the sound rays are refracted back towards the minimum sound speed is called the deep sound speed channel or the SOFAR (SOund Fixing And Ranging) channel.

The fact that the physical properties of the ocean give rise to the sound speed channel is highly significant for long range sound transmission through the ocean. Sound rays are trapped within the sound speed channel and the acoustic energy can travel over vast distances, through the open ocean, without intersecting with either the ocean surface or the ocean bottom.

The two dimensional environment that was described in this section, where the ocean is horizontally stratified and the only variation occurs in the vertical plane, gives rise to range independent models, which were defined in section 2.2.

Range independent ray tracing models are easy to formulate using the ray tracing equations, Snell's law and the radius of curvature. (This theory is equally applicable to the two dimensional, horizontal environment, and useful when analyzing the effects of horizontal variations in the medium.)

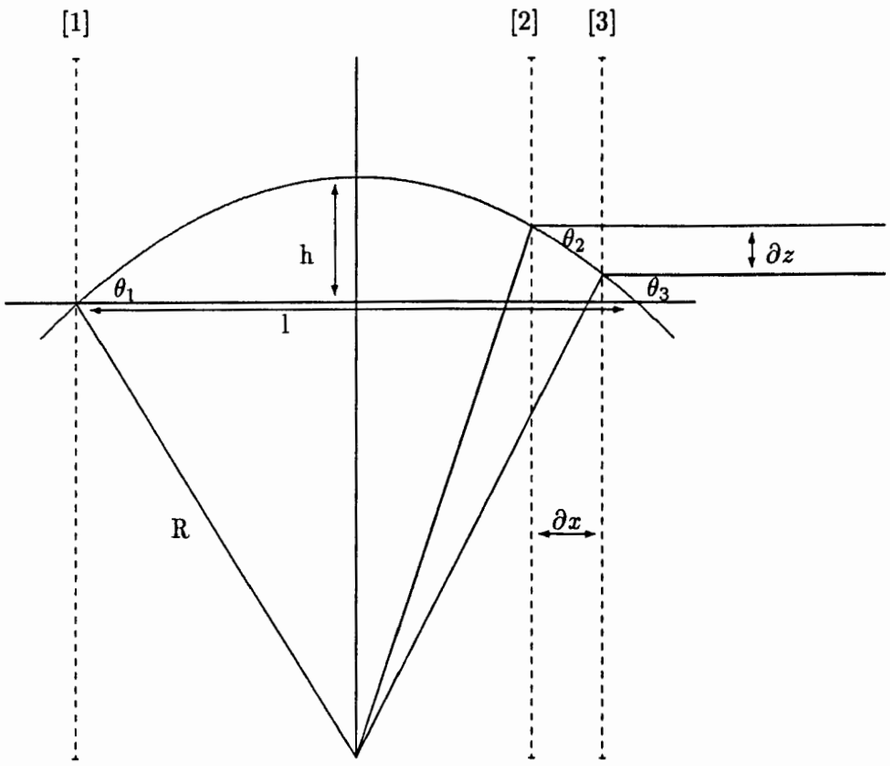

Figure 3.5: Diagram To Determine The Ray Tracing Procedure (Burdic, 1984)

Considering figure 3.5 and a ray with start position at [1] and direction of propagation θ_1 . The maximum height reached, above the initial position, by the ray is: $h = R(1 - \cos\theta_1)$, where: $R = -\frac{c_1}{g\cos\theta_1}$. The cord length is

given by: $l = 2R\sin\theta_1$, l is the horizontal distance from the source to the point where the ray returns to the starting depth.
For arbitrary points: [2] and [3] :

$$\begin{aligned} \delta z &= R(\cos\theta_3 - \cos\theta_2) = \frac{(c_3 - c_2)}{g} \\ \delta x &= R(\sin\theta_2 - \sin\theta_3) \end{aligned}$$

These equations can be used to trace a ray through a medium which varies in two dimensions. Burdic (1984) contains a worked ray tracing example, which makes use of these equations.

Within an undisturbed ocean the temperature field, and hence sound speed field, has a high degree of stratification with depth, and since isotherms are nearly parallel to the horizontal plane this structure is known as horizontal stratification (Weinberg, 1978). However while the underlying ocean is horizontally uniform it does consist of a number of anomalies, for instance ocean currents and eddies. From previous theoretical and experimental evidence it is known that these features have a significant effect on the sound propagation through them. This is due to variations in the acoustic field within the disturbances, primarily because of their anomalous temperature structure and the fact that their perimeters act as ocean fronts.

An ocean front, defined in terms of ocean acoustics, is a discontinuity within the sound speed field which significantly alters the sound propagation pattern. An ocean front can be responsible for changes in sound speed of the order of thirty meters per second and a variation in sound channel depth of the order of $750\ m$. These variations result in refraction of a sound rays as they cross an

ocean front obliquely. (Etter, 1991).

Usually when one thinks of an ocean front one considers for example a convergence zone. However the perimeter of ocean currents and mesoscale eddies represent a form of ocean front, since they are separate water mass entities contained within their own circulation and surrounded by water with different characteristics.

In the same way that rays bend towards the sound speed minimum in the vertical, so rays refract towards lower sound speeds in the horizontal. This has to be taken into consideration when analyzing the results of propagation studies through features such as currents and eddies.

3.5 Hamiltonian Ray Tracing

In this section the theory of ray tracing, which has been developed previously in this chapter, for a homogeneous environment (that is a stationary and linearly stratified environment) is generalized. Lighthill (1978) provides the link between the generalized ray tracing equations and Hamilton's equations for a conservative dynamical system. An outline of Lighthill's work is given here and the Hamiltonian ray equations are derived. The theory is then extended further and the Hamiltonian ray tracing equations for sound propagation through a current are derived.

In this section, to assist the explanation, the suffix notation introduced in section 3.3 is used again. Once again waves where the wavenumber vector, $\underline{k}$,

varies only gradually on a scale of a wavelength are considered.

In a homogeneous system this would permit the use of a standard form for waves:

$$p(x_1, x_2, x_3, t) = A(x_1, x_2, x_3, t)e^{i\psi(x_1,x_2,x_3,t)} .$$

The phase function, ψ satisfies the following phase equations:

$$\frac{\partial\psi}{\partial x_i} = -k_i \quad \text{and} \quad \frac{\partial\psi}{\partial t} = \omega$$

The local frequency , ω , and the wavenumber vector, $\underline{k}$ are connected by a dispersion relationship:

$$\omega = \omega(k_1, k_2, k_3)$$

In a non-homogeneous environment, that is within a moving environment, the time derivatives change to reflect the Doppler shift. The new time derivatives are of the form: $(\frac{\partial}{\partial t} - \underline{V}.\nabla)$ (Apel, 1987), giving the continuity equation:

$$\frac{1}{\rho_o}(\frac{\partial}{\partial t} - \underline{V}.\nabla)\rho = -\nabla.\underline{u}$$

and the force equation:

$$(\frac{\partial}{\partial t} - \underline{V}.\nabla)\underline{u} = -\frac{1}{\rho_o}\nabla p$$

which gives:

$$\frac{1}{\rho_o}(\frac{\partial}{\partial t} - \underline{V}.\nabla)^2\rho = \frac{1}{\rho_o}\nabla^2 p$$

and introducing the sound speed, c , gives the acoustic wave equation in a moving environment as:

$$(\frac{\partial}{\partial t} - \underline{V}.\nabla)^2 p = c^2\nabla^2 p$$

In a non homogeneous system the same form of solution for the wave equation as mentioned previously is appropriate, provided that the fluid properties defining the dispersion relationship also vary slowly on a scale of wavelengths (for example the refractive index, N). This allows the waves to have the same phase equations as previously but ω specified for a given k_i in a way that varies with position as well, so:

$$\omega = \omega(k_1, k_2, k_3, x_1, x_2, x_3)$$

In a region where c is locally fixed, $c = c_o$, a solution of the form above is a good approximation in a moving environment provided:

$$(\omega - \underline{V}.\underline{k})^2 = c^2 \underline{k}.\underline{k} \, ,$$

which is a Doppler shifted dispersion relation.

However in a region where A, $\underline{V}$ and c are all slowly varying (that is they can be treated as constants when taking derivatives) the solution is of the form:

$$p = Ae^{i(\omega t - k_o W)}$$

with a dispersion relation:

$$-(\omega - k_o \underline{V}.\nabla W)^2 = -c^2 {k_o}^2 (\nabla W)^2$$

An extension of the previously defined refractive index, N , to a vector form, $\underline{N} = (\alpha N, \beta N, \gamma N)$ is introduced and $\nabla W = \underline{N}$. Now this vector form must also incorporate the Doppler shift and becomes:

$$N = \frac{\nabla W}{|-\frac{1}{c_o}\underline{V}\nabla W|}$$

As shown in section 3.3 locally the energy propagation velocity has approximately the value $U_j = \frac{\partial \omega}{\partial k_j}$.

In a non-homogeneous system wave energy propagated at this group velocity is expected to suffer refraction, that is changes to the wavenumber due to non-homogeneity.

From the phase equations:

$$\frac{\partial \psi}{\partial t} = \omega(-\frac{\partial \psi}{\partial x_1}, -\frac{\partial \psi}{\partial x_2}, -\frac{\partial \psi}{\partial x_3}, x_1, x_2, x_3)$$

Differentiating this with respect to x_i gives:

$$\frac{\partial^2 \psi}{\partial x_i \partial t} = (\frac{\partial \omega}{\partial k_j})(\frac{-\partial^2 \psi}{\partial x_i \partial x_j}) + \frac{\partial \omega}{\partial x_i}$$
$$\Rightarrow \quad \frac{\partial k_i}{\partial t} + U_j(\frac{\partial k_i}{\partial x_j}) = -\frac{\partial \omega}{\partial x_i}$$

Here the left hand side represents the rate of change of k_i with time at a position working with group velocity U_j , that is changes satisfying $\frac{\partial x_i}{\partial t} = U_j$. In changes like these

$$\frac{\partial k_i}{\partial t} = \frac{-\partial \omega}{\partial x_i} .$$

This equation specifies the refraction of wave energy, that is the rate of change of wavenumber along paths traversed at the energy propagation velocity, U_j , that is along rays. The equations governing these in general curved rays take a more symmetrical form if $\frac{\partial x_j}{\partial t} = U_j$ is written:

$$\frac{\partial x_i}{\partial t} = \frac{\partial \omega}{\partial k_i}$$

While refraction in a nonhomogeneous system is expected, the frequency ω should remain unchanged. In order to prove that ω remains constant along a

ray it is shown that the rate of change of ω with time for arbitrary rates of change of k_i and x_i is zero.

$$\frac{\partial \omega}{\partial t} = (\frac{\partial \omega}{\partial k_i})(\frac{\partial k_i}{\partial t}) + (\frac{\partial \omega}{\partial x_i})(\frac{\partial x_i}{\partial t}) = 0$$

Since: $\frac{\partial k_i}{\partial t} = -\frac{\partial \omega}{\partial x_i}$

and $\frac{\partial x_i}{\partial t} = \frac{\partial \omega}{\partial k_i}$

These last two equations parallel the characteristic form (symmetric except for a '- sign') of Hamilton's equations, for a conservative dynamical system, exactly. Written in terms of the Hamiltonian function:

$$H(p_1, p_2, \ldots p_n, q_1, q_2, \ldots q_n) \ ,$$

which is the systems total energy (kinetic and potential) expressed as a function of generalized coordinates $q_1, q_2, \ldots q_n$ and associated generalized momenta $p_1, p_2, \ldots p_n$. Hamilton's equations then take the form:

$$\frac{\partial p_i}{\partial t} = -\frac{\partial H}{\partial q_i} \qquad \text{(Hamiltonian Equations)}$$
$$\frac{\partial q_i}{\partial t} = \frac{\partial H}{\partial p_i} \qquad for\ i = 1 \ldots n$$

The previous equations were of this form, for $i = 1 \ldots 3$ and k_i , x_i and ω replacing p_i , q_i and H respectively. The verification that ω remains constant along a ray is an exact parallel to the standard verification that for any solution of the equations of motion the total energy, H remains constant.

Notice that the Hamiltonian ray tracing equations:

$$\frac{\partial k_i}{\partial t} = -\frac{\partial \omega}{\partial x_i} \qquad \text{(Hamiltonian Ray Equations)}$$
$$\frac{\partial x_i}{\partial t} = \frac{\partial \omega}{\partial k_i} \qquad for\ i = 1 \ldots 3$$

are already in a form suitable for the application of standard computer routines, for ordinary differential equations, to obtain their solutions under a wide variety of initial conditions. In such computations the fact that ω remains constant along a ray can be used as an accuracy check.

At this stage the general theory of ray tracing is extended to wave propagation through a fluid in motion. The basic assumption, that the flow field and properties that influence the waves in a fluid at rest vary gradually on a scale of wavelengths, is kept for this derivation. Here the concern is wave propagation through a non-uniform flow, such as a current. At each point, as sound propagates through the current, a frame of reference can be chosen so that locally there is no mean flow and the waves are propagating through the fluid at rest. However the frame of reference is different at different points and therefore modifying the energetics of wave propagation.

Let $\underline{V} = (V_1, V_2, V_3)$ represent the mean velocity field through which the sound waves would propagate. Consider a local frame of reference, moving at a particular value of the mean velocity flow, then within that frame of reference there is locally no current and the waves have frequency:

$$\omega_r = \omega_r(k_1, k_2, k_3, x_1, x_2, x_3)$$

This frequency, ω_r , is appropriate to a fluid at rest, and is the frequency of the motions relative to the local mean velocity.

Assume that the properties of the fluid vary so gradually that only their local values effect the local dispersion relationship. Also assume that changes in

the mean flow within a wavelength are so slight that they effect the dispersion relationship negligibly.

A simple relationship exists between the absolute frequency ω (frequency of oscillations occurring at a fixed point in space) and the relative frequency ω_r (frequency of oscillations occurring at a point moving with velocity $\underline{V}$).

In terms of a phase function $\psi(x_1, x_2, x_3, t)$ the absolute frequency ω and wavenumber vector k_i are given by its partial derivatives:

$$\frac{\partial \psi}{\partial x_i} = -k_i \text{ and } \frac{\partial \psi}{\partial t} = \omega$$

The relative frequency, ω_r , is the rate: $\frac{\partial \psi}{\partial t} + V_j \frac{\partial \psi}{\partial x_j}$ at which the phase changes for a point moving with velocity $\underline{V}$

$$\Rightarrow \quad \omega_r = \omega - V_j k_j.$$

This relationship relates the frequencies of the same wave in two different frames of reference and is called the Doppler relationship.

For sound waves whose wavenumber vector, $\underline{k}$ (perpendicular to the wave crests), makes an angle, ϕ , with the current velocity V_j , the usual relationship:

$$\omega_r = c_o({k_1}^2 + {k_2}^2 + {k_3}^2)^{\frac{1}{2}}$$

satisfied by ω_r

$$\begin{aligned} \Rightarrow V_j k_j &= V({k_1}^2 + {k_2}^2 + {k_3}^2)^{\frac{1}{2}} cos\phi \\ &= \omega_r(\tfrac{V}{c_o})cos\phi \end{aligned}$$

where V is the current speed.

Now: $\omega_r = \omega - V_j k_j$

$\Rightarrow \quad \omega = k_j V_j(x_1, x_2, x_3) + \omega_r(k_1, k_2, k_3, x_1, x_2, x_3)$

From the generalized Hamiltonian ray tracing equations the velocity, $\frac{\partial x_i}{\partial t} = \frac{\partial \omega}{\partial k_i}$, of a wave packet along its ray becomes:

$$\frac{\partial x_i}{\partial t} = V_i + \frac{\partial \omega_r}{\partial k_i} = V_i + U_i$$

That is the vector sum of the current velocity and the group velocity in a fluid at rest. Also, in a current the equation governing refraction, $\frac{\partial k_i}{\partial t} = -\frac{\partial \omega}{\partial x_i}$ takes the form:

$$\frac{\partial k_i}{\partial t} = -k_j \frac{\partial V_j}{\partial x_i} - \frac{\partial \omega_r}{\partial x_i}$$

The first term represents refraction due to the current gradient and the second term due to changing fluid properties (such as N).

In conclusion the generalized Hamiltonian ray tracing equations for sound propagation through a fluid in motion are:

$$\frac{\partial k_i}{\partial t} = -k_j \frac{\partial V_j}{\partial x_i} - \frac{\partial \omega_r}{\partial x_i} \qquad \text{(Hamiltonian Ray Tracing Equations In A Curren}$$

$$\frac{\partial x_i}{\partial t} = V_i + \frac{\partial \omega_r}{\partial k_i} \qquad for\ i = 1 \ldots 3$$

As in the generalized theory, the result : $\frac{\partial \omega}{\partial t} = 0$ shows that the frequency ω remains constant along rays, however the relative frequency ω_r may vary, in fact:

$$\begin{aligned} \frac{\partial \omega_r}{\partial t} &= \left(\frac{\partial \omega_r}{\partial k_i}\right)\left(\frac{\partial k_i}{\partial t}\right) + \left(\frac{\partial \omega_r}{\partial x_i}\right)\left(\frac{\partial x_i}{\partial t}\right) \\ &= -U_i k_j \frac{\partial V_j}{\partial x_i} + V_i \frac{\partial \omega_r}{\partial x_i} \end{aligned}$$

Two examples using the Hamiltonian ray tracing equations in a current are given. In order to separate the current velocity and sound speed effects a region with a fixed sound speed is considered. The purpose of these examples is to illustrate the effects of a velocity structure on sound propagation through them and thus provide insight to the results for the velocity only scenario's presented in Chapter Six. However it must be mentioned that the model used, $\mathcal{HARPO}$, can include both the velocity and sound speed structure associated with mesoscale current features and thus provide more realistic scenario's.

Consider a region with a fixed sound speed, then:

$$\omega_r{}^2 = c_o(\underline{k}.\underline{k})$$

$$\Rightarrow \quad \frac{\partial \omega_r}{\partial x_i} = 0 \quad \text{and} \quad \frac{\partial \omega_r}{\partial k_i} = c_o \frac{k_i}{\sqrt{\underline{k}.\underline{k}}}$$

Example 1: Firstly consider a zonal current of the form $\underline{V} = (0, V_2(x_1), 0)$, where $(x_1, x_2, x_3) \equiv (latitude, longitude, depth)$:

then:	$\frac{\partial k_1}{\partial t} = -k_2 \frac{\partial V_2}{\partial x_1}$	$\frac{\partial k_2}{\partial t} = 0$	$\frac{\partial k_3}{\partial t} = 0$
and:	$\frac{\partial x_1}{\partial t} = c_o \frac{k_1}{\sqrt{\underline{k}.\underline{k}}}$	$\frac{\partial x_2}{\partial t} = V_2 + c_o \frac{k_2}{\sqrt{\underline{k}.\underline{k}}}$	$\frac{\partial x_3}{\partial t} = c_o \frac{k_3}{\sqrt{\underline{k}.\underline{k}}}$

Suppose the initial direction of the wave front is taken to be $\underline{k} = (k_1, 0, 0)$

then:	$\frac{\partial k_1}{\partial t} = 0$	$\frac{\partial k_2}{\partial t} = 0$	$\frac{\partial k_3}{\partial t} = 0$
and:	$\frac{\partial x_1}{\partial t} = c_o$	$\frac{\partial x_2}{\partial t} = V_2$	$\frac{\partial x_3}{\partial t} = 0$

These equations demonstrate that while the sound wave remains in its initial direction (that is $\underline{k}$ remains unchanged) the wave is refracted by the current.

The zonal current is extended to a vertically sheared zonal current of the form

$\underline{V} = (0, V_2(x_1, x_3), 0)$, which represents the current through which sound rays were propagated for this experiment. A full description of the current is given in Chapter Five, and the sound propagation results through the current are given in Chapter Six. If $\underline{V} = (0, V_2(x_1, x_3), 0)$

then: $\frac{\partial k_1}{\partial t} = -k_2 \frac{\partial V_2}{\partial x_1}$ $\frac{\partial k_2}{\partial t} = 0$ $\frac{\partial k_3}{\partial t} = -k_2 \frac{\partial V_2}{\partial x_3}$

and: $\frac{\partial x_1}{\partial t} = c_o \frac{k_1}{\sqrt{\underline{k}.\underline{k}}}$ $\frac{\partial x_2}{\partial t} = V_2 + c_o \frac{k_2}{\sqrt{\underline{k}.\underline{k}}}$ $\frac{\partial x_3}{\partial t} = c_o \frac{k_3}{\sqrt{\underline{k}.\underline{k}}}$

If the initial wave front direction is again taken to be $(k_1, 0, 0)$ then k_2 is always zero, since $\frac{\partial k_2}{\partial t} = 0$ and the equations reduce to those of the scenario above, that is sound propagation through a zonal current with the initial direction remaining constant and refraction in the horizontal plane occurring.

Suppose the initial ray is not perpendicular to the current, for example an initial wave front direction of $\underline{k} = (k_1, 0, k_3)$, then the wave front direction will still be conserved but refraction would occur in both the horizontal and vertical planes, that is:

$$\frac{\partial x_1}{\partial t} = c_o \frac{k_1}{\sqrt{\underline{k}.\underline{k}}} \qquad \frac{\partial x_2}{\partial t} = V_2 \qquad \frac{\partial x_3}{\partial t} = c_o \frac{k_3}{\sqrt{\underline{k}.\underline{k}}}$$

Finally suppose the initial non-perpendicular direction of the wave front is $\underline{k} = (k_1, k_2, 0)$ then since $k_2 \neq 0$ the wave front direction is not conserved and varies as the ray travels through the current. This follows since while the value of k_2 remains constant the values of $k_1$and k_3 vary with time, that is:

$$\frac{\partial k_1}{\partial t} = -k_2 \frac{\partial V_2}{\partial x_1} \qquad \frac{\partial k_2}{\partial t} = 0 \qquad \frac{\partial k_3}{\partial t} = -k_2 \frac{\partial V_2}{\partial x_3}$$

Once again refraction occurs in both the horizontal and the vertical planes:

$$\frac{\partial x_1}{\partial t} = c_o \frac{k_1}{\sqrt{\underline{k}.\underline{k}}} \qquad \frac{\partial x_2}{\partial t} = V_2 + c_o \frac{k_2}{\sqrt{\underline{k}.\underline{k}}} \qquad \frac{\partial x_3}{\partial t} = c_o \frac{k_3}{\sqrt{\underline{k}.\underline{k}}} \ .$$

Example 2: Secondly consider a horizontal current of the form:

$$\underline{V} = (0, V_2(x_1, x_2, x_3), V_3(x_1, x_2, x_3)) \ ,$$

where $(x_1, x_2, x_3) \equiv (depth, latitude, longitude)$. This current is a generalized form of the equations used to describe the anticlockwise vortex through which sound rays were propagated for this numerical experiment. A detailed description of the vortex and its equations are presented in Chapter Five and the sound propagation results are presented in Chapter Six.

If $\underline{V} = (0, V_2(x_1, x_2, x_3), V_3(x_1, x_2, x_3))$

then: $\frac{\partial k_1}{\partial t} = -k_2 \frac{\partial V_2}{\partial x_1} - k_3 \frac{\partial V_3}{\partial x_1}$ $\frac{\partial k_2}{\partial t} = -k_2 \frac{\partial V_2}{\partial x_2} - k_3 \frac{\partial V_3}{\partial x_2}$ $\frac{\partial k_3}{\partial t} = -k_2 \frac{\partial V_2}{\partial x_3} - k_3 \frac{\partial V_3}{\partial x_3}$

and: $\frac{\partial x_1}{\partial t} = c_o \frac{k_1}{\sqrt{\underline{k}.\underline{k}}}$ $\frac{\partial x_2}{\partial t} = V_2 + c_o \frac{k_2}{\sqrt{\underline{k}.\underline{k}}}$ $\frac{\partial x_3}{\partial t} = V_3 + c_o \frac{k_3}{\sqrt{\underline{k}.\underline{k}}}$

Suppose this current is confined in the horizontal and vertical planes so that the initial ray is outside the feature and suppose the initial wavefront direction is $\underline{k} = (0, k_2, 0)$

then: $\frac{\partial k_1}{\partial t} = -k_2 \frac{\partial V_2}{\partial x_1}$ $\frac{\partial k_2}{\partial t} = -k_2 \frac{\partial V_2}{\partial x_2}$ $\frac{\partial k_3}{\partial t} = -k_2 \frac{\partial V_2}{\partial x_3}$

and: $\frac{\partial x_1}{\partial t} = 0$ $\frac{\partial x_2}{\partial t} = V_2 + c_o$ $\frac{\partial x_3}{\partial t} = V_3$

These equations show that once the ray enters the current the wave front direction varies continuously and refraction occurs in the horizontal plane.

Bibliography

[1] Apel J.R. (1987).
Principles of ocean physics.
Academic Press Inc. London. pp634.

[2] Burdic W.S. (1984).
Underwater acoustic systems analysis.
Prentice-Hall Inc. New Jersey. pp445.

[3] Etter P.C. (1991).
Underwater Acoustic Modeling: principles, techniques and applications.
Elsevier Science Publishers Ltd. New York. pp305.

[4] Lighthill J. (1978).
Waves in fluids.
University Press. Cambridge. pp504

[5] Kinsler L.E., Frey A.R., Coppins A.B. and Sanders J.V. (1982).
Fundamentals of Acoustics (Third Edition).
John Wiley & Sons. U.S.A. pp480.

[6] Seto W.W. (1971).

Schaum's outline of theory and problems of acoustics.

Mcgraw-hill publishing company. U.S.A. pp195.

[7] Ross D. (1976).

Mechanics of underwater noise.

Permagon press. U.S.A. pp 375.

[8] Urick R.J. (1982).

Sound Propagation in the Sea.

Peninsula Publishing. California. pp 149.

[9] Weinberg H. (1978).

Application of ray theory to acoustic propagation in horizontally stratified oceans.

Journal of Acoustic Society of America. vol 58. no1. pp97-109.

Chapter 4

THE AGULHAS CURRENT REGION

This thesis is concerned with the modeling of acoustic propagation through the Agulhas Current region. The area of interest, south of Africa, contains the Agulhas Current System. The oceanography of the Agulhas Current System has been examined by many researchers, a comprehensive source book containing a number of papers was compiled by Lutjeharms (1983). The location and features of the Agulhas Current System are described in this chapter, in order to provide the setting for the acoustic modeling which follows. A basic understanding of the real environment is necessary to provide a realistic model environment.

This location is of particular interest to acoustic oceanographers because of the high degree of variability found there. There are two distinct types of variability found within the region: firstly that variability associated with semipermanent features of the Agulhas Current System, for example the Agulhas Current, the

Agulhas Return Current and the Retroflection, while the position of these features does not vary very much in time the features themselves are in continuous motion. The second type of variability found in this region is associated with the prolific mesoscale eddies, not only are these features constantly varying position, they are also in continuous motion, yet they still maintain there definition over a long time scale.

4.1 Geographical Location

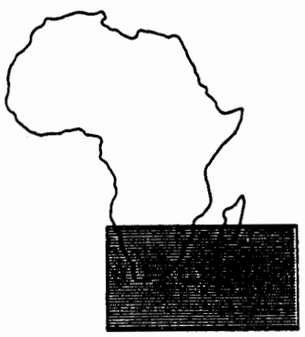

Figure 4.1: Map Showing The Location Of The Agulhas Current Region

The area of interest is the large area south and east of southern Africa (see figure 4.1) which contains the Agulhas Current System, this is a large circulation which can be divided into four main sections (Van Foreest, 1977):

- The Source Region: including part of the Mozambique channel, at about $20°S$;
- The Agulhas Current: which flows in a south westerly direction along the south east coast of Africa;
- The Retroflection Region: which extends to approximately $15°E$, and

- The Return Current: between $40°S$ and $41°S$.

The eastern boundary of the current system defined by Van Foreest (1977), was $45°E$, since to the east of this recycling between the Agulhas Current and the Agulhas Return current seemed to occur.

4.2 The Topography Of The Region

The bottom topography of this region is important, because it has a direct influence on the flow pattern of the Agulhas Current System. A map containing the bottom topography of the region is included in figure 4.2.

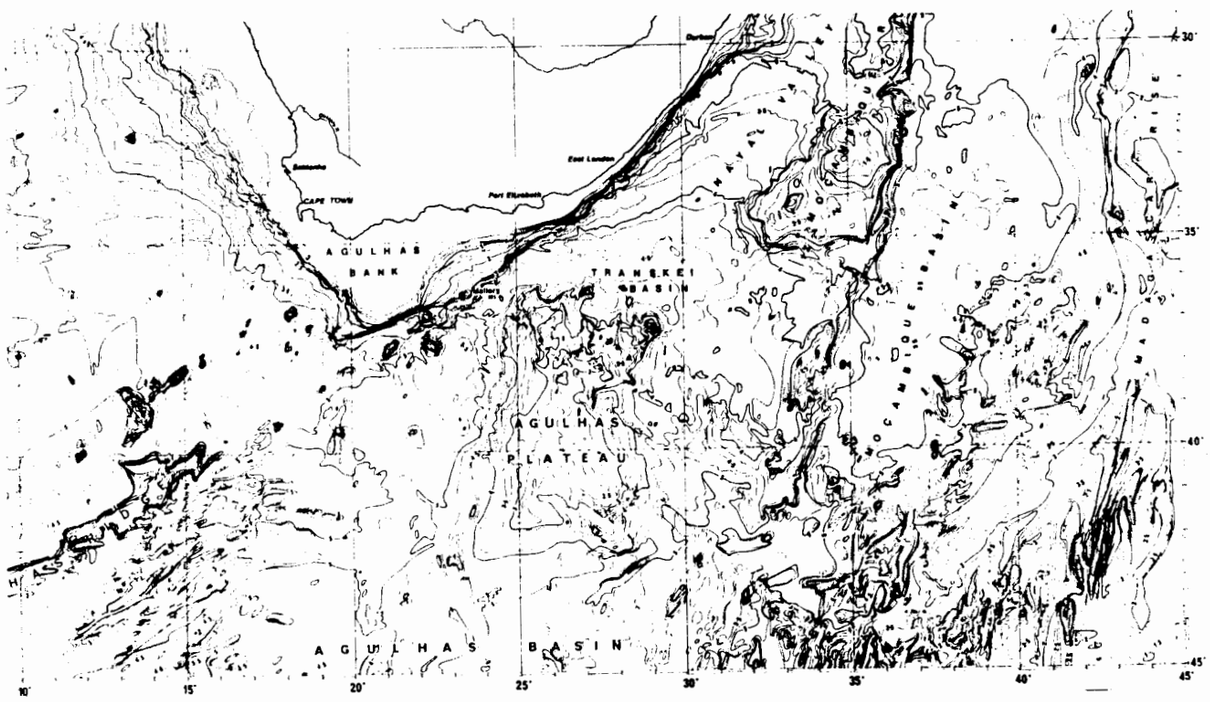

Figure 4.2: Map Showing The Topography Of The Region

One of the most important features of the bottom topography is the narrow, almost shear edged continental shelf along the east coast of southern Africa. South of Port Elizabeth the continental shelf widens out to form the Agulhas Bank. Other important topographic features, that directly influence the flow within the Agulhas Current System are the Agulhas Plateau, at $40^{o}S$, and the Mozambique Ridge and Madagascar Rise, which also extend to $40^{o}S$.

4.3 The Course Of The Agulhas Current System

The Agulhas Current System forms part of the South West Indian Ocean Circulation. A schematic diagram demonstrating the course of the Agulhas Current is included, refer to figure 4.3. Water from the South Equatorial Current flowing through the Mozambique Channel and water flowing down the East coast of Madagascar combine together to form the origin of the Agulhas Current, north of Durban.

Between Durban and Port Elizabeth the current reaches its full stature as regards volume flux and velocity (Lutjeharms, 1981). The current is a typical well developed western boundary current flowing close to the shore (Pickard and Emery, 1990). The course of the Agulhas Current is strongly dependent on the bottom topography. The continental shelf is relatively narrow in this region and the shelf slope is steep. The core of the current is deeper than the continental shelf and the current is therefore forced to flow parallel to the coastline on the seaward side of the shelf. As the bottom topography becomes more aligned in an east-west direction south of East London, so the current follows this trend (Darbyshire, 1972).

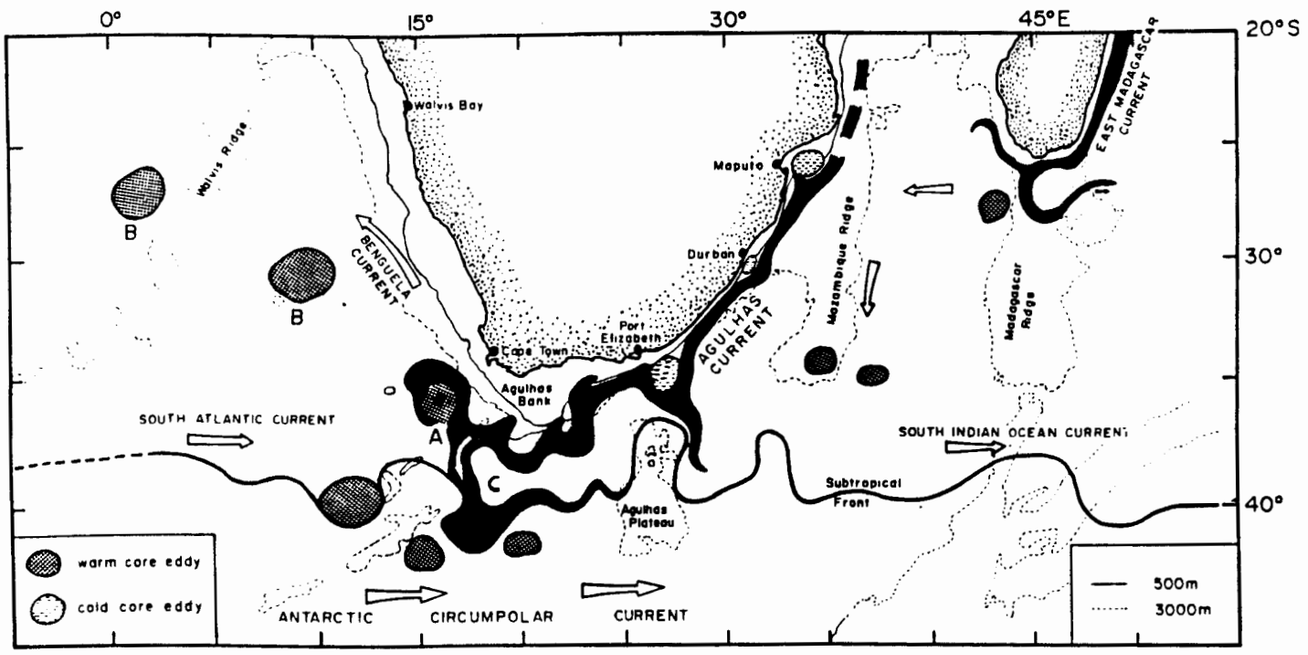

Figure 4.3: A Conceptual Representation Of The Agulhas Current System And Surrounding Mesoscale Features. Important Oceanographic Features Are Labeled As: A - An Agulhas Ring Shed From The Agulhas Retroflection; B - Agulhas Eddies Moving Into The South East Atlantic Ocean; and C - The Agulhas Current Retroflection Loop (adapted from Van Ballegooyen et al 1991)

Further downstream from Port Elizabeth the continental shelf widens, into the Agulhas Bank, this causes the current to diverge away from the coast. As the current moves away from the Agulhas Bank, south of Africa, it undergoes an abrupt turn about - this is known as the retroflection region.

The retroflection has been observed by several authors (Grundlingh, 1978; Lutjeharms, 1981) and is particularly apparent in infra-red satellite images, which are becoming readily available to oceanographers as an observation tool. The Agulhas Retroflection does not follow any consistent path, it is a semi-permanent feature that exhibits considerable spatial variability and does not have a fixed position, typically it has a longitude of between 13^o and 22^oE . The region of the Retroflection is recognized as one of the most highly variable regions of the world oceans.

The area of the retroflection is one of extreme current variability and flux. In this region interaction takes place between the large scale currents of both the Atlantic and Indian oceans, as well as the West Wind Drift which flows from west to east in the Southern Ocean. The result is a confined area of relatively high dynamic variability. A number of investigations have been devoted to the a detailed description and explanation of the local mesoscale features, which are a direct result of this variability. Section 4.5 includes a discussion on mesoscale eddies within this region.

Grundlingh (1978) describes the drift pattern of a buoy released into the southern Agulhas Current. The buoy traveled in a south westerly direction, with the Agulhas Current, until it reached the Retroflection area south of Cape Town. Here the current underwent a severe deflection of about 135^o . Having twisted through the retroflection the current flows eastwards, as the Agulhas Return Current, forming the northern border with the Antarctic Circumpolar Current. According to Grundlingh (1978) the Return Current is practically zonal, with an

axis at approximately $40^{o}S$.

However as the current flows towards the east a number of topographically induced meanders occur. Specifically, as the current flows towards the east it encounters a large obstruction in the form of the Agulhas plateau, which rises to within $1500\ m$ of the sea surface. The effect of a sudden decrease in depth on an relatively deep eastward flowing current is to deflect the path of the current towards the equator. As the current returns to deeper water so it is deflected back to its previous latitude. In this way a planetary wave is set up (Grundlingh and Lutjeharms, 1978). So the Return Current describes a series of meanders as it coincides with important topographic features - such as the Agulhas plateau, the Mozambique ridge and the Madagascar rise.

It is interesting to observe the rapid decrease in velocity of the Return Current as it flows towards the east (Grundlingh, 1978). The drift speed of a satellite tracked buoy decreased from $1.30\ m.s^{-1}$ at $15 - 25^{o}E$ to a much lower value of $0.40\ m.s^{-1}$ at $55 - 63^{o}E$.

Satellite photographs, mentioned previously, are becoming more available to oceanographers and are being used more and more to plot the course of ocean currents. The following figure (figure 4.4) is a satellite photograph which clearly demonstrates the usefulness of these images when observing the course of the Agulhas Current.

The NOAA AVHRR satellite image, in figure 4.4, was taken using an infrared sensor on 24 March 1992. The image data was received and processed at

the Satellite Application Center of the CSIR. The image was calibrated to represent the sea surface temperature at that time, warm water has been depicted dark and cool waters light. The white areas over the southern areas of the image and over the subcontinent are indicative of cloud cover.

The warm (dark) Agulhas Current can be clearly seen as it traveled down the east coast of Southern Africa, diverging away from the subcontinent downstream of Port Elizabeth. The retroflection south west of Cape Town is clearly visible in the satellite image, and a ring, warmer than the surrounding waters, which would have budded off the Agulhas Current System can be seen to the north west of the retroflection. The Agulhas Return Current can be seen just north of the cold waters of the Antarctic Circumpolar Current. In the region of the Agulhas Plateau the topographically induced meander, mentioned previously is visible, as well as a distinct warm core eddy within the cooler waters that have intruded from the south onto the Agulhas Plateau.

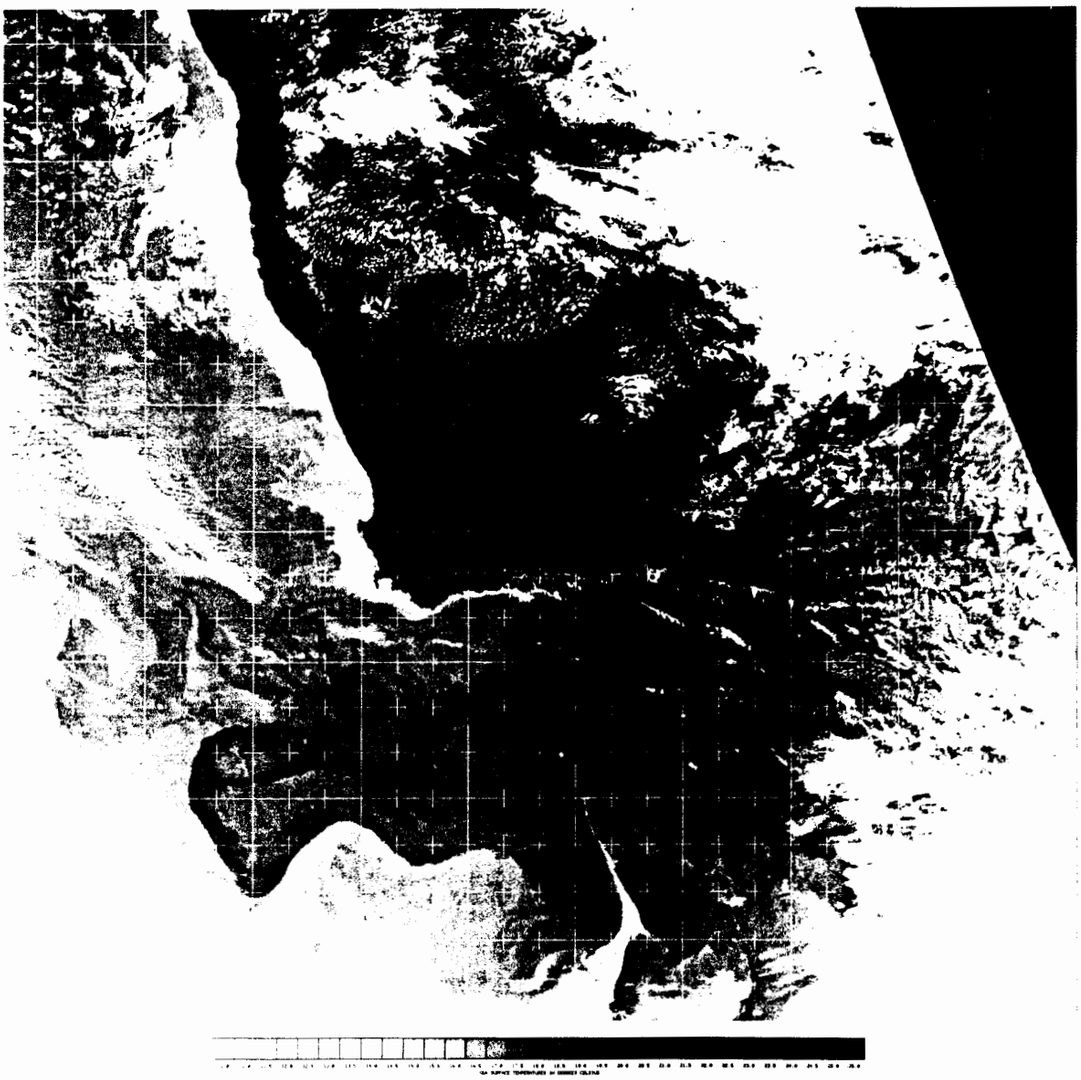

Figure 4.4: Satellite Photograph Demonstrating The Course Of The Agulhas Current

4.4 Characteristics And Structure Of The Agulhas Current.

The Agulhas current is a typical warm core western boundary current bringing warm water from the tropics to the south east coast of Africa. It forms part of the Western Boundary current system of the south east indian ocean and is therefore dynamically similar to the Gulf stream and Kurishio system. The Agulhas current is characterized by a warm fast flowing central filament, where speeds up to $2.5\ m.s^{-1}$ have been recorded, with the current decreasing gradually as one travels away from the central filament (Grundlingh, 1977). The current is typically narrow, with a width of about $100\ km$ and has a transport reported to average $50\ Sv$ and rise to as much as $80\ Sv$ (Pickard and Emery, 1990).

The current consists of three distinct regions (Pearce, 1977):

1. The Western Boundary Of The Current: the inshore, cyclonic shear region, with relatively high thermal and velocity gradients separates the current from from cooler water on the continental shelf.

2. The Current Core: a warm, high speed, $> 1\ m.s^{-1}$ filament with a peak speed of $2.5\ m.s^{-1}$ (Grundlingh, 1977). The highest surface temperatures are typically associated with peak current speeds.

3. The Eastern Boundary Of The Current: offshore, anticyclonic region, the temperature and velocity are much lower than in cyclonic shear region.

A case study is provided here in order to demonstrate the main features of the current (see figure 4.5). A cross-section of CTD (Conductivity, Temperature,

Depth) data from the KNORR 104-5 Agulhas Retroflection Cruise was used, taken from Camp et al (1986). The figure includes temperature, salinity and sound speed profiles, as well as a map showing the corresponding cruise track. The cross-section, from stations [48] - [58], began at a latitude of about $35^{o}S$ and extended to a latitude of $42^{o}S$, it includes a cross section through both the Agulhas and Return Currents. At this stage in the current circulation the current has started to move away from the sub-continent. The core of the Agulhas current, in this example, is at $37^{o}S$ and the Return current core at $39^{o}S$.

The depths of the profiles extended to $1500\ m$. The temperature and salinity were shown to increase in the region of both of the currents, resulting in a corresponding increase of sound speed in these regions as well. In the figure the downward forcing of the sound speed minimum, due to the overlying warm water, is clearly evident. The sound channel has deepened from $750\ m$ to approximately $1500\ m$ for the Agulhas Current, while the sound speed in the current core has increased by approximately $10\ m.s^{-1}$. In both the Agulhas and the Return currents the temperature, salinity and sound speed contours were steeper and closer together on their inshore edges than on their offshore edges, this indicates the shear region which was discussed previously. The depth and intensity of the parameter gradients are not as pronounced in the Return Current as they are in the Agulhas Current itself.

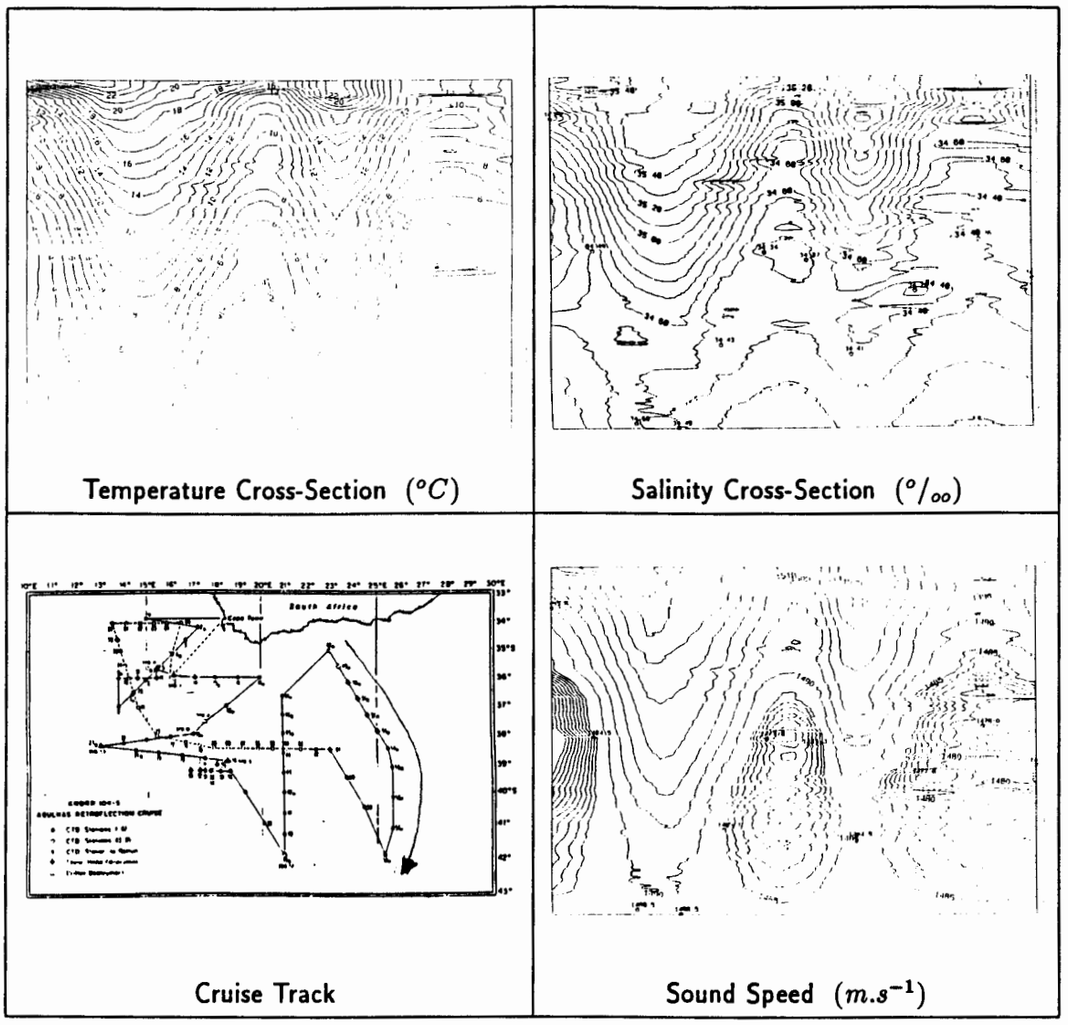

Figure 4.5: Cross-Section Through The Agulhas And Return Currents, 0 – 1500 m Depth (Camp et al, 1986)

4.5 Mesoscale Features Within The Region

The region of the Agulhas Current system has been observed to be rich in mesoscale features. Eddies and other mesoscale disturbances to the average flow of the current system have been observed in all areas of the region, they have been tracked by buoys, observed in hydrographic sections and traced using satellite imagery. They have also been found to be the main disturbance to the general flow in the south west Indian Ocean. Grundlingh M.L. (1983) provides an essay on mesoscale eddies within the Agulhas Current system, and is used as a reference throughout this section.

Eddies are important to ocean dynamics for a number of reasons. Apart from influencing the behavior of ocean currents they carry vast amounts of heat, which may influence local weather and climate. Also eddies are responsible for the transport of large amounts of organisms from one ocean area to another and thus dispersing biota.

Eddies in this region are formed by a number of processes and for this reason there are no 'typical' features but rather a variety of dynamic mesoscale features, which occur throughout the course of the Agulhas Circulation. These eddies can be cold cyclonic or warm anticyclonic features, with diameters of up to $200\ km$ and extending to $2500\ m$ in depth.

Upstream of Port Elizabeth the position of the Agulhas Current is very stable, demonstrating little meandering from side to side. Its inshore front is sharp and except for small shear eddy features usually stable. These small eddies are

formed by a process of vortex shedding and are mostly confined to the continental shelf. These eddies have a diameter of between 20 and 30 km wide, and surface velocities of up to 1 $m.s^{-1}$. South of Port Elizabeth where the continental shelf widens and the current moves away from the coast shear eddies are formed, due to the friction between the fast flowing current and the almost stagnant water on the continental shelf.

Periodically, as the current travels through the highly variable retroflection region, the retroflection becomes occluded and large warm core rings are shed from the western termination of the retroflection region, from there they drift into the South Atlantic Ocean. These rings quickly lose their surface temperature expression, but they retain their deep thermal and acoustic characteristics as they move into the South Atlantic Ocean (Krige and Brundrit, in press). A number of eddies formed in this way have been observed and can now be tracked using satellite imagery. Grundlingh (1983) discusses a characteristic eddy in this region, centered at $(40^{o}S,\ 15^{o}E)$, with a diameter of between 150 and 200 km and extending to a depth greater than 2000 m . The surface velocities of eddies such as these is in general greater than 1 $m.s^{-1}$.

As the current travels away from the retroflection region, as the approximately zonal Agulhas Return Current, it encounters a barrier in the form of the Agulhas Plateau. As the current meets the plateau it experiences a strong northward deflection, when it reaches deeper water north of the plateau it is deflected back to its original latitude, of $40^{o}S$, on the eastern side of the plateau. Similar large topographically induced meanders occur at the Mozambique Ridge (and further east at the Madagascar Rise). Intense shear forces exist between the

north and southward flowing meanders of the Return current, this results in the formation of a number of highly variable eddies within this region. The northward intrusion of cold water as a consequence of the topographically induced eddies, results in nutrient rich cold waters from south of the subtropical convergence to be introduced into this area.

In summary, there are three main types of mesoscale feature within the Agulhas Current region: shear edge eddies on the landward side of the Agulhas Current, those which are the result of large meanders becoming occluded in the retroflection region and those which are topographically induced along the subtropical convergence.

A similar case study, to that in the previous section, section 4.4 is provided here, this time demonstrating the characteristics of a mesoscale feature within the retroflection region (refer to figure 4.6). This figure includes the temperature, salinity and sound speed profiles as well as a map showing the cruise track through the feature. Comparable changes to the sound speed minimum beneath the Agulhas Current can be seen.

The feature had a diameter just slightly larger than one degree of latitude (approximately 111 km), centered at about $(38^{o}S; 15^{o}E)$. The profiles extend to 1500 m , clearly the feature extended to deeper than this. The surface temperature, of approximately $18^{o}C$ is lower than that in the Agulhas current case study, but it is clearly warmer than the surrounding waters. This feature is symmetric and as in the case of the warm currents the sound speed minimum is forced downwards by a substantial amount.

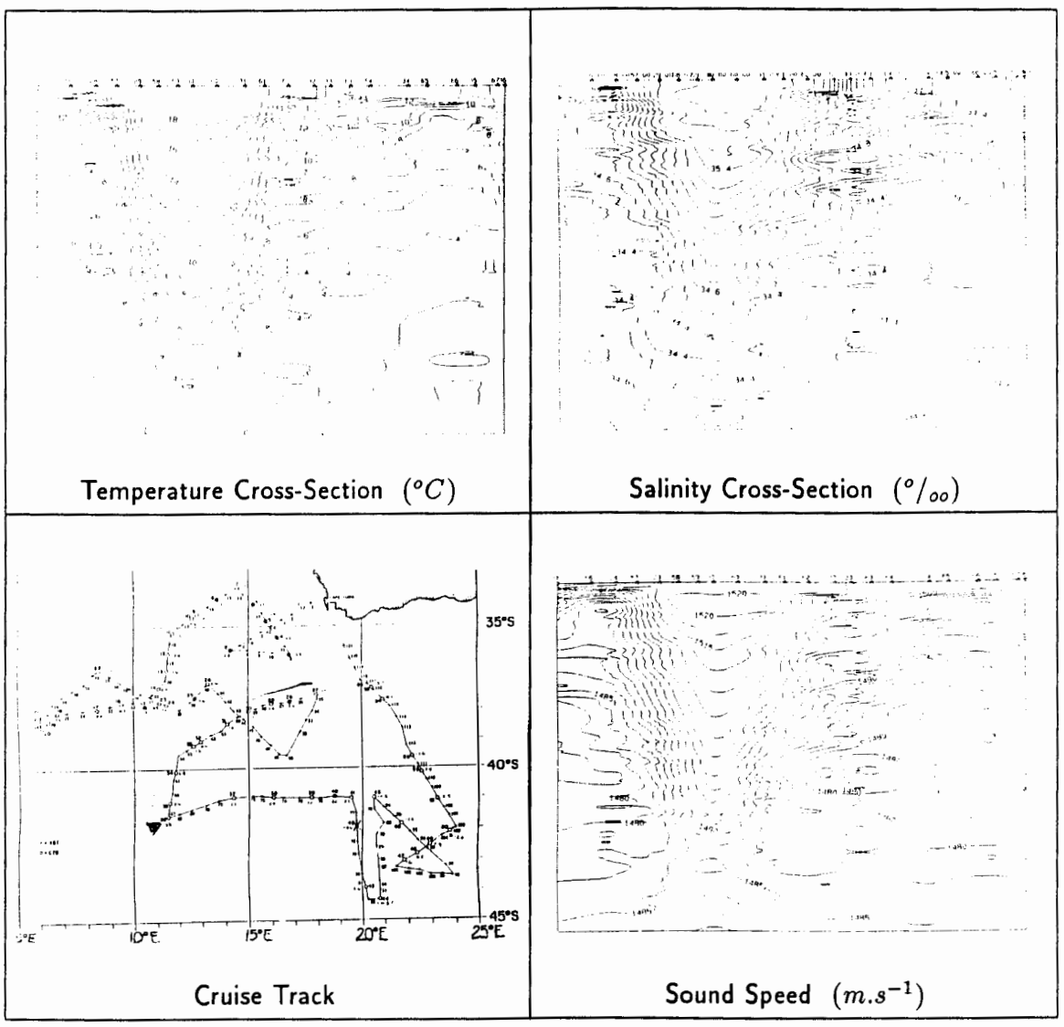

Figure 4.6: Cross-Section Through A Mesoscale Feature In The Retroflection Region, $0 - 1500\ m$ Depth (Valentine et al, 1988)

Bibliography

[1] Camp D.B., Haines W.E., Huber B.A., Rennie S.E. and Gordon A.L. (1986)
The Agulhas Retroflection Cruise Hydrographic (CTD) Data Report.
Lamont-Doherty Geological Observatory Technical Report. LDGO-86-1, pp392.

[2] Darbyshire J. (1972).
The effect of bottom topography on the Agulhas Current.
Reviews of Pure and Applied Geophysics. 101. ix. pp208-220.

[3] Grundlingh M.L. (1977).
Drift Observations from Nimbus VI satellite tracked buoys in the south-western Indian Ocean.
Deep Sea Research. 24(10). pp903-913.

[4] Grundlingh M.L. (1978).
Drift of a satellite-tracked buoy in the southern Agulhas Current and Agulhas Return Current.
Deep Sea Research. 25(12). pp1209-1224.

[5] Grundlingh M.L. (1983).
Eddies in the Southern Ocean and Agulhas Current.

In Robinson A.R.
Eddies in Marine science
Springer-Verlag. Germany. pp609.

[6] Grundlingh M.L. and Lutjeharms J.R.E (1978).
Large Scale Flow Patterns Of The Agulhas Current System.
South African Journal of Science, vol 75, June, pp269-270.

[7] Krige L. and Brundrit G.B. (in press).
Heard Island signals through the Agulhas Retroflection Region.
Journal of the Acoustical Society of America, Special Edition.

[8] Lutjeharms J.R.E. (1981).
Features of the Southern Agulhas Current Circulation from satellite remote sensing.
South African Journal of Science. 77(May). pp231-236.

[9] Lutjeharms J.R.E. (1983).
The Agulhas Current Source Book.
Stellenbosch. South Africa.

[10] Pearce A.F. (1977).
Some features of the upper 500m of the Agulhas Current.
Journal of Marine Research. 35(4). pp731-753.

[11] Pickard G.L. and Emery W.J. (1990).
Descriptive Physical Oceanography: an Introduction.
Permagon Press. England. pp320.

[12] Valentine H.R., Duncombe Rae C.M., Van Ballegooyen R.C. and Lutjeharms J.R.E. (1988).
The Subtropical Convergence and Agulhas Retroflection Cruise (SCARC) Data Report.
CSIR Report T/SEA8804, pp258.

[13] Van Ballegooyen R.C., Valentine H.R. and Lutjeharms J.R.E. (1991).
Modeling the Agulhas Current.
South African Journal of Science. 87(Nov/Dec). pp569-571

[14] Van Foreest (1977).
The Agulhas Current System Above the Intermediate Level.
MSc Thesis. U.C.T. pp116

Chapter 5

SIMULATED OCEAN ENVIRONMENTS

The purpose of this chapter is to describe a number of model environments which were used to simulate aspects of the real ocean environment. A variety of environments are introduced in order to consider the effects different oceanic features have on sound propagating through them. *HARPO* - 'a Hamiltonian Acoustic Ray tracing Program for the Ocean' (Georges, Jones and Lawrence, 1990; Jones, Riley and Georges, 1986)and its associated environmental submodels were used to define environments specific to the Agulhas Current region.

A detailed description of each submodel is included in the last section of this chapter. The submodel equations were taken directly from the *HARPO* manual. The model parameters are shown within the text in order to describe the features within the model environments. The model equations corresponding to the input parameters are included into the last section of this chapter for com-

pleteness and the reading of the last section is not required for an understanding of the numerical experiments or results, which are described in Chapter Six.

5.1 The Location Of The Experiment

An ideal position for an acoustic receiver is one fixed within the sound channel within the deep ocean. Another important factor is that the station be close to the coast so that the amount of cable required to reach the shore is a minimum in order to facilitate easy monitoring of the station. East London off the southern coast of South Africa, where the continental shelf is narrow, was chosen as the receiver site for these experiments because it satisfies the above 'source-receiver site' conditions.

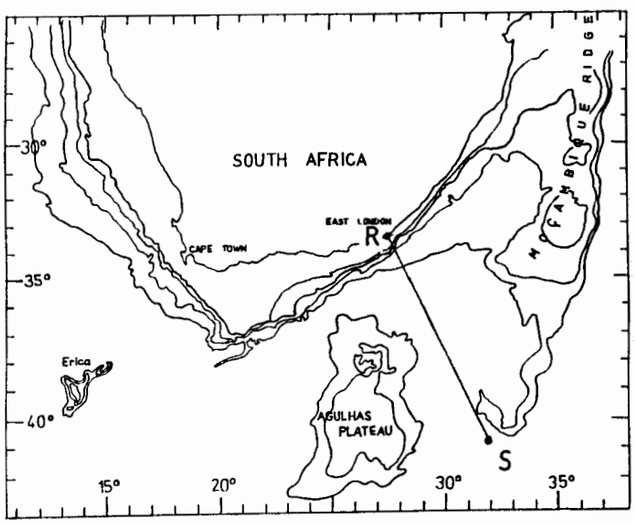

Figure 5.1: Map Showing The Area Of Interest, Including The Source (S) And Receiver Site (R) At East London. The horizontal distance between source and receiver is approximately 894.91 km

In this experiment a ray traveling perpendicularly towards the coast is considered ideal since there can be no intrusion of bottom topography into the sound channel until the ray reaches the continental shelf, where the receiver is positioned. The map shown in figure 5.1 shows the position of the source (S) offshore and the receiver (R) at the coast at East London.

A description of the coordinate system used for this experiment is described here (see table 5.1). The conventional positional frame of reference for an experiment of this nature is: $[latitude, longitude, depth]$, however since the coastline is slightly oblique to this co-ordinate system at East London the frame of reference was adapted to a more realistic one: $[coastline, perpendicular\ to\ the\ coastline, depth]$.

Sound rays travel along the shortest path available to them, and so a ray travels along the great circle path between source and receiver. When a great circle path coincides with a line of longitude, the great circle path is a straight line in the model domain. Small deviations in the ray path due to perturbations in the ocean environment are easier to interpret if they are deviations from a straight line, rather than the arc of a circle. For this reason the co-ordinate system was transformed again, so that it appeared as if the ray was traveling along a line of longitude.

The transformation was this: the ' $coastline - axis$ ' was reinterpreted as a line of latitude, and the ' $perpendicular\ to\ the\ coast - axis$ ' as the twenty eight degree east line of longitude, and the ' $depth - axis$ ' remained the ' $depth - axis$ '.

Coordinate System	Representation
Conventional:	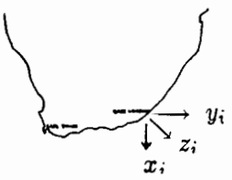
[latitude, longitude, depth] ⇓ $[x_i,\ y_i,\ z_i]$	
Environmental:	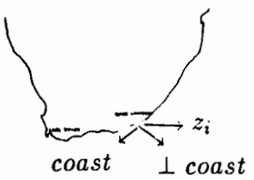
[coastline, ⊥ coastline, depth] ⇓ [coast, ⊥ coast, z_i]	
Used: Profile Taken ⊥ To The Coast:	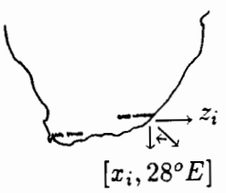
[latitude, 28^oE , depth] ⇓ $[x_i,\ 28^oE,\ z_i]$	

Table 5.1: The Coordinate System Used

From now on the meridional ray path used in the experiments is understood as a ray traveling perpendicular to the coast. This coordinate system is useful not only for easy interpretation of the results but it also facilitated the inputting of data into the model, for example the Agulhas Current was modeled as a zonal current flowing parallel to the coastline.

5.2 Model Plan And Description

The $\mathcal{HARPO}$ model was described in Chapter Two as having two distinct sections: the Hamiltonian ray tracing section and the environmental models which define the region through which sound rays travel. When setting up any model environment, using $\mathcal{HARPO}$, a number of submodels have to be used to describe aspects of the environment, they are as follows:

- a dispersion relation routine
- a background (and perturbation) current model
- a background (and perturbation) sound speed model
- a background (and perturbation) bottom model
- a background (and perturbation) surface model
- an absorption (loss) (and perturbation) model
- a receiver surface model

Initially a very simple ocean environment, rather than a physically realistic one, was set up in order to determine the fundamental features of acoustic propagation through the ocean. Thereafter this simple model environment was used as the background environment and a number of oceanic features were superimposed onto it. This allowed for deviations from the ray traveling through the simple environment to be measured. Throughout the numerical experiment, while different model environments were used, the ray parameters remained

constant, the purpose of this was to make it easier to determine variations due to the anomalies included into the model environment.

5.3 Modeling The Ray

The source was positioned at $(41S, 28E)$, where twenty eight degrees east was chosen because it is the longitude of East London, and forty-one degrees south so that the Agulhas and Agulhas Return Currents can both be included into the model.

The transmitter height was positioned at a depth of $1000\ m$ below sea level. This is because the sound speed minimum specified in the sound speed model was also positioned at this depth. Positioning the source at this depth ensures that the ray travels through the SOFAR channel.

Throughout the experiment the initial elevation angle of the ray was eight degrees, with no stepping in elevation angle. This elevation angle provided a large SOFAR channel, but not so large as to interact with either the ocean surface or the ocean bottom. The acoustic frequency of the ray was four hundred hertz and there was no stepping in frequency. The model was insensitive to any changes in the magnitude of the acoustic frequency, indicating that the choice of frequency was not noteworthy.

Two different rays were used when considering the perturbations included into the model. Firstly one with an azimuth angle of zero degrees, this ray crossed any of the anomalies, described later, orthogonally. The other ray had an az-

imuth angle of three-hundred-and-fifty degrees and crossed the model environment obliquely. The reason for considering two rays was this: a ray intersecting a perturbation orthogonally is not refracted through the perturbation field in the same way that a ray traveling obliquely through the perturbation field is.

5.4 A Horizontally Stratified Ocean

Initially a horizontally stratified ocean was modeled. It contained: no current field; a very simple sound speed profile; a flat bottom; a flat ocean surface and no perturbations.

The acoustic wave dispersion routine used throughout the experiment was $\mathcal{AWCWL}$ - Acoustic With Currents, With Losses. While more efficient dispersion routines are available, for example without ocean currents, the more efficient routines only suited the experiment initially, for this reason it was decided to keep the dispersion relation consistent throughout the experiment.

The background current model chosen for this experiment was $\mathcal{WLINEAR}$ (see pp 97 for details). With this model it is possible to represent a constant current, either radial (upwards), eastward or southward, and allows for a linear gradient in the eastward component. For this experiment all the current model parameters were set to zero in order to define a region containing no current effects. The current perturbation model $\mathcal{NPCURR}$ was used since no current perturbation was required.

$\mathcal{CTANH}$ (see pp 98 for details) was the background sound speed model used

throughout the experiment. In this exercise it represented a horizontally stratified ocean with a sound speed minimum at a depth of 1000 m below the ocean surface. $CTANH$ is a general purpose model that is able to fit tabular sound speed data profiles with linear segments, which are smoothly joined by hyperbolic functions. Rather than going through the data points the final profile smooths around the data points. Figure 5.2 shows the relationship between the sound speed data that was used and the corresponding function derived for the model environment. No sound speed perturbation model was required, because only a horizontally stratified ocean environment (range - independent) was being considered at this stage, so the sound speed perturbation model $NPSPEED$ was used.

The ocean absorption model $SLLOSS$ (see pp 99 for details) was used throughout the experiment even though absorption losses were not considered in this experiment, the reason for this was to keep the model consistent. $SLLOSS$ is an empirical absorption model and depends only on the acoustic frequency. The no absorption perturbation model, $NPABSR$, was used.

The surface model $SHORIZ$ (see pp 100 for details) is able to describe a spherical ocean surface at a specified height above mean sea level. For this experiment the height above mean sea level of the ocean surface was taken to be zero. No ocean surface perturbation was needed for this experiment so $NPSURF$ was used. The background bottom model that was used $GHORIZ$ (see pp 101 for details) is similar to the surface model used. $GHORIZ$ can be used to specify an ocean bottom a constant spherical surface, concentric with the earth, below the mean sea level. In this experiment

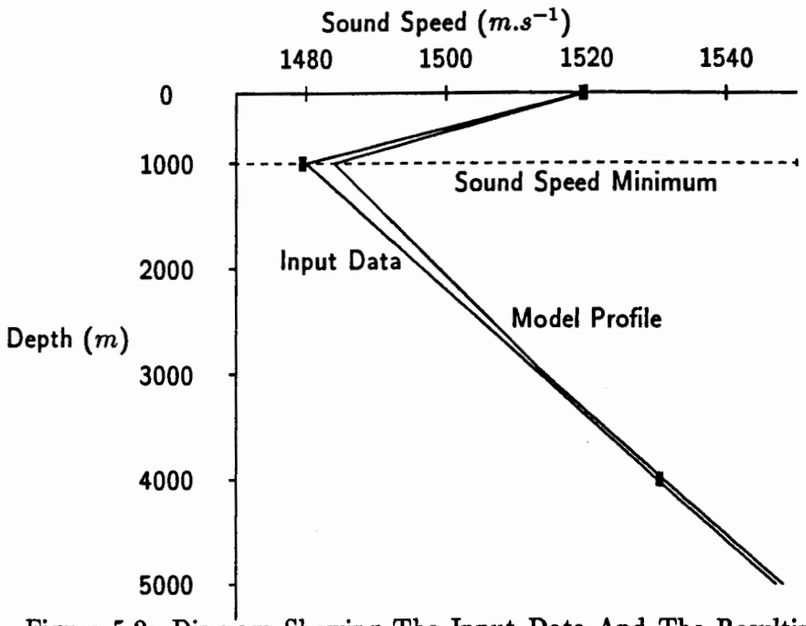

Figure 5.2: Diagram Showing The Input Data And The Resulting Model Profile

the depth of the ocean was chosen to be 5000 m below the mean sea level. No bottom perturbation was required so the bottom perturbation model used was $\mathcal{NPBOTM}$.

$\mathcal{RVERT}$ was the receiver surface model used throughout the experiment. This receiver model, $\mathcal{RVERT}$ (see pp 102 for details), specifies the receiver as a vertical surface a constant distance away from the source. In this case the receiver surface was positioned 8^o from the source at $(41^oS, 28^oE)$, so as to coincide with the receiver positioned at East London, $(33^oS, 28^oE)$.

The combination of models described here produced the horizontally stratified ocean environment, a representation is given in figure 5.3. This model

environment is required as a background model environment for future experimentation. Notice that the horizontally stratified ocean that is described here represents a range independent acoustic model, defined in section 2.2 and discussed in section 3.4.

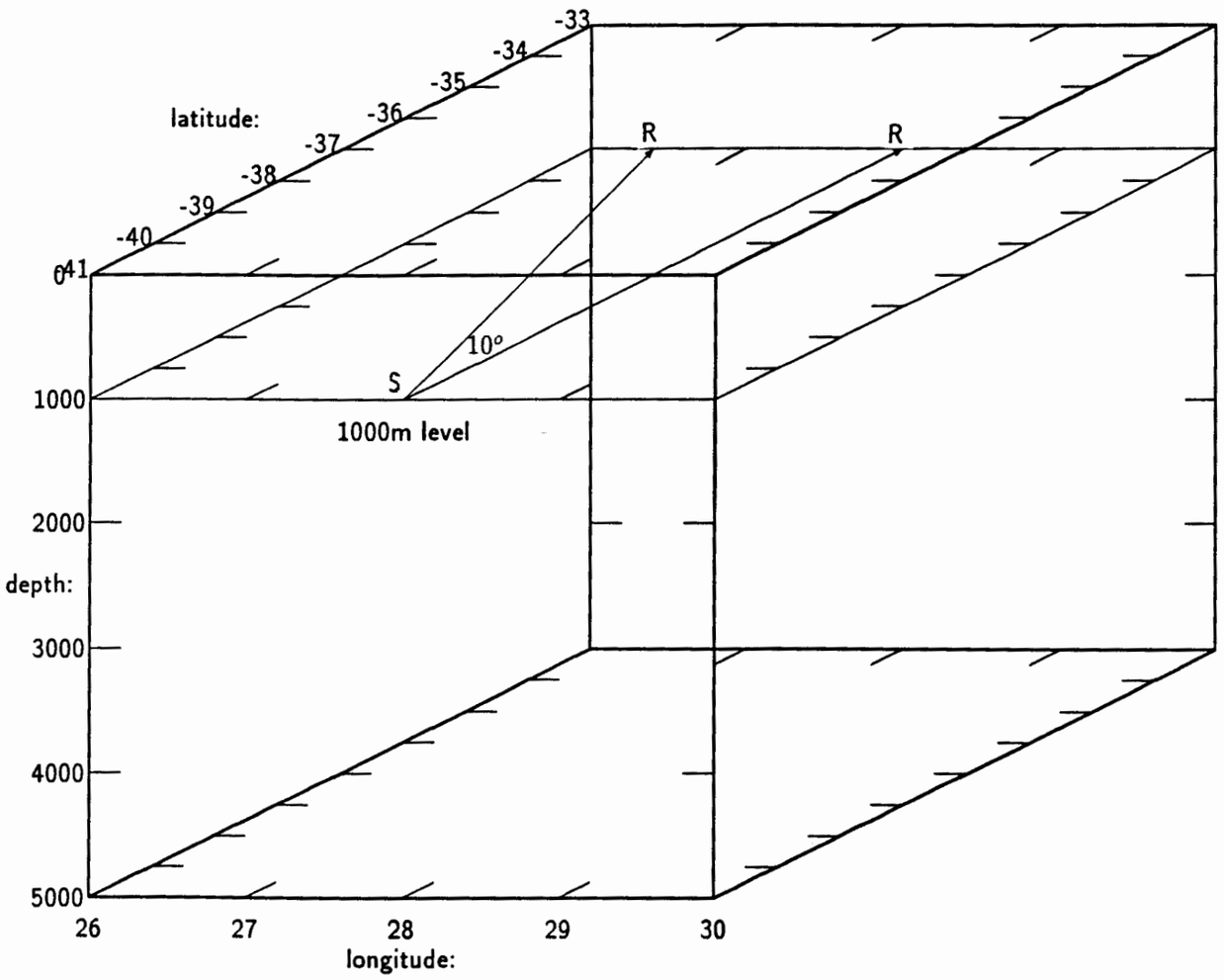

Figure 5.3: Schematic Representation Of The Horizontally Stratified Ocean Environment, Showing The Orthogonal And Oblique Rays

5.5 A Current Feature Environment

The most obvious feature, within the area of interest, to consider in terms of its acoustic properties is the Agulhas Current, which was described in detail in section 4.4. From the description of the Current given in Chapter Four there are two distinct components of the Agulhas Current that have to be considered, these are the temperature and the velocity components. These components were included into the horizontally stratified model, both separately and combined together, in order to determine their effects on sound propagation through them. Figure 5.4 shows a schematic representation of both the velocity and temperature components which were included into the horizontally stratified ocean.

Firstly the velocity structure was included into the horizontally stratified model by replacing the current model $\mathcal{WLINEAR}$ with $\mathcal{WGAUSS}2$ (see pp 103 for details). This model represents a zonal (eastward) current whose intensity decays in all three directions. Setting the gaussian, zonal or meridional width to zero results in no space variation in that direction. A maximum current speed of $-3\ m.s^{-1}$ was chosen, the negative sign represents a westerly current. The current maximum was positioned at $33.5^{o}S$ and $28^{o}E$, also the current maximum was specified at the ocean surface. The zonal width of the current was set to zero, which results in no variation in the east-west direction. Otherwise the meridional width was chosen to be 1^{o} and a gaussian height of $1000\ m$ is chosen.

So the Agulhas Current model velocity structure was described as a surface westerly current flowing at $3\ m.s^{-1}$, positioned at $33.5^{o}S$ with a current

width of 1^o and extending to $1000\ m$ below the sea surface.

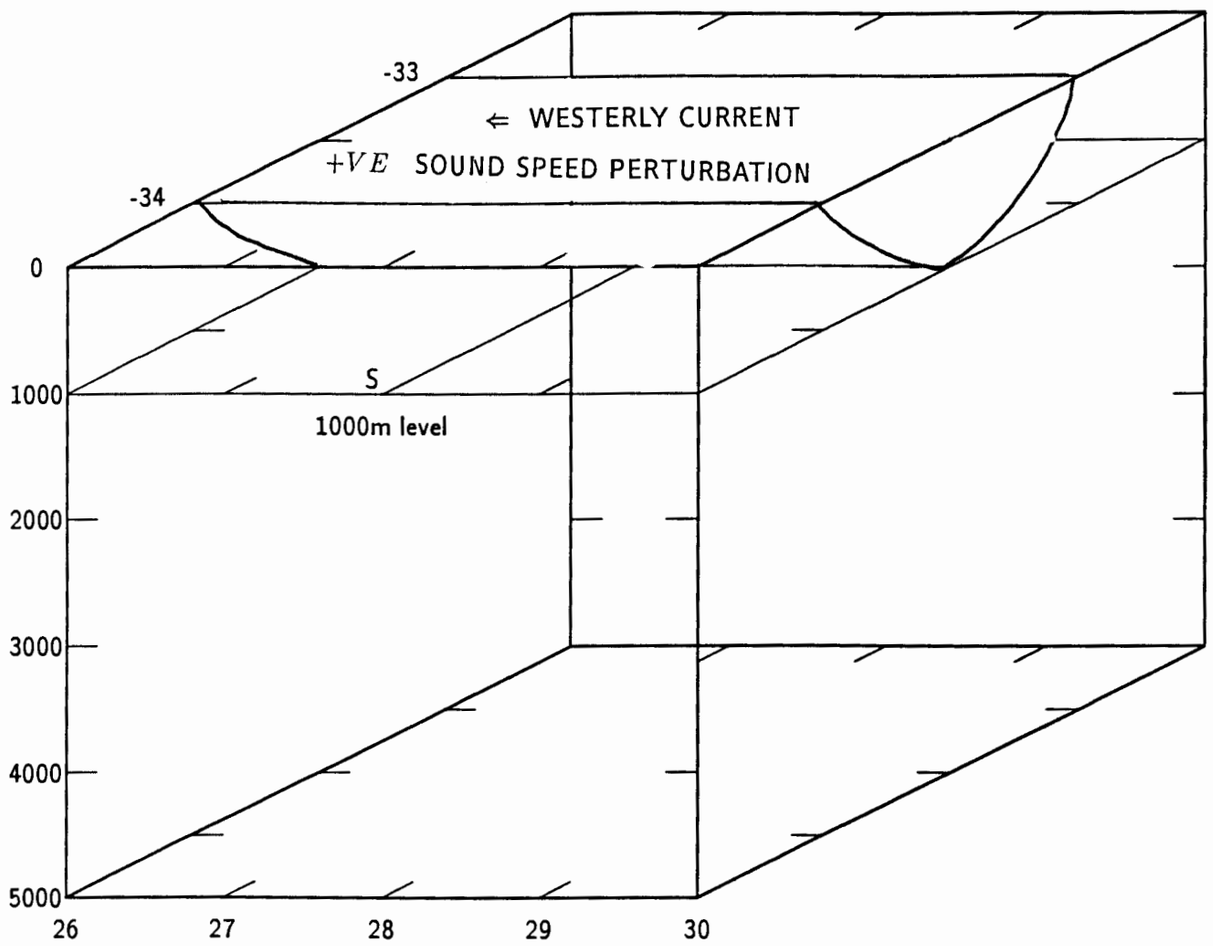

Figure 5.4: Schematic Representation Of The Temperature And Velocity Structure Associated With The Agulhas Current Included Into The Horizontally Stratified Ocean Environment

The temperature structure associated with the Agulhas Current was also included into the horizontally stratified ocean environment. In Chapter Three it

was shown that a change in sound speed indicates, through the equation of state, a variation in the temperature structure. An increase in sound speed is indicative of an increase in temperature, similarly a decrease in sound speed responds to a decrease in temperature. So the warm temperature structure associated with the Agulhas Current was included into the model by using the sound speed perturbation model $\mathcal{CBLOB}4$ (see pp 105 for details).

$\mathcal{CBLOB}4$ describes an increase (or decrease) in sound speed, in up to three localized regions, that decay in a gaussian manner in all three directions. A 2% increase in sound speed was chosen to represent the Agulhas Current sound speed structure, this represents a variation in the sound speed of about $30\ m.s^{-1}$. The sound speed perturbation was positioned so as to coincide with the velocity structure, that is the maximum perturbation was centered on the surface at $33.5^{o}S$ with no zonal variation, the meridional width of the perturbation was chosen to be 1^{o} extending to $1000\ m$ below sea level.

Another consideration in this region is that of the Agulhas Return Current, which was discussed in section 4.3. The velocity and temperature structures were included in the same way as for the Agulhas Current, into the horizontally stratified ocean. The Return Current velocity structure was modeled in the same way that the Agulhas Current velocity structure was, again using $\mathcal{WGAUSS}2$. The Return Current velocity structure was modeled as a surface easterly current, positioned at $40^{o}S$, with no zonal variation, the meridional width of the current was 1^{o} and the current effect extended to $1000\ m$. Similarly the temperature structure was included into the model using $\mathcal{CBLOB}4$, with a 2% perturbation at the surface, at $40^{o}S$, with a meridional width of 1^{o} and

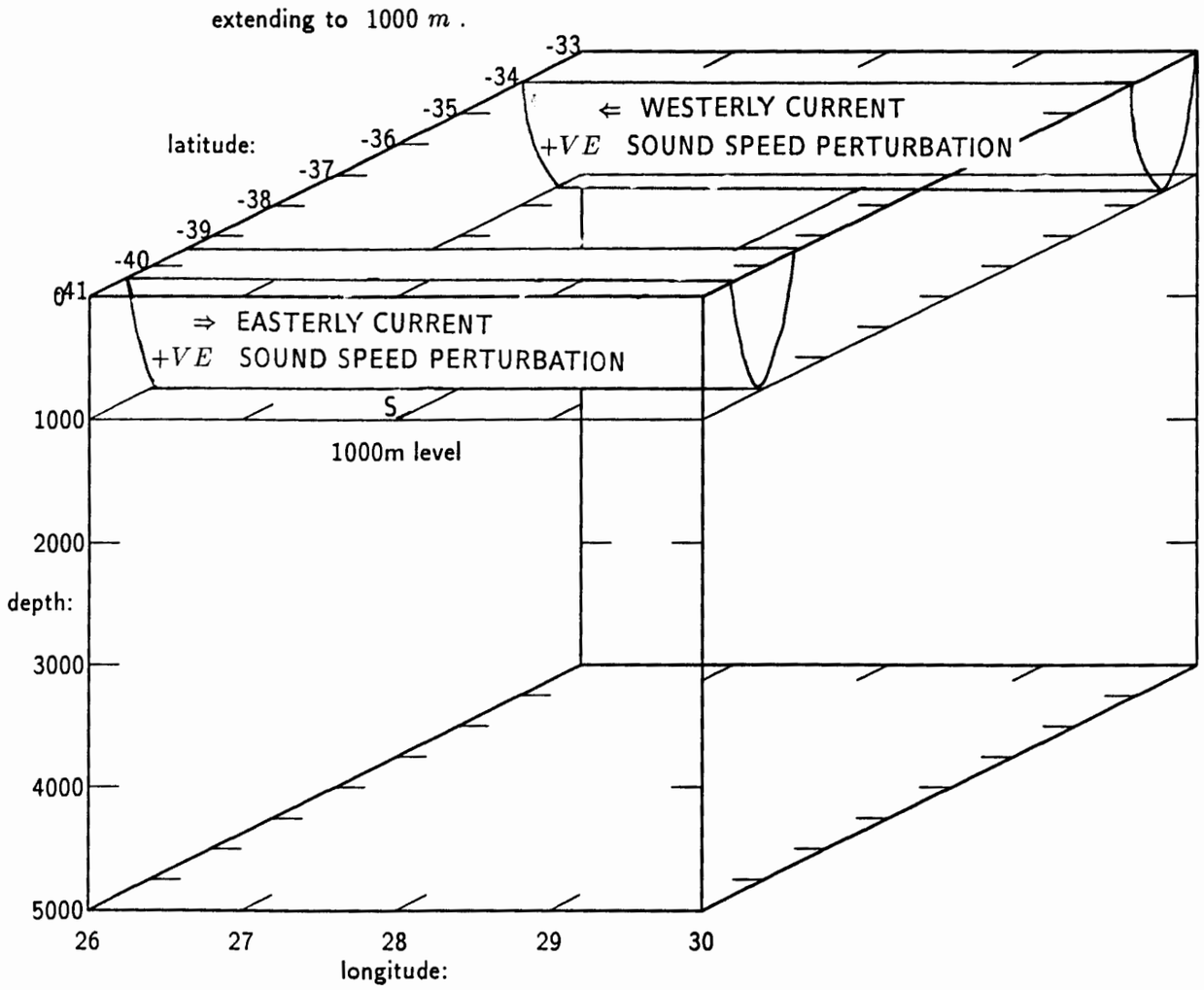

Figure 5.5: Schematic Representation Of The Temperature And Velocity Structure Associated With The Agulhas And Agulhas Return Currents Included Into The Horizontally Stratified Ocean Environment

A limitation of *HARPO* is that only one velocity structure can be included into a model environment at a time. However using *CBLOB4* , it is possible

to include the sound speed structure, the implied temperature structure, associated with both the Agulhas Current and the Agulhas Return Current. Figure 5.5 includes a schematic representation of both the Agulhas and the Agulhas Return Currents, which were included into the horizontally stratified ocean environment.

5.6 An Eddy Feature Environment

Another typical feature of the Agulhas Current region that is considered is that of a mesoscale eddy, features such as these were described in section 4.5. Warm and cold core eddy features have been observed to have very different properties and so results of sound propagating through a warm and a cold core eddy are very different, not only because of the differences in eddy dynamics, but also because of the differences in acoustic propagation properties through warm and cold features. In this experiment a warm core anticyclonic feature was considered, since that corresponds to an eddy which buds off the Agulhas Current, for instance in the retroflection region.

Firstly the temperature structure associated with a warm core eddy was represented by a 2% increase in sound speed, again using the sound speed perturbation model $CBLOB4$. The feature was positioned with the maximum variation at the surface, with the center at $(37^{o}S, 28^{o}E)$. The feature had a radius of 0.5^{o} and extended to a depth of $1000\ m$ below the ocean surface.

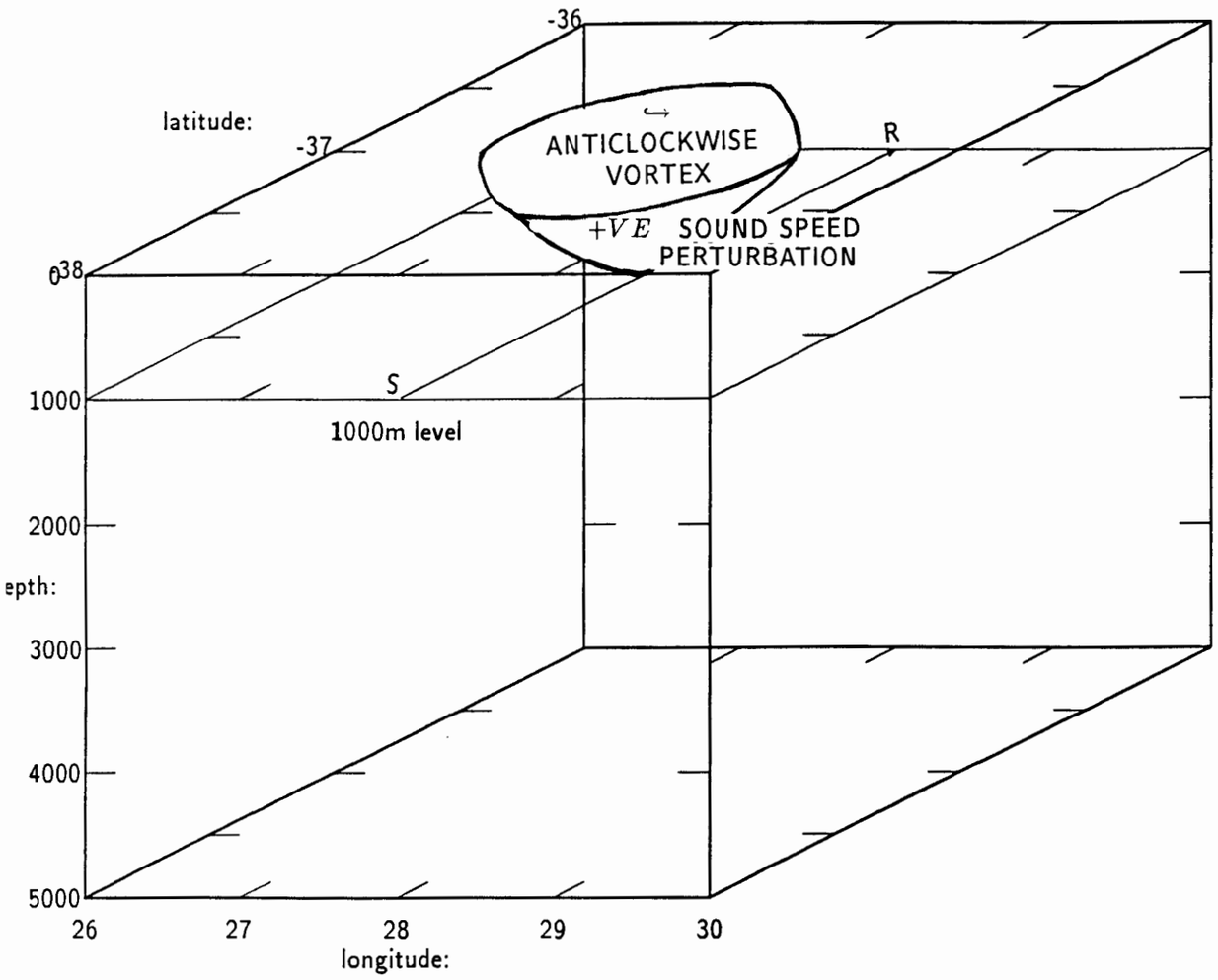

Figure 5.6: Representation Of The Temperature And Velocity Structure Associated With A Warm Core Anticyclonic Eddy

The velocity structure associated with a warm core eddy, which has an anticlockwise rotation in the southern hemisphere was included using the velocity model $\mathcal{VVORTX}3$ (see pp 108 for details). This model describes a rotating current structure with a viscous core and a gaussian intensity profile in the ver-

tical. The axis of the vortex is vertical and was positioned in the same place as the temperature structure, that is centered at $(37°S, 28°E)$. Now the vortex rotates anticlockwise looking down and the maximum tangential current is chosen to be $1.5\ m.s^{-1}$ at the surface. The radius of the vortex, where the vortex core reaches its maximum velocity, was taken to be $0.5°$. The vortex core, within the radius, is essentially a solid rotating fluid, while outside the vortex core decreases as the inverse radius. The vortex extends to $1000\ m$ in depth below the mean sea level. Figure 5.6 shows a schematic representation of a warm core eddy, which was included into the horizontally stratified ocean environment.

5.7 Models Used

In this section the details of each of the environmental submodels used is given. The equations for each submodel are given, they were taken directly from the *HARPO* manual. Following the model equations the input variables that were used for this demonstration and the resulting model equations are provided. Table 5.2 includes a list of background and perturbation models used to construct the model environments. Table 5.3 contains a list of the submodels used to construct each of the model environments, as well as the relevant page number for each of the submodels.

	Background Models	Perturbation Models
Current Model	*WLINEAR* ; *WGAUSS2*; *VVORTX3*	*NPCURR*
Sound Speed Model	*CTANH*	*NPSPEED* ; *CBLOB4*
Surface Model	*SHORIZ*	*NPSURF*
Bottom Model	*GHORIZ*	*NPBOTM*
Absorption (loss) Model	*SLLOSS*	*NPABSR*
Receiver Surface Model	*RVERT*	

Table 5.2: Models Used In This Experiment

	Relevant Page Number	Horizontally Stratified Environment	Zonal Current And Temperature Structure	Warm Core Anticlockwise Vortex
WLINEAR	pp 97	√		
WGAUSS2	pp 103		√	
VVORTX3	pp 108			√
NPCURR		√	√	√
CTANH	pp 98	√	√	√
NPSPEED		√		
CBLOB4	pp 105		√	√
SHORIZ	pp 100	√	√	√
NPSURF		√	√	√
GHORIZ	pp 101	√	√	√
NPBOTM		√	√	√
SLOSS	pp 99	√	√	√
NPABSR		√	√	√
RVERT	pp 102	√	√	√

Table 5.3: Models Used For Each Environment

Current Velocity Model $\mathcal{WLINEAR}$:

Specifies a constant radial (upward), eastward and southward current, allowing a linear height gradient of the eastward component.

$$
\begin{aligned}
u_\theta &= U_{\theta o} \\
u_\phi &= U_{\phi o} + \frac{\partial u_\phi}{\partial z} \cdot z \\
u_r &= U_{ro}
\end{aligned}
$$

where: $z = r - r_e$

r_e = earth radius

r = is the radial coordinate of the ray point

input: 'LINEAR CURRENT SET TO ZERO FOR NO CURRENT FIELD'

the constant upward current, $U_{ro} = 0.\ km.s^{-1}$

the constant southward current, $U_{\theta o} = 0.\ km.s^{-1}$

the ground value of the eastward current, $U_{\phi o} = 0.\ km.s^{-1}$

the height gradient of u_ϕ, $\frac{\partial u_\phi}{\partial z} = 0.\ km.s^{-1}.km^{-1}$

giving:

$$
\begin{aligned}
u_\theta &= 0. \\
u_\phi &= 0. \\
u_r &= 0.
\end{aligned}
$$

Sound Speed Model $\mathcal{CTANH}$:

This model represents the sound speed profile by a sequence of linear segments that are smoothly joined by hyperbolic functions.

$$C = C_o + \frac{b_1}{2}(z - z_o) + \sum_{i=1}^{n} \delta_i \left(\frac{b_{i+1} - b_i}{2}\right) \ln \left\{ \frac{cosh\left(\frac{z - z_i}{\delta_i}\right)}{cosh\left(\frac{z_i - z_o}{\delta_i}\right)} \right\} + \frac{b_{n+1}}{2}(z - z_o)$$

$$b_i = \frac{(C_i - C_{i-1})}{(z_i - z_{i-1})}$$

where: z = $r - r_e$

r_e = earth radius

r = is the radial coordinate of the ray point

δ_i = the half thickness of a region centered at approximately z_i km , in which $\frac{\partial C}{\partial z}$ changes from b_i to b_{i+1}

Start by drawing a profile with linear segments, get C_i and z_i from the corners, select δ_i to round the corners. The final profile will not go through (C_i, z_i) .

input: 'TYPICAL SOUND SPEED PROFILE, MINIMUM AT 1000M'

n = 'number of points in the profile -2 ' = $n = 1$.

the profile:	i	z_i (m)	C_i $(m.s^{-1})$	δ_i (m)
	0	0.0	1520.	0.0
	1	$-1000.$	1480.	$-250.$
	2	$-4000.$	1531.	0.0

giving: $b_1 = 0.04$

$b_2 = -0.017$

$$C(z) = C_o + \frac{b_1}{2}(z - z_o) + \delta_1 \left(\frac{b_2 - b_1}{2}\right) \ln \left\{ \frac{cosh\left(\frac{z - z_1}{\delta_1}\right)}{cosh\left(\frac{z_1 - z_o}{\delta_1}\right)} \right\} + \frac{b_2}{2}(z - z_o)$$

$$C(z) \simeq 1496.436284 + 0.0115(z) + 7.125[\ln\{\cosh(-0.004z - 4.)\}]$$

Ocean Absorption Model $\mathcal{SLLOSS}$:

This absorption model depends only on the acoustic wave frequency $\omega\ (rad.s^{-1})$ according to the formula:

$$\alpha = a\frac{\omega^2}{\omega_1^2} + b\frac{\omega^2}{\omega_2^2+\omega^2}$$

The following values for the coefficients correspond to the model of 'Skretting-Leroy':

$a = 0.006\ \ dB.km^{-1}$; $\quad \omega_1 = 6283.2\ rad.s^{-1} \quad (= 1000.\ Hz)$

$b = 0.2635\ dB.km^{-1}$; $\quad \omega_2 = 10681.4\ rad.s^{-1} \quad (= 1700.\ Hz)$

Ocean Surface Model $\mathcal{SHORIZ}$:

An ocean surface model that is horizontal (i.e. a sphere concentric with the earth). The ocean surface is where the following function is zero.

$$s(r, \theta, \phi) = z_s - h$$

where: $h = r - r_e$

r_e = earth's radius

r = radial coordinate of ray point

input: 'OCEAN SURFACE A SPHERE AT MSL'

the height of the ocean surface above the mean sea level, $z_s = 0.\ m$

giving: $s(r, \theta, \phi) = r_e - r$

Ocean Bottom Model $\mathcal{GHORIZ}$:

A constant height bottom model (i.e. a sphere concentric with the earth).

$$g(r,\theta,\phi) = h - z_o$$

where: $h = r - r_e$

r_e = earth's radius

r = radial coordinate of ray point

input: 'BOTTOM MODEL A SPHERE 6KM DEEP'

constant bottom height, $z_o = -5.\ km$

(negative if below mean sea level).

giving: $g(r,\theta,\phi) = r - r_e + 5.$

Receiver Surface Model $\mathcal{RVERT}$:

A receiver surface that is a vertical (canonical) surface a constant distance from a given origin on the earths surface.

$$f(r,\theta,\phi) = \sin\lambda_o\cos\theta + \cos\lambda_o\sin\theta\cos(\phi-\phi_o) - \cos\alpha_o$$

input: 'RECEIVER SURFACE A VERTICAL SURFACE'

the distance of the surface from the origin, $\alpha_o = 8.^o$

the latitude of the origin, $\lambda_o = -41.^o$

the longitude of the origin, $\alpha_o = 28.^o$

giving: $f(r,\theta,\phi) \simeq -0.656\cos\theta + 0.755\sin\theta\cos(\phi - 28.^o) - 0.990$

Current Velocity Model $\mathcal{WGAUSS}2$:

This subroutine specifies a zonal (eastward) current field whose intensity decays in a gaussian manner in all three space dimensions.

$$u_\phi = U_{\phi o}\ exp\left\{-\left(\frac{z-z_o}{W_z}\right)^2 - \left(\frac{\theta-\theta_o}{W_\theta}\right)^2 - \left(\frac{\phi-\phi_o}{W_\phi}\right)^2\right\}$$

where:

z	=	$r - r_e$
r_e	=	earth radius
r	=	is the radial coordinate of the ray point
δ_i	=	the half thickness of a region centered at approximately $z_i\ km$, in which
θ	=	co-latitude
θ_o	=	$90^o - \lambda_o$
ϕ	=	longitude

Note: This current field does not satisfy continuity if $W_\phi \neq 0$.

Note: Setting W_z, W_θ or $W_\phi = 0$ results in no variation in that direction.

input: 'ZONAL MODEL OF THE AGULHAS CURRENT'

the maximum value of u_ϕ, $U_{\phi o} = -0.003\ km.s^{-1}$

the height where u_ϕ maximizes, $z_o = 0.\ km$

the gaussian width in height of u_ϕ, $W_z = 1.\ km$

the latitude where u_ϕ maximizes, $\lambda_o = -33.5^o$

the meridional width of u_ϕ, $W_\theta = 0.5^o$

the longitude where u_ϕ maximizes, $\phi_o = 28.^o$

the zonal width of u_ϕ, $W_\phi = 0.^o$

Giving:

$$u_\phi = -0.003 \exp\left\{-(z)^2 - 4(\theta - 123.5)^2\right\}$$

input: 'ZONAL MODEL OF THE RETURN CURRENT'

the maximum value of u_ϕ, $U_{\phi o} = 0.003\ km.s^{-1}$

the height where u_ϕ maximizes, $z_o = 0.\ km$

the gaussian width in height of u_ϕ, $W_z = 1.\ km$

the latitude where u_ϕ maximizes, $\lambda_o = -40.^o$

the meridional width of u_ϕ, $W_\theta = 0.5^o$

the longitude where u_ϕ maximizes, $\phi_o = 28.^o$

the zonal width of u_ϕ, $W_\phi = 0.^o$

Giving:

$$u_\phi = 0.003exp\left\{-(z)^2 - 4(\theta - 130.0)^2\right\}$$

Sound Speed Perturbation Model $\mathcal{CBLOB4}$:

An increase (or decrease) in squared sound speed, in up to three localized regions, that decays in a gaussian manner in all three spatial directions.

$$C^2(r,\theta,\phi) = {C_o}^2(r,\theta,\phi)\left\{1 + \Sigma_{i=1}^{n}\Delta_i \exp\left[-\left(\frac{z-z_i}{W_{zi}}\right)^2 - \left(\frac{\theta-\theta_i}{W_{\theta i}}\right)^2 - \left(\frac{\phi-\phi_i}{W_{\phi i}}\right)^2\right]\right\}$$

where:

	z	=	$r - r_e$
	r_e	=	earth's radius
	(r,θ,ϕ)	=	earth centered spherical - polar coordinates
	${C_0}^2(r,\theta,\phi)$	=	background sound speed model
	λ_i	=	$\frac{\pi}{2} - \theta_i$

Note: Setting W_z, W_θ or $W_\phi = 0.$ results in no space variation in that direction.

input: 'PERTURBATION ASSOCIATED WITH THE AGULHAS CURRENT'

the strength of the fractional increase (or decrease), $\Delta_i = 0.02$

the height of the maximum effect, $z_o = 0.\ km$

the latitude of the maximum effect, $\lambda_o = -33.5^o$

the longitude of the maximum effect, $\phi_o = 28.^o$

the gaussian width in height of the effect, $W_z = 1.\ km$

the meridional width of the effect, $W_\theta = 0.5^o$

the zonal width of the effect, $W_\phi = 0.^o$

Giving:

$$C^2(r,\theta,\phi) = {C_o}^2(r,\theta,\phi)\left\{1 + 0.02\ exp\left[-(z)^2 - 4(\theta - 123.5)^2\right]\right\}$$

input: 'PERTURBATION ASSOCIATED WITH THE RETURN CURRENT'

the strength of the fractional increase (or decrease), $\Delta_i = 0.02$

the height of the maximum effect, $z_o = 0.\ km$

the latitude of the maximum effect, $\lambda_o = -40.^o$

the longitude of the maximum effect, $\phi_o = 28.^o$

the gaussian width in height of the effect, $W_z = 1.\ km$

the meridional width of the effect, $W_\theta = 0.5^o$

the zonal width of the effect, $W_\phi = 0.^o$

Giving:

$$C^2(r,\theta,\phi) = {C_o}^2(r,\theta,\phi)\left\{1 + 0.02 \exp\left[-(z)^2 - 4(\theta - 130.0)^2\right]\right\}$$

input: 'WARM CORE PERTURBATION '

the strength of the fractional increase (or decrease), $\Delta_i = 0.02$

the height of the maximum effect, $z_o = 0.\ km$

the latitude of the maximum effect, $\lambda_o = -37.^o$

the longitude of the maximum effect, $\phi_o = 28.^o$

the gaussian width in height of the effect, $W_z = 1.\ km$

the meridional width of the effect, $W_\theta = 0.5^o$

the zonal width of the effect, $W_\phi = 0.5^o$

Giving:

$$C^2(r,\theta,\phi) = {C_o}^2(r,\theta,\phi)\left\{1 + 0.02\exp\left[-z^2 - 4(\theta - 127.)^2 - 4(\phi - 28.0)^2\right]\right\}$$

Current Velocity Model $\mathcal{VVORTX}3$:

This subroutine models a vortex with a viscous core and a gaussian intensity profile in the vertical. The axis of the vortex is vertical and may be positioned above the any geographic latitude and longitude. The vortex rotates anticlockwise looking down. The core (inside r_o) is essentially a solid rotating fluid, while outside r_o, $\mid U \mid$ falls off as the inverse radius.

$$u_\theta = \frac{-1.397\ R_e\ U_o\ r_o}{r^2}\left(1 - \exp\frac{-1.26.r^2}{{r_o}^2}\right)(\phi - \phi_o)e^{-\left(\frac{h-h_{max}}{W_H}\right)^2}$$

$$u_\phi = \frac{1.397\ R_e\ U_o\ r_o}{r^2}\left(1 - \exp\frac{-1.26.r^2}{{r_o}^2}\right)(\theta - \theta_o)e^{-\left(\frac{h-h_{max}}{W_H}\right)^2}$$

where:

r = the radial distance from the vortex center

R_e = Earths radius - 6370 km throughout

θ = co-latitude

θ_o = $\frac{\pi}{2} - \lambda_o$

ϕ = longitude

h = height above sea level

input: 'ANTICLOCKWISE VORTEX'

the maximum tangential current, $U_o = 0.0015\ km.s^{-1}$

the radius of the vortex core to $u = U_o, r_o = 55.\ km$

the latitude of the vortex center, $\lambda_o = -37.^o$

the longitude of the vortex center, $\phi_o = 28.^o$

the gaussian width in height of the vortex, $W_H = 1.\ km$

the height of the vortex, $h_{max} = 0.\ m$

Giving:

$$u_\theta = \frac{-734.1584}{r^2}\left(1 - e^{\frac{-1.26.r^2}{3025^2}}\right)(\phi - 28.)e^{h^2}$$

$$u_\phi = \frac{734.1584}{r^2}\left(1 - e^{\frac{-1.26.r^2}{3025^2}}\right)(\theta - 127.)e^{h^2}$$

Bibliography

[1] Georges T.M., Jones R.M. and Lawrence R.S. (1990).
A PC version of the HARPO ocean acoustic ray tracing program.
NOAA Report. Wave propagation Laboratory. Boulder CO. pp18.

[2] Jones R.M., Riley J.P. and Georges T.M. (1986).
HARPO - A versatile three dimensional Hamiltonian ray tracing program for acoustic waves in an ocean with irregular bottom.
NOAA Report. Environmental Research Laboratories. Boulder CO. pp455.

Chapter 6

SOUND PROPAGATION EXPERIMENTS AND RESULTS

The previous chapters in this thesis provided the groundwork for this chapter, in which the use of *HARPO* as an acoustic modeling tool is demonstrated. The results of sound propagating through the model environments, which were defined in Chapter Five, are presented here. Also comparisons between the observed model results and the expected results, using the mathematical methods developed in Chapter Three are performed in order to validate the use of *HARPO* as a modeling tool. The experimental philosophy described in Chapter Two has been applied to the modeling procedure, beginning with sound propagating through a simple horizontally stratified ocean environment and then including more complex features such as an ocean current and a warm core eddy into the environment. Finally the results for the current and eddy scenar-

ios are applied to the Agulhas Current Region described in Chapter Four.

It is important to say that every effort was made throughout the numerical experiment to include realistic parameters into the model and hence realistic model environments were set up. This is a useful practice since it allows one to compare experimental data with model results.

6.1 The Presentation Of Results

An explanation regarding the presentation of results is necessary before considering the results themselves. The ray diagrams that resulted from the numerical sound propagation experiments are presented in Appendix A, Appendix B and Appendix C. The purpose of including all the ray diagrams is that they comprise a complete set of results that demonstrate the development of the experiment from the initial stages of sound propagating through a horizontally stratified ocean environment in Appendix A, a current environment in Appendix B and an anticyclonic warm core eddy environment in Appendix C. In order to ensure that the appendices are useful a table comprising of a list of all the ray diagrams relevant to that appendix and the position of the ray diagram within the appendix was compiled and is included at the start of each appendix.

Each of the experiments through distinct features, for example through the Agulhas Current, the Return Current and a warm core eddy, have three distinct categories of ray diagrams: those of sound propagation through the velocity structure, the sound speed (implied temperature) structure associated with the

feature, as well as a combined scenario that includes both the velocity and sound speed structure of the feature. For the eddy feature there are four more categories of ray diagram, within each of the three experimental categories, these are for the ray propagating through the center, $\frac{1}{2}$ *a radius* , 1 *radius* and $1\frac{1}{2}$ *radii* from the eddy center, as the eddy traveled towards the east.

For each of the scenarios provided two ray diagrams were produced, one in the vertical plane and one in the horizontal plane, all of these ray diagrams are included into the appendices. In scenarios where no downwards displacement in the vertical plane or refraction in the horizontal plane occurred, the ray diagrams are included for completeness. Clearly the vast number of ray diagrams produced could not be presented within the text, but were necessary not only for completeness, but to explain the results and determine conclusions.

Within the following text a number of ray diagrams are presented within tables of results, each of these ray diagrams has a reference number, $A.1 \ldots A.3$; $B.1 \ldots B.8$; $C.1 \ldots C.24$, which refers to the same figure within the appendices.

The size of the diagrams in the appendices are the same as the size of the diagrams produced by $\mathcal{HARPO}$, with a vertical scale of

$$2\ cm : 1000\ m$$

and a horizontal scale of

$$5.4\ cm : 1000\ m.$$

In the warm core eddy scenario a different horizontal scale was used,

$$5.4\ cm : 2000\ m,$$

because the horizontal refraction was so much greater than that in the current scenario.

These scales were used to approximately determine the observed magnitude of the downward displacement and horizontal refraction for all the vertical and horizontal ray diagrams respectively.

In certain of the ray diagrams a relatively small amount of downwards displacement or horizontal refraction can be observed, because of the scale of the diagrams it is not possible to determine an actual amount for these results, for this reason the magnitude of the variation that occurs to a sound ray propagating through a feature can not always be determined. In cases such as these where a feature has perturbed the ray, but the effect is not measurable the results are represented by $\star\star\star$ in the relevant table.

An important factor to notice is that throughout this research the horizontal ray diagrams shown were all taken at the $1000\ m$ level, that is the depth of the source and the sound speed minimum. This was done in order to facilitate comparisons when more complicated features, which result in horizontal variations, were included into the environment. Another factor is that each ray diagram, in both the vertical and horizontal plane, in the experiments that follow have the ray propagating through a horizontally stratified ocean included into them, this was done in order to assess the effects each feature has upon the ray propagating through them.

Throughout this thesis the observed horizontal refraction taken from the ray diagrams was determined by measuring the longitudinal distance between the refracted ray and the horizontal ray at the receiver site. The downwards displacement, measured in the vertical plane, was taken as the maximum displacement

of the ray from the ray propagating through a horizontally stratified ocean.

6.2 Sound Propagation Through A Horizontally Stratified Ocean

In Section 5.4 a horizontally stratified ocean model environment was set up, using $\mathcal{HARPO}$, sound rays were then propagated through the environment. Apart from providing a basis for further modeling the horizontally stratified ocean was modeled to demonstrate the fundamental features of acoustic propagation through the ocean. A schematic representation for this environment was presented in figure 5.3. The results of this particular experiment, that is sound propagation through a uniform ocean environment are presented in table 6.1, which includes both the vertical and the horizontal ray diagrams, as well as the vertical ray diagram for an oblique ray.

Consider the first figure in table 6.1, that is sound propagation through a uniform ocean environment in the vertical plane. The SOFAR channel, which was introduced in section 3.4, has been clearly demonstrated by the ray which continuously bends towards the sound speed minimum.

Uniform Ocean	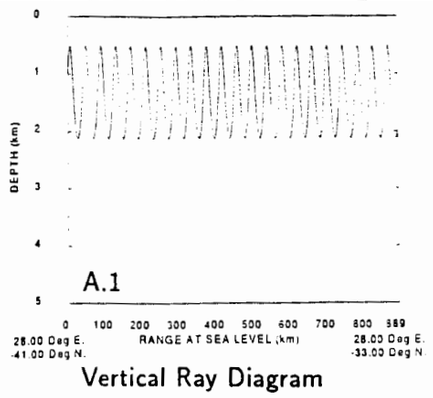 Vertical Ray Diagram
Uniform Ocean	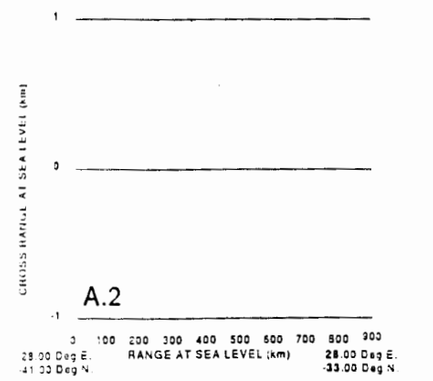 Horizontal Ray Diagram
Oblique Ray	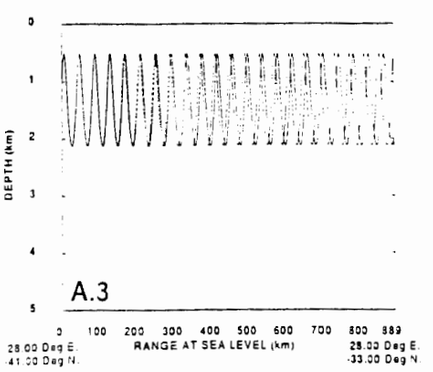 Vertical Ray Diagram

Table 6.1: Results For A Ray Propagating Through A Uniform Ocean Environment

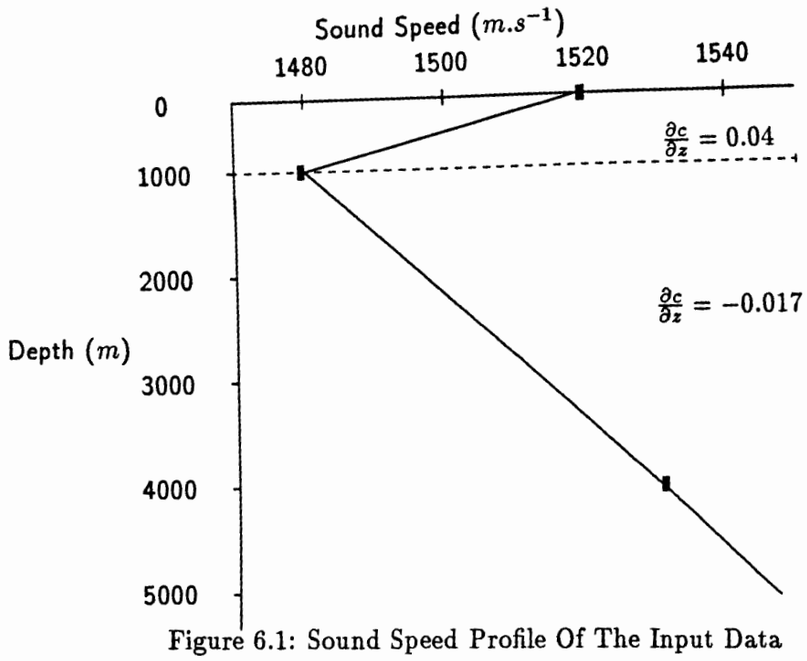

Figure 6.1: Sound Speed Profile Of The Input Data

In the vertical plane the variation from the sound speed minimum, above and below the sound speed minimum, is determined by the magnitude of the sound speed gradient, $|\frac{\partial c}{\partial z}|$ within that region. In Section 3.4 the radius of curvature was defined by $R = -\frac{c_o}{g}$, where $g = \frac{\partial c}{\partial z}$. From this it can be deduced that for a large sound speed gradient the radius of curvature is small and so the deviation from the sound channel axis is small. Conversely a small sound speed gradient results in a large radius of curvature and hence in a large deviation from the sound channel axis.

Consider figure 6.1, where $|\frac{\partial c}{\partial z}| \simeq 0.04\ s^{-1}$ above the sound speed minimum (a relatively large sound speed gradient), the maximum deviation from the sound speed minimum is fairly small, approximately $50\ m$. Below the sound speed gradient, where $|\frac{\partial c}{\partial z}| \simeq -0.017\ s^{-1}$ a large maximum variat

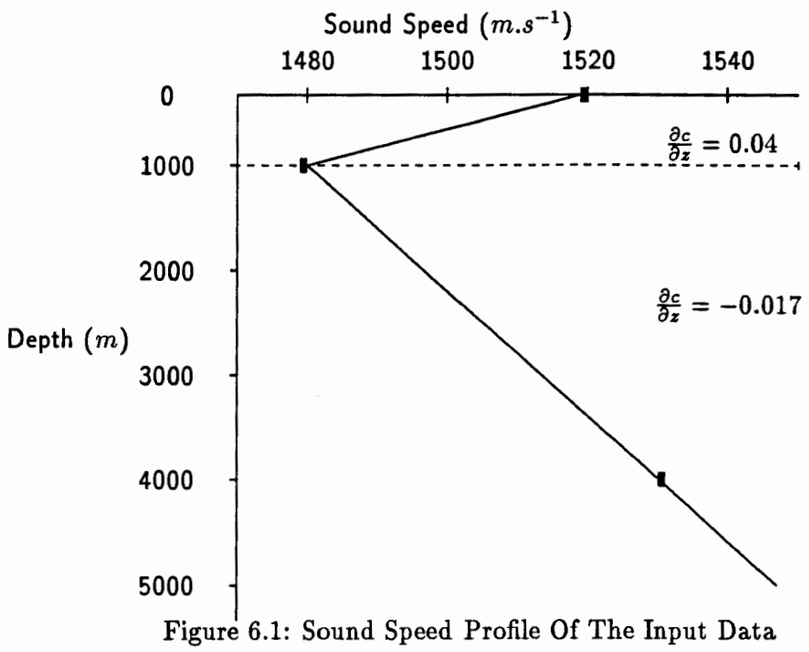

Figure 6.1: Sound Speed Profile Of The Input Data

In the vertical plane the variation from the sound speed minimum, above and below the sound speed minimum, is determined by the magnitude of the sound speed gradient, $|\ \frac{\partial c}{\partial z}\ |$ within that region. In Section 3.4 the radius of curvature was defined by $R = -\frac{c_o}{g}$, where $g = \frac{\partial c}{\partial z}$. From this it can be deduced that for a large sound speed gradient the radius of curvature is small and so the deviation from the sound channel axis is small. Conversely a small sound speed gradient results in a large radius of curvature and hence in a large deviation from the sound channel axis.

Consider figure 6.1, where $|\ \frac{\partial c}{\partial z}\ | \simeq 0.04\ s^{-1}$ above the sound speed minimum (a relatively large sound speed gradient), the maximum deviation from the sound speed minimum is fairly small, approximately $50\ m$. Below the sound speed gradient, where $|\ \frac{\partial c}{\partial z}\ | \simeq -0.017\ s^{-1}$ a large maximum variation

from the sound channel axis of about $1150\ m$ is observed. Also, as mentioned in Section 3.4, the sound speed gradient above the sound channel axis was positive and resulted in the downwards bending of the ray towards the sound speed minimum and in the region below the sound channel axis the sound speed gradient was negative which resulted in the upward bending of the ray towards the sound speed minimum.

In a range-independent or a horizontally stratified environment, such as the one considered here, where by definition there is no variation to the sound speed in a horizontal plane, there was no refraction in the horizontal plane. Refer to the second figure in table 6.1, the horizontal line through the center of the figure represents the unrefracted ray.

At this stage it is necessary to notice that with the position of the receiver at East London and the ray traveling perpendicularly towards the coast from the source the bathymetry of the region would not affect a sound ray propagating through it. That is nowhere along the route of the ray path does the bottom topography rise to a depth that intrudes into the sound channel. In section 4.2 the bottom topography of the region was discussed, even when other features were included into the model which cause the ray to refract and be displaced in the vertical plane, the bottom topography is so deep here that it never interacts with the sound channel. For this reason the ocean bottom was kept at a constant depth of $5000\ m$ throughout the experiment, even though it is possible, using $\mathcal{HARPO}$, to include topographic features into the model environment.

A variation on the horizontally stratified ocean scenario was to consider a

ray crossing the environment obliquely. Starting with an azimuth angle of 0^o (perpendicular to the environment), the ray was propagated through the environment with 1^o decremental steps in azimuth angle until an azimuth angle of 350^o was reached. The resulting ray diagram in the vertical plane, for the ray propagating through the environment with an azimuth angle of 350^o is presented in the third diagram of table 6.1.

The oblique ray appears to have a different wavelength to the ray traveling perpendicularly through the environment, this is a result of the different observation position relative to the ray and hence a different perspective on the ray. Initially this ray was included throughout the experiment in order to determine the effects of a ray that propagates through a feature obliquely. However the results were insignificant in that variation to a ray as it traveled through a feature, with an azimuth angle of 350^o , were negligible, in both the vertical and horizontal planes. For this reason, apart from this initial example, the oblique rays are omitted from all the figures that follow.

6.3 Sound Propagation Through A Current Feature

In the previous Chapter a model environment was established that included the velocity and temperature structures of the Agulhas and Agulhas Return Currents, these structures were superimposed onto the horizontally stratified ocean environment. Figure 5.4 and figure 5.5 represented the Agulhas and Agulhas Return Current model environments that were used for this part of the experiment. Sound rays were propagated through the velocity structure, the temperature structure and finally the combined velocity and temperature struc-

tures. The results for the Agulhas Current scenario are presented in table 6.2.

Table 6.2 is divided into three parts: firstly sound propagation through the velocity structure associated with the Agulhas Current; secondly sound propagation through the temperature structure associated with the Agulhas Current; and thirdly sound propagation through the combined velocity and temperature structures associated with the Agulhas Current.

The vertical and horizontal effects of each feature on sound propagation through them are outlined, and the relevant ray diagrams are presented. The horizontal ray diagram (taken at $1000\ m$) of sound propagation through the velocity structure, the vertical ray diagram showing sound propagation through the temperature structure and the horizontal ray diagram (taken at $1000\ m$) of sound propagation through the combined structures are included into the table.

Firstly the velocity structure associated with the Agulhas Current described in section 5.4 is considered. The velocity structure had no vertical effect on a ray traveling through it and the vertical ray diagram was the same as that for sound propagation through a horizontally stratified ocean environment (refer to figure A.1). However in the horizontal plane refraction in the direction of the current flow occurred. This refraction only took place in the region of the current, between 33 and $34^{o}S$, about $800\ km$ from the source.

Velocity Structure	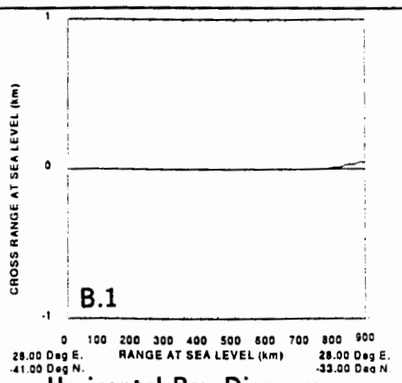 Horizontal Ray Diagram
• vertical effect: none • horizontal effect: refraction in the direction of the current flow	
Temperature Structure	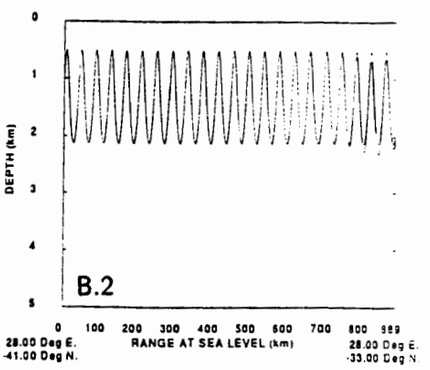 Vertical Ray Diagram
• vertical effect: downwards displacement of of the ray in the region of the perturbation • horizontal effect: none	
Combined Scenario	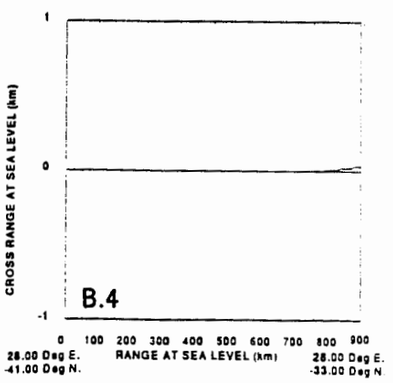 Horizontal Ray Diagram
• vertical effect: same as that for the temperature only scenario • horizontal effect: less refraction in the direction of the current flow than in the velocity only scenario	

Table 6.2: Results For A Ray Propagating Through The Agulhas Current Scenario

Ocean Bottom Model $\mathcal{GHORIZ}$:

A constant height bottom model (i.e. a sphere concentric with the earth).

$$g(r,\theta,\phi) = h - z_o$$

where: $h = r - r_e$

r_e = earth's radius

r = radial coordinate of ray point

input: 'BOTTOM MODEL A SPHERE 6KM DEEP'

constant bottom height, $z_o = -5.\ km$

(negative if below mean sea level).

giving: $g(r,\theta,\phi) = r - r_e + 5.$

Receiver Surface Model $\mathcal{RVERT}$:

A receiver surface that is a vertical (canonical) surface a constant distance from a given origin on the earths surface.

$$f(r,\theta,\phi) = \sin\lambda_o \cos\theta + \cos\lambda_o \sin\theta \cos(\phi - \phi_o) - \cos\alpha_o$$

input: 'RECEIVER SURFACE A VERTICAL SURFACE'

the distance of the surface from the origin, $\alpha_o = 8.^o$

the latitude of the origin, $\lambda_o = -41.^o$

the longitude of the origin, $\alpha_o = 28.^o$

giving: $f(r,\theta,\phi) \simeq -0.656\cos\theta + 0.755\sin\theta\cos(\phi - 28.^\circ) - 0.990$

Current Velocity Model $\mathcal{WGAUSS}2$:

This subroutine specifies a zonal (eastward) current field whose intensity decays in a gaussian manner in all three space dimensions.

$$u_\phi = U_{\phi o}\ exp\left\{-\left(\frac{z-z_o}{W_z}\right)^2 - \left(\frac{\theta-\theta_o}{W_\theta}\right)^2 - \left(\frac{\phi-\phi_o}{W_\phi}\right)^2\right\}$$

where:

z	=	$r - r_e$
r_e	=	earth radius
r	=	is the radial coordinate of the ray point
δ_i	=	the half thickness of a region centered at approximately $z_i\ km$, in which
θ	=	co-latitude
θ_o	=	$90^o - \lambda_o$
ϕ	=	longitude

Note: This current field does not satisfy continuity if $W_\phi \neq 0$.

Note: Setting W_z, W_θ or $W_\phi = 0$ results in no variation in that direction.

input: 'ZONAL MODEL OF THE AGULHAS CURRENT'

the maximum value of u_ϕ, $U_{\phi o} = -0.003\ km.s^{-1}$

the height where u_ϕ maximizes, $z_o = 0.\ km$

the gaussian width in height of u_ϕ, $W_z = 1.\ km$

the latitude where u_ϕ maximizes, $\lambda_o = -33.5^o$

the meridional width of u_ϕ, $W_\theta = 0.5^o$

the longitude where u_ϕ maximizes, $\phi_o = 28.^o$

the zonal width of u_ϕ, $W_\phi = 0.^o$

Giving:

$$u_\phi = -0.003 \exp\left\{-(z)^2 - 4(\theta - 123.5)^2\right\}$$

input: 'ZONAL MODEL OF THE RETURN CURRENT'

the maximum value of u_ϕ, $U_{\phi o} = 0.003\ km.s^{-1}$

the height where u_ϕ maximizes, $z_o = 0.\ km$

the gaussian width in height of u_ϕ, $W_z = 1.\ km$

the latitude where u_ϕ maximizes, $\lambda_o = -40.^o$

the meridional width of u_ϕ, $W_\theta = 0.5^o$

the longitude where u_ϕ maximizes, $\phi_o = 28.^o$

the zonal width of u_ϕ, $W_\phi = 0.^o$

Giving:

$$u_\phi = 0.003 exp\left\{-(z)^2 - 4(\theta - 130.0)^2\right\}$$

Sound Speed Perturbation Model *CBLOB4* :

An increase (or decrease) in squared sound speed, in up to three localized regions, that decays in a gaussian manner in all three spatial directions.

$$C^2(r,\theta,\phi) = {C_o}^2(r,\theta,\phi)\left\{1 + \Sigma_{i=1}^{n}\Delta_i \exp\left[-\left(\frac{z-z_i}{W_{zi}}\right)^2 - \left(\frac{\theta-\theta_i}{W_{\theta i}}\right)^2 - \left(\frac{\phi-\phi_i}{W_{\phi i}}\right)^2\right]\right\}$$

where:

	z	=	$r - r_e$
	r_e	=	earth's radius
	(r,θ,ϕ)	=	earth centered spherical - polar coordinates
	${C_0}^2(r,\theta,\phi)$	=	background sound speed model
	λ_i	=	$\frac{\pi}{2} - \theta_i$

Note: Setting W_z, W_θ or $W_\phi = 0.$ results in no space variation in that direction.

input: 'PERTURBATION ASSOCIATED WITH THE AGULHAS CURRENT'

the strength of the fractional increase (or decrease), $\Delta_i = 0.02$

the height of the maximum effect, $z_o = 0.\ km$

the latitude of the maximum effect, $\lambda_o = -33.5^o$

the longitude of the maximum effect, $\phi_o = 28.^o$

the gaussian width in height of the effect, $W_z = 1.\ km$

the meridional width of the effect, $W_\theta = 0.5^o$

the zonal width of the effect, $W_\phi = 0.^o$

Giving:

$$C^2(r,\theta,\phi) = {C_o}^2(r,\theta,\phi)\left\{1 + 0.02\ exp\left[-(z)^2 - 4(\theta - 123.5)^2\right]\right\}$$

input: 'PERTURBATION ASSOCIATED WITH THE RETURN CURRENT'

the strength of the fractional increase (or decrease), $\Delta_i = 0.02$

the height of the maximum effect, $z_o = 0.\ km$

the latitude of the maximum effect, $\lambda_o = -40.^o$

the longitude of the maximum effect, $\phi_o = 28.^o$

the gaussian width in height of the effect, $W_z = 1.\ km$

the meridional width of the effect, $W_\theta = 0.5^o$

the zonal width of the effect, $W_\phi = 0.^o$

Giving:

$$C^2(r,\theta,\phi) = {C_o}^2(r,\theta,\phi)\left\{1 + 0.02\exp\left[-(z)^2 - 4(\theta - 130.0)^2\right]\right\}$$

input: 'WARM CORE PERTURBATION '

the strength of the fractional increase (or decrease), $\Delta_i = 0.02$

the height of the maximum effect, $z_o = 0.\ km$

the latitude of the maximum effect, $\lambda_o = -37.^o$

the longitude of the maximum effect, $\phi_o = 28.^o$

the gaussian width in height of the effect, $W_z = 1.\ km$

the meridional width of the effect, $W_\theta = 0.5^o$

the zonal width of the effect, $W_\phi = 0.5^o$

Giving:

$$C^2(r,\theta,\phi) = {C_o}^2(r,\theta,\phi)\left\{1 + 0.02\exp\left[-z^2 - 4(\theta - 127.)^2 - 4(\phi - 28.0)^2\right]\right\}$$

Current Velocity Model $\mathcal{VVORTX}3$:

This subroutine models a vortex with a viscous core and a gaussian intensity profile in the vertical. The axis of the vortex is vertical and may be positioned above the any geographic latitude and longitude. The vortex rotates anticlockwise looking down. The core (inside r_o) is essentially a solid rotating fluid, while outside r_o, $\mid U \mid$ falls off as the inverse radius.

$$u_\theta = \frac{-1.397\ R_e\ U_o\ r_o}{r^2}\left(1 - \exp\frac{-1.26.r^2}{{r_o}^2}\right)(\phi - \phi_o)e^{-\left(\frac{h-h_{max}}{W_H}\right)^2}$$

$$u_\phi = \frac{1.397\ R_e\ U_o\ r_o}{r^2}\left(1 - \exp\frac{-1.26.r^2}{{r_o}^2}\right)(\theta - \theta_o)e^{-\left(\frac{h-h_{max}}{W_H}\right)^2}$$

where: r = the radial distance from the vortex center

R_e = Earths radius - 6370 km throughout

θ = co-latitude

θ_o = $\frac{\pi}{2} - \lambda_o$

ϕ = longitude

h = height above sea level

input: 'ANTICLOCKWISE VORTEX'

the maximum tangential current, $U_o = 0.0015\ km.s^{-1}$

the radius of the vortex core to $u = U_o, r_o = 55.\ km$

the latitude of the vortex center, $\lambda_o = -37.^o$

the longitude of the vortex center, $\phi_o = 28.^o$

the gaussian width in height of the vortex, $W_H = 1.\ km$

the height of the vortex, $h_{max} = 0.\ m$

Giving:

$$u_\theta = \frac{-734.1584}{r^2}\left(1 - e^{\frac{-1.26.r^2}{3025^2}}\right)(\phi - 28.)e^{h^2}$$

$$u_\phi = \frac{734.1584}{r^2}\left(1 - e^{\frac{-1.26.r^2}{3025^2}}\right)(\theta - 127.)e^{h^2}$$

Bibliography

[1] Georges T.M., Jones R.M. and Lawrence R.S. (1990).
A PC version of the HARPO ocean acoustic ray tracing program.
NOAA Report. Wave propagation Laboratory. Boulder CO. pp18.

[2] Jones R.M., Riley J.P. and Georges T.M. (1986).
HARPO - A versatile three dimensional Hamiltonian ray tracing program for acoustic waves in an ocean with irregular bottom.
NOAA Report. Environmental Research Laboratories. Boulder CO. pp455.

Chapter 6

SOUND PROPAGATION EXPERIMENTS AND RESULTS

The previous chapters in this thesis provided the groundwork for this chapter, in which the use of *HARPO* as an acoustic modeling tool is demonstrated. The results of sound propagating through the model environments, which were defined in Chapter Five, are presented here. Also comparisons between the observed model results and the expected results, using the mathematical methods developed in Chapter Three are performed in order to validate the use of *HARPO* as a modeling tool. The experimental philosophy described in Chapter Two has been applied to the modeling procedure, beginning with sound propagating through a simple horizontally stratified ocean environment and then including more complex features such as an ocean current and a warm core eddy into the environment. Finally the results for the current and eddy scenar-

ios are applied to the Agulhas Current Region described in Chapter Four.

It is important to say that every effort was made throughout the numerical experiment to include realistic parameters into the model and hence realistic model environments were set up. This is a useful practice since it allows one to compare experimental data with model results.

6.1 The Presentation Of Results

An explanation regarding the presentation of results is necessary before considering the results themselves. The ray diagrams that resulted from the numerical sound propagation experiments are presented in Appendix A, Appendix B and Appendix C. The purpose of including all the ray diagrams is that they comprise a complete set of results that demonstrate the development of the experiment from the initial stages of sound propagating through a horizontally stratified ocean environment in Appendix A, a current environment in Appendix B and an anticyclonic warm core eddy environment in Appendix C. In order to ensure that the appendices are useful a table comprising of a list of all the ray diagrams relevant to that appendix and the position of the ray diagram within the appendix was compiled and is included at the start of each appendix.

Each of the experiments through distinct features, for example through the Agulhas Current, the Return Current and a warm core eddy, have three distinct categories of ray diagrams: those of sound propagation through the velocity structure, the sound speed (implied temperature) structure associated with the

feature, as well as a combined scenario that includes both the velocity and sound speed structure of the feature. For the eddy feature there are four more categories of ray diagram, within each of the three experimental categories, these are for the ray propagating through the center, $\frac{1}{2}$ *a radius* , 1 *radius* and $1\frac{1}{2}$ *radii* from the eddy center, as the eddy traveled towards the east.

For each of the scenarios provided two ray diagrams were produced, one in the vertical plane and one in the horizontal plane, all of these ray diagrams are included into the appendices. In scenarios where no downwards displacement in the vertical plane or refraction in the horizontal plane occurred, the ray diagrams are included for completeness. Clearly the vast number of ray diagrams produced could not be presented within the text, but were necessary not only for completeness, but to explain the results and determine conclusions.

Within the following text a number of ray diagrams are presented within tables of results, each of these ray diagrams has a reference number, $A.1 \ldots A.3$; $B.1 \ldots B.8$; $C.1 \ldots C.24$, which refers to the same figure within the appendices.

The size of the diagrams in the appendices are the same as the size of the diagrams produced by $\mathcal{HARPO}$, with a vertical scale of

$$2\ cm : 1000\ m$$

and a horizontal scale of

$$5.4\ cm : 1000\ m.$$

In the warm core eddy scenario a different horizontal scale was used,

$$5.4\ cm : 2000\ m,$$

because the horizontal refraction was so much greater than that in the current scenario.

These scales were used to approximately determine the observed magnitude of the downward displacement and horizontal refraction for all the vertical and horizontal ray diagrams respectively.

In certain of the ray diagrams a relatively small amount of downwards displacement or horizontal refraction can be observed, because of the scale of the diagrams it is not possible to determine an actual amount for these results, for this reason the magnitude of the variation that occurs to a sound ray propagating through a feature can not always be determined. In cases such as these where a feature has perturbed the ray, but the effect is not measurable the results are represented by $\star\star\star$ in the relevant table.

An important factor to notice is that throughout this research the horizontal ray diagrams shown were all taken at the $1000\ m$ level, that is the depth of the source and the sound speed minimum. This was done in order to facilitate comparisons when more complicated features, which result in horizontal variations, were included into the environment. Another factor is that each ray diagram, in both the vertical and horizontal plane, in the experiments that follow have the ray propagating through a horizontally stratified ocean included into them, this was done in order to assess the effects each feature has upon the ray propagating through them.

Throughout this thesis the observed horizontal refraction taken from the ray diagrams was determined by measuring the longitudinal distance between the refracted ray and the horizontal ray at the receiver site. The downwards displacement, measured in the vertical plane, was taken as the maximum displacement

of the ray from the ray propagating through a horizontally stratified ocean.

6.2 Sound Propagation Through A Horizontally Stratified Ocean

In Section 5.4 a horizontally stratified ocean model environment was set up, using $\mathcal{HARPO}$, sound rays were then propagated through the environment. Apart from providing a basis for further modeling the horizontally stratified ocean was modeled to demonstrate the fundamental features of acoustic propagation through the ocean. A schematic representation for this environment was presented in figure 5.3. The results of this particular experiment, that is sound propagation through a uniform ocean environment are presented in table 6.1, which includes both the vertical and the horizontal ray diagrams, as well as the vertical ray diagram for an oblique ray.

Consider the first figure in table 6.1, that is sound propagation through a uniform ocean environment in the vertical plane. The SOFAR channel, which was introduced in section 3.4, has been clearly demonstrated by the ray which continuously bends towards the sound speed minimum.

Uniform Ocean	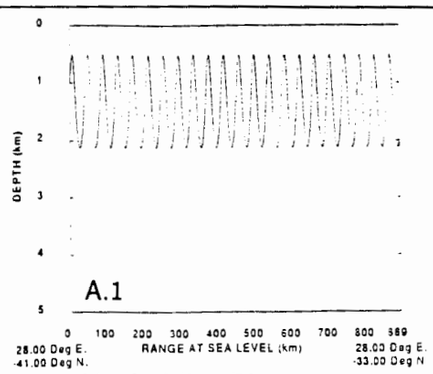 Vertical Ray Diagram
Uniform Ocean	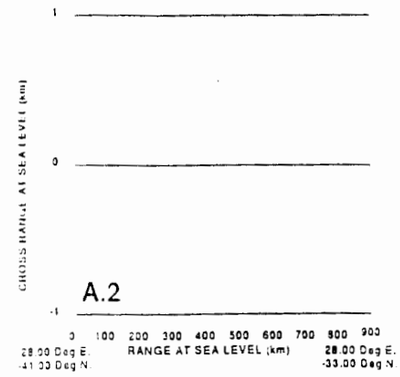 Horizontal Ray Diagram
Oblique Ray	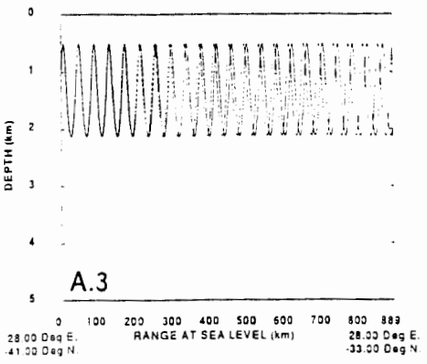 Vertical Ray Diagram

Table 6.1: Results For A Ray Propagating Through A Uniform Ocean Environment

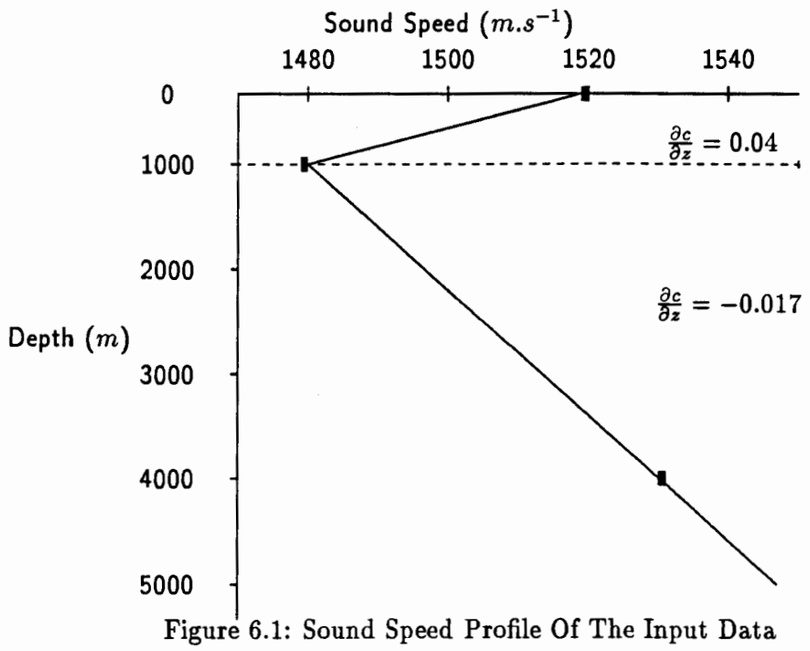

Figure 6.1: Sound Speed Profile Of The Input Data

In the vertical plane the variation from the sound speed minimum, above and below the sound speed minimum, is determined by the magnitude of the sound speed gradient, $|\frac{\partial c}{\partial z}|$ within that region. In Section 3.4 the radius of curvature was defined by $R = -\frac{c_o}{g}$, where $g = \frac{\partial c}{\partial z}$. From this it can be deduced that for a large sound speed gradient the radius of curvature is small and so the deviation from the sound channel axis is small. Conversely a small sound speed gradient results in a large radius of curvature and hence in a large deviation from the sound channel axis.

Consider figure 6.1, where $|\frac{\partial c}{\partial z}| \simeq 0.04\ s^{-1}$ above the sound speed minimum (a relatively large sound speed gradient), the maximum deviation from the sound speed minimum is fairly small, approximately $50\ m$. Below the sound speed gradient, where $|\frac{\partial c}{\partial z}| \simeq -0.017\ s^{-1}$ a large maximum variation

from the sound channel axis of about 1150 m is observed. Also, as mentioned in Section 3.4, the sound speed gradient above the sound channel axis was positive and resulted in the downwards bending of the ray towards the sound speed minimum and in the region below the sound channel axis the sound speed gradient was negative which resulted in the upward bending of the ray towards the sound speed minimum.

In a range-independent or a horizontally stratified environment, such as the one considered here, where by definition there is no variation to the sound speed in a horizontal plane, there was no refraction in the horizontal plane. Refer to the second figure in table 6.1, the horizontal line through the center of the figure represents the unrefracted ray.

At this stage it is necessary to notice that with the position of the receiver at East London and the ray traveling perpendicularly towards the coast from the source the bathymetry of the region would not affect a sound ray propagating through it. That is nowhere along the route of the ray path does the bottom topography rise to a depth that intrudes into the sound channel. In section 4.2 the bottom topography of the region was discussed, even when other features were included into the model which cause the ray to refract and be displaced in the vertical plane, the bottom topography is so deep here that it never interacts with the sound channel. For this reason the ocean bottom was kept at a constant depth of 5000 m throughout the experiment, even though it is possible, using $\mathcal{HARPO}$, to include topographic features into the model environment.

A variation on the horizontally stratified ocean scenario was to consider a

ray crossing the environment obliquely. Starting with an azimuth angle of 0^o (perpendicular to the environment), the ray was propagated through the environment with 1^o decremental steps in azimuth angle until an azimuth angle of 350^o was reached. The resulting ray diagram in the vertical plane, for the ray propagating through the environment with an azimuth angle of 350^o is presented in the third diagram of table 6.1.

The oblique ray appears to have a different wavelength to the ray traveling perpendicularly through the environment, this is a result of the different observation position relative to the ray and hence a different perspective on the ray. Initially this ray was included throughout the experiment in order to determine the effects of a ray that propagates through a feature obliquely. However the results were insignificant in that variation to a ray as it traveled through a feature, with an azimuth angle of 350^o , were negligible, in both the vertical and horizontal planes. For this reason, apart from this initial example, the oblique rays are omitted from all the figures that follow.

6.3 Sound Propagation Through A Current Feature

In the previous Chapter a model environment was established that included the velocity and temperature structures of the Agulhas and Agulhas Return Currents, these structures were superimposed onto the horizontally stratified ocean environment. Figure 5.4 and figure 5.5 represented the Agulhas and Agulhas Return Current model environments that were used for this part of the experiment. Sound rays were propagated through the velocity structure, the temperature structure and finally the combined velocity and temperature struc-

tures. The results for the Agulhas Current scenario are presented in table 6.2.

Table 6.2 is divided into three parts: firstly sound propagation through the velocity structure associated with the Agulhas Current; secondly sound propagation through the temperature structure associated with the Agulhas Current; and thirdly sound propagation through the combined velocity and temperature structures associated with the Agulhas Current.

The vertical and horizontal effects of each feature on sound propagation through them are outlined, and the relevant ray diagrams are presented. The horizontal ray diagram (taken at $1000\ m$) of sound propagation through the velocity structure, the vertical ray diagram showing sound propagation through the temperature structure and the horizontal ray diagram (taken at $1000\ m$) of sound propagation through the combined structures are included into the table.

Firstly the velocity structure associated with the Agulhas Current described in section 5.4 is considered. The velocity structure had no vertical effect on a ray traveling through it and the vertical ray diagram was the same as that for sound propagation through a horizontally stratified ocean environment (refer to figure A.1). However in the horizontal plane refraction in the direction of the current flow occurred. This refraction only took place in the region of the current, between 33 and $34^{o}S$, about $800\ km$ from the source.

Velocity Structure	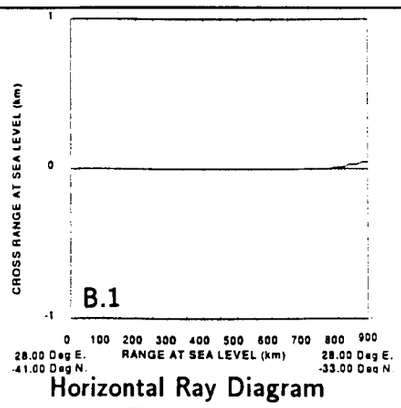 Horizontal Ray Diagram
• vertical effect: none • horizontal effect: refraction in the direction of the current flow	
Temperature Structure	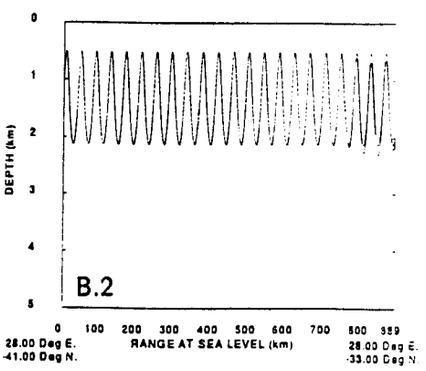 Vertical Ray Diagram
• vertical effect: downwards displacement of of the ray in the region of the perturbation • horizontal effect: none	
Combined Scenario	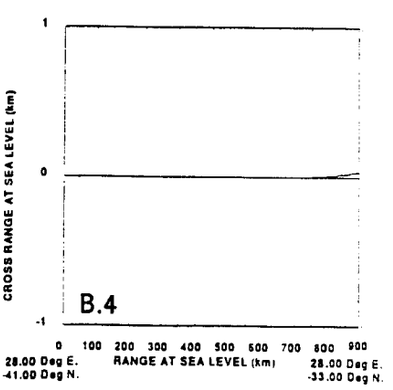 Horizontal Ray Diagram
• vertical effect: same as that for the temperature only scenario • horizontal effect: less refraction in the direction of the current flow than in the velocity only scenario	

Table 6.2: Results For A Ray Propagating Through The Agulhas Current Scenario

Using the displacement equations derived in **example 1** at the end of section 3.5, which made use of the generalized Hamiltonian ray tracing equations within a current:

$$\frac{\partial x_1}{\partial t} = c_o \qquad \frac{\partial x_2}{\partial t} = V_2(x_1, x_3) \quad \frac{\partial x_3}{\partial t} = 0$$

In this experiment the current used was provided by the model $\mathcal{WGAUSS}2$ (refer to pp 103). At the source depth of $1000\ m$:

$$V_2(x_1, x_3) = V_2(x_1, -1) = -0.003e^{-1-4(x_1-123.5)^2}$$

Now at $1000\ m$: $c = 1480\ m.s^{-1}$

$$\Rightarrow \quad \Delta t \ = \ \frac{distance\ traveled}{sound\ speed} \ = \ \frac{110000\ m}{1480\ m.s^{-1}} \ \simeq \ 74.3\ s$$

Therefore the predicted ray displacement would be:

$$\int_0^{74.3} - 0.003e^{-1-(\frac{t-37.2}{37.2})^2)} \partial t \simeq 61.32\ m$$

However the observed refraction, taken from the horizontal ray diagram in table 6.2 is only about $46.3\ m$ in the direction of the current flow. This indicates that while the observed experiment results appear to be realistic they are not necessarily numerically correct.

In Section 3.1 it was stated that a change in sound speed indicates, through the equation of state, a variation in the temperature structure. An increase in sound speed would be indicative of an increase in temperature, for this reason the temperature structure associated with the Agulhas Current was included as a positive sound speed perturbation. The results for a ray propagating through a positive sound speed perturbation, associated with the warm temperature

structure of the Agulhas Current, are presented in table 6.2.

No horizontal variation occurred to the ray and therefore the horizontal ray diagram is the same as that for the horizontally stratified ocean (see figure A.2). However, in the vertical plane a downwards displacement of approximately $200\ m$ was observed in the region of the perturbation, with the largest effect occurring at the latitude of the current axis, $33.5^{o}S$.

It is important to notice that while a warm core feature, such as that associated with the Agulhas Current, result in a downwards displacement of the sound speed minimum, the inclusion of a positive sound speed perturbation does not necessarily have this effect. For example the sound speed perturbation used for this experiment, represented in figure 6.2, results in an increase in the magnitude of the sound speed gradient above the sound speed minimum, which remains unchanged at a depth of $1000\ m$.

The 2% increase in sound speed resulted in approximately a $30\ m.s^{-1}$ increase in the sound speed at the surface, this in turn resulted in an increase in the magnitude of the sound speed gradient above the sound speed minimum. Therefore the perturbation resulted in an increase in the sound speed gradient above the sound speed minimum. The new magnitude of the sound speed gradient above the sound speed minimum was $\mid \frac{\partial c}{\partial z} \mid = 0.07\ s^{-1}$.

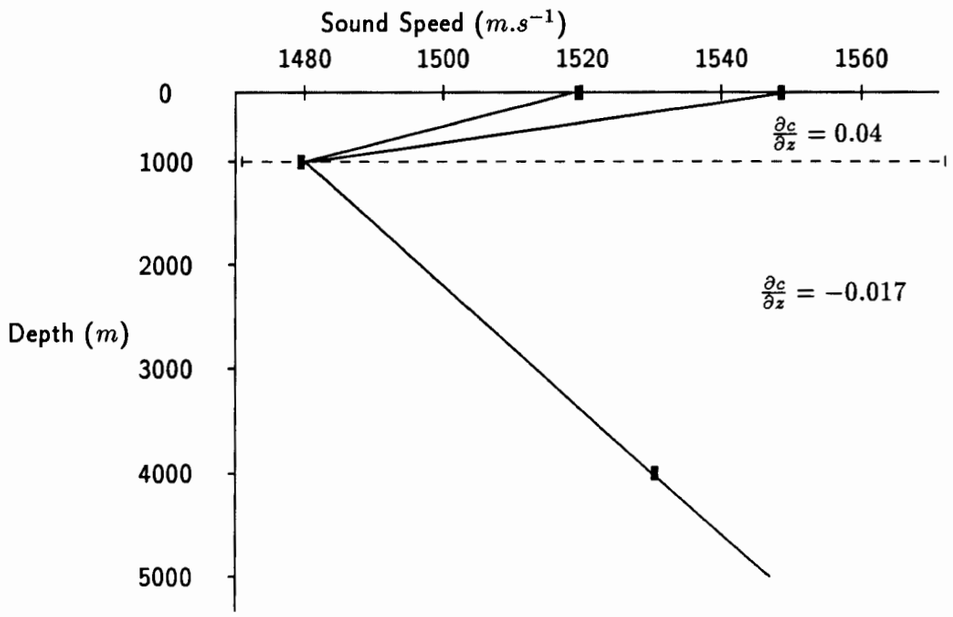

Figure 6.2: Diagram Of The Sound Speed Profile At The Maximum Variation On The Current Axis.

An increase in the magnitude of the sound speed gradient, which occurred above the sound speed minimum as a result of the positive sound speed perturbation, results in a decrease to the maximum deviation of the ray from the sound speed minimum in that region. This in turn results in a larger entry angle into the layer beneath the sound channel, which results in a larger deviation of the ray from the sound speed minimum (according to the definition of h in section 3.4). In table 6.2 the downwards displacement of the ray in the region of the current is clearly evident, with the maximum downwards displacement below the channel as a result of the sound speed perturbation was approximately $200\ m$.

After considering the two components separately the ray was propagated through

an environment containing both the temperature and velocity structures associated with the Agulhas Current. In the vertical plane no difference could be detected between the ray diagram for the combined velocity and temperature scenario and the temperature only scenario. This indicates that the velocity structure did not affect sound propagation in the vertical plane. However in the horizontal plane the amount of refraction, while still in the direction of the current flow, was significantly less than in the velocity only scenario, about $35.2\ m$. This indicates that the temperature structure had a dampening effect on the horizontal velocity effect.

At this stage the experiment was extended to include the Agulhas Return Current. The Agulhas Return Current velocity and temperature structures were included into the horizontally stratified ocean environment. The structures had the same parameters as the Agulhas Current feature, but the latitudinal axis was positioned at $40^{o}S$ and the current direction was reversed so as to correspond to the easterly direction of the Return Current.

The results of this experiment are presented in the table 6.3, in the same way as for the Agulhas Current results in table 6.2. Table 6.3 includes the horizontal ray diagram (taken at $1000\ m$) associated with propagation through the velocity structure, the vertical ray diagram associated with propagation through the temperature structure and finally the horizontal ray diagram (taken at $1000\ m$) associated with the combined velocity and temperature structures which represented the Return Current and the Agulhas Current temperature structure.

It was mentioned in section 5.4 that it was not possible, using $\mathcal{HARPO}$,

to include both the Agulhas and Agulhas Return velocity structures into the same model environment. So the velocity structure associated with the Agulhas Return Current was considered on its own.

The velocity structure resulted in no variation in the vertical plane, but as for the Agulhas Current scenario horizontal refraction of about $55.6\ m$ in the direction of the current flow was observed. However a feature of the refraction that was not observed in the Agulhas Current velocity scenario, because of the close proximity of the coast and the receiver to the 'coast-edge' of the current, is that the horizontal refraction only occurs within the region of the current, thereafter the ray proceeds parallel to the $28^{o}E$ line of longitude. This result corresponded to the mathematical prediction, derived at the end of section 3.5, where for the first example the displacement equations indicated that once the ray was no longer within the current region the ray would continue to propagate in its initial direction.

It was possible to include both the sound perturbation associated with the Agulhas and the Agulhas Return Current into the same model environment. No horizontal variation was experienced by the ray as it propagated through the sound speed perturbations. The vertical effect of sound propagating through the positive sound speed perturbation associated with the warm Agulhas Return Current was the same as that for the Agulhas Current, only in the position of the Agulhas Return Current.

Velocity Structure	
• vertical effect: none • horizontal effect: refraction in the direction of the current flow	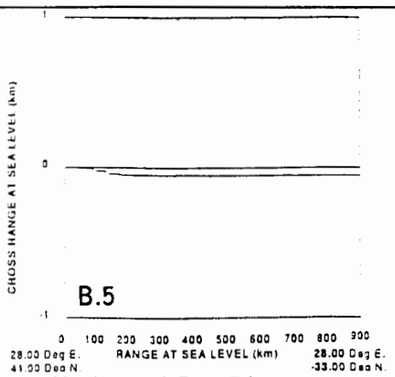 Horizontal Ray Diagram
Temperature Structure	
• vertical effect: downwards displacement of of the ray in the region of the perturbations • horizontal effect: none	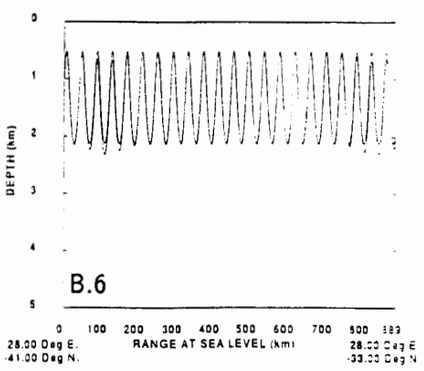 Vertical Ray Diagram
Combined Scenario	
• vertical effect: same as that for the temperature only scenario • horizontal effect: less refraction in the direction of the current flow than in the velocity only scenario	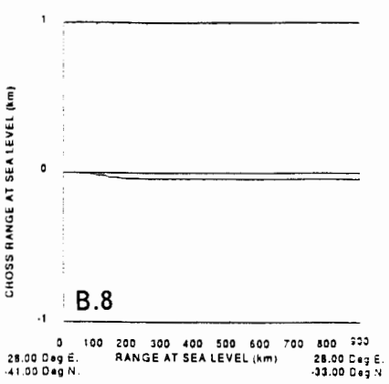 Horizontal Ray Diagram

Table 6.3: Results For A Ray Propagating Through The Return Current Scenario

Finally the velocity and temperature structure associated with the Agulhas Return Current and the temperature structure associated with the Agulhas Current were included into the horizontally stratified ocean environment. The results were similar to that of the Agulhas Current Scenario. In the vertical plane the downwards displacement was the same as that for the temperature only scenario. In the horizontal plane refraction of approximately $37.0\ m$, in the region of the Return Current, was again observed to be less than that for the velocity only scenario. No further refraction occurred to the ray on entering the temperature structure associated with the Agulhas Current.

6.4 Sound Propagation Through A Warm Core Eddy

Before considering the results of sound propagating through an eddy environment it must be mentioned that a large amount of research has been done on sound propagating through mesoscale eddies (Baer, 1980). Kamenkovich et al (1986) provided an overview on previous research done with respect to acoustic propagation through mesoscale eddies. Most of the previous research done with respect to mesoscale eddies has been performed on intense mesoscale features within the Gulf Stream Region, in fact very little has been published on the more typical, less energetic eddy fields.

Mesoscale eddies have been shown to have significant effects on the sound speed structure of the ocean, this is primarily as a result of the large temperature variations associated with them (Henrick et al, 1979). Another primary component of an eddy, which effects acoustic propagation through them, is the

rotational velocity structure, which can either accelerate or decelerate the propagation sound signal.

There are two distinct eddy types which are defined by their direction of rotation: firstly a cyclonic eddy, which consists of a cold core of water which spins in a clockwise direction in the Southern Hemisphere; and secondly an anticyclonic eddy, which consists of a warm core of water which spins in an anticlockwise direction in the Southern Hemisphere. Within these two categories of eddy large variations can be in the eddy structure and intensity. Diameters ranging from 100 km to 500 km and current speeds from 3 $m.s^{-1}$ to 1.5 $m.s^{-1}$ have been observed (Henrick, 1977).

An experiment pertaining to the effects of an eddy on a sound ray propagating through it would not be complete without mentioning the paper by Munk (1980), in which Munk mentions that the presence of a warm or cold mesoscale feature results in the spreading or focusing respectively of acoustic energy in both the vertical and horizontal planes. In his paper Munk states that the horizontal angular deflection of a ray path through a circular eddy is approximately double that of the fractional variation in sound speed at the eddy center.

Because warm core and cold core eddies have such very different structures and dynamics they have very different acoustic properties and hence very different effects on sound propagating through them. In this experiment a warm core anticyclonic eddy was considered because of the frequency of this type of eddy experienced in the Retroflection Region, south of Africa. According to Munk (1980) as rays propagate through a warm core eddy they refract in a direction

away from the eddy center, this is primarily because sound rays refract towards regions of lower sound speed and hence towards cooler water. (Conversely rays passing through a cold core eddy would refract towards the eddy center).

The anticlockwise warm core eddy that was considered for this experiment was depicted in figure 5.6. As in the previous experiments described in this Chapter the velocity and sound speed (implied temperature) structures are considered first separately and then combined together. Another factor which was included into the experiment was that the eddy was moving in an easterly direction, and the ray was still transmitted along the $28°E$ line of longitude. An eddy traveling in a westerly direction would have produced symmetric results. Rays passing through the center, $\frac{1}{2}$ *a radius* , 1 *radius* and $1\frac{1}{2}$ *radii* from the center of the eddy were considered. Figure 6.3 shows the orientation that was used, for the experiment and in the corresponding ray diagrams, of the ray to the eddy as the eddy traveled towards the east. This was done in order to compare results with Munk (1980), who performed a similar experiment.

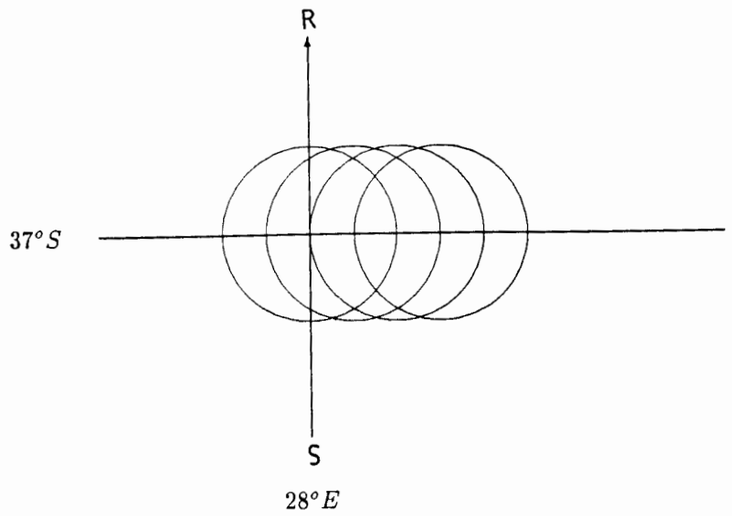

Figure 6.3: Diagram Showing That As The Eddy Travels Towards The East So The Ray Propagates Through The Center, $\frac{1}{2}$ *a radius* , 1 *radius* And $1\frac{1}{2}$ *radii* From The Center Of The Eddy.

The experiment to demonstrate sound propagation through an eddy feature was performed in the same way that sound propagation through a current feature was. A sound ray was propagated through the velocity structure associated a warm core eddy in the Southern Hemisphere, that is an anticlockwise vortex. This was followed by propagating the sound ray through the temperature (or implied sound speed structure) associated with a warm core eddy. Finally a sound ray was propagated through the combined scenario, which included the velocity and temperature structures associated with a warm core eddy.

The results are presented in two tables: table 6.4, which contains all the vertical ray diagrams associated with the eddy experiment; and table 6.5 contains all the horizontal ray diagrams (all taken at 1000 m) associated with the eddy

experiment.

So each table contains the ray diagrams associated with sound propagation through an anticlockwise vortex, a warm core sound speed perturbation and the combined scenario of a warm core anticlockwise vortex. For each of these scenarios four ray diagrams are presented, corresponding to a ray propagating through the center, $\frac{1}{2}$ *a radius* , 1 *radius* and $1\frac{1}{2}$ *radii* a radius from the center of an eddy as the eddy traveled towards the east.

First the results for sound propagation through the velocity structure, an anticlockwise vortex were considered. As the ray propagated through the anticlockwise vortex no vertical displacement was observed, in fact the same vertical ray diagram as for the horizontally uniform ocean, presented in figure A.1, was produced. This indicates that a horizontal current does not effect a ray propagating through it in the vertical plane. This corresponds to the first displacement equation for each of the examples presented at the end of section 3.5:

$$\frac{\partial x_1}{\partial t} = 0 .$$

However in the same way that there appeared to be a variation in wavelength when observing the oblique ray in table 6.1, there appeared to be a slight variation as the ray traveled through the vortex at $\frac{1}{2}$ *a radius* , 1 *radius* and $1\frac{1}{2}$ *radii* from the vortex center. This effect follows since these rays would be intersecting the feature obliquely.

Downwards Displacement	Velocity Structure
$R = 0$: • velocity: 0 m • temperature: 200 m • combined: 200 m	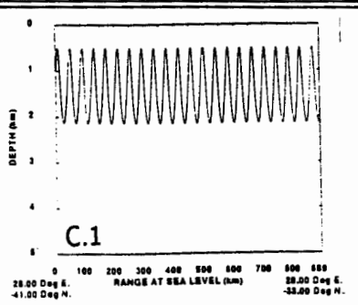
$R = \frac{1}{2}$: • velocity: 0 m • temperature: 150 m • combined: 150 m	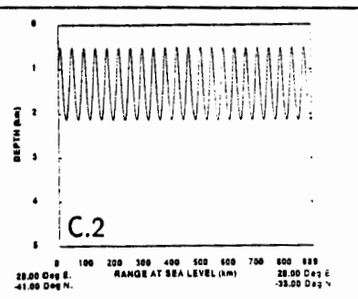
$R = 1$: • velocity: 0 m • temperature: 60 m • combined: 50 m	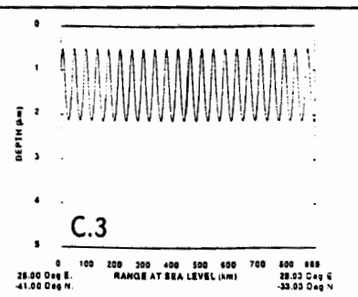
$R = 1\frac{1}{2}$: • velocity: 0 m • temperature: $\star\star\star$ • combined: 0 m	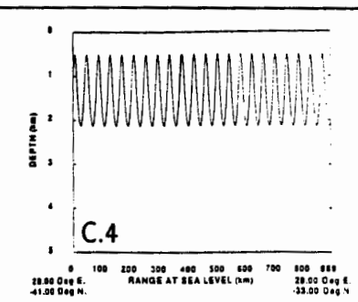

Table 6.4: Table Showing The Vertical Ray Diagrams Produced For The Eddy Experiment, Demonstrating Sound Propagation Through A Warm Core Eddy Feature.

Temperature Structure	Combined Scenario
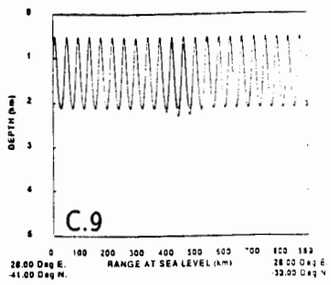	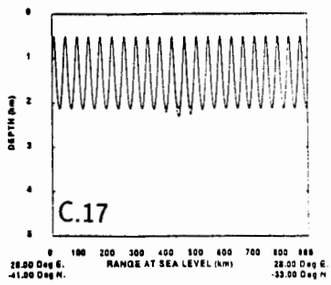
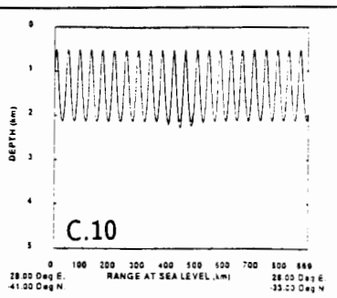	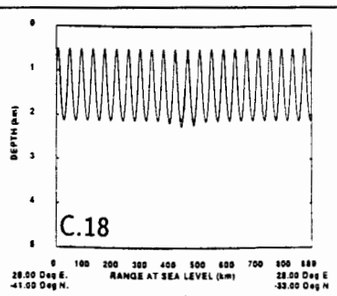
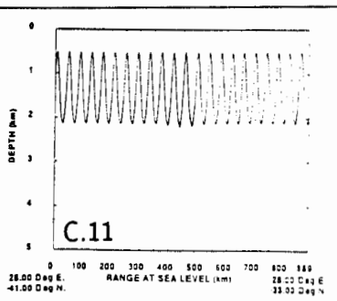	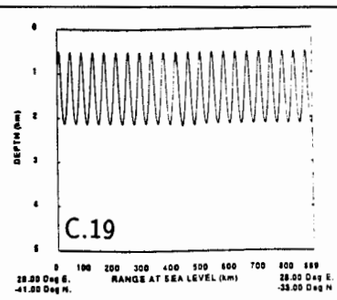
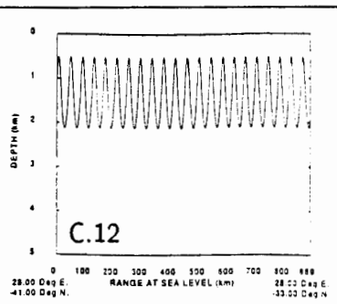	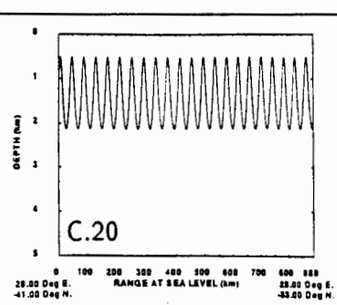

This experiment was followed by considering sound propagation through a positive sound speed perturbation, which corresponds to the warm temperature structure associated with a warm core eddy. The perturbation was designed to coincide with the location of the anticlockwise vortex, and the maximum sound speed variation occurred at the center of the feature, where the sound speed profile was the same as that in figure 6.2.

For the sound speed perturbation scenario, as expected the most downwards displacement occurred to the ray propagating through the center of the feature, where the perturbation was the most intense. The amount of downwards displacement decreased as the eddy traveled towards the east and the ray propagated through progressively less intense regions of the perturbation.

The maximum downwards displacement, below the sound speed minimum, was approximately $200\ m$ more than that for the ray propagating through the horizontally stratified ocean. Once again the downwards displacement of the sound channel was a direct result of the increase in magnitude of the sound speed gradient above the sound speed minimum was a result of the positive sound speed perturbation. The maximum downwards displacement of the ray propagating through the perturbation at $\frac{1}{2}\ a\ radius$ was approximately $150\ m$, the downwards displacement through $1\ radius$ was approximately $60\ m$ and for the ray propagating through $1\frac{1}{2}\ radii$ away from the eddy center downwards displacement did occur but it was too small to measure on the ray diagram.

The anticlockwise vortex and the positive sound speed perturbation were combined together and included into the horizontally stratified ocean, representing

a warm core eddy. As in the case of the sound speed perturbation scenario, the maximum amount of downwards displacement occurred to the ray traveling through the center of the eddy, the amount of downwards displacement then decreased as the eddy traveled towards the east. However, for the two outer rays, the downwards displacement was less for the eddy scenario, in each case, than for the sound speed perturbation only scenario.

The ray traveling through the center of the feature experienced a downwards displacement of approximately $200\ m$. The amount of downwards displacement to the ray traveling through the eddy eddy at $\frac{1}{2}\ a\ radius$ was approximately $150\ m$, for the ray traveling through the eddy at $1\ radius$ the downwards displacement was approximately $50\ m$ and there was no downwards displacement for the ray traveling through the eddy $1\frac{1}{2}\ radii$ from the eddy center.

In the same way that the vertical results are presented in table 6.4 so the horizontal results were presented in table 6.5. Consider first the results for a ray propagating through the eddy velocity structure, that was through an anticlockwise vortex. In the horizontal plane the anticlockwise vortex produced the largest horizontal refraction, away from the vortex, to the ray traveling through the center of the vortex, that was where the velocity structure was the most intense. Thereafter the amount of refraction decreased as the eddy traveled towards the east.

Horizontal Refraction	Velocity Structure
$R = 0$: • velocity: 722.2 m • temperature: 0 m • combined: 611.1 m	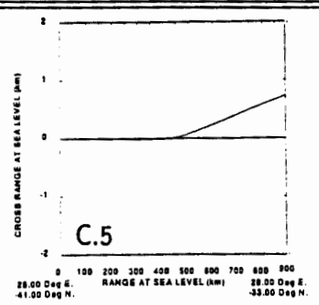
$R = \frac{1}{2}$: • velocity: 518.5 m • temperature: 1556.6 m • combined: 2074.1 m	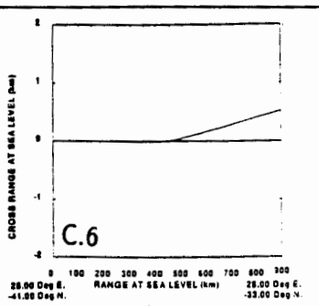
$R = 1$: • velocity: 166.7 m • temperature: 1629.6 m • combined: 1833.3 m	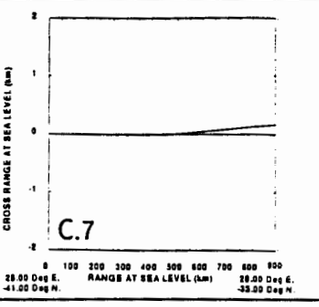
$R = 1\frac{1}{2}$: • velocity: 7.4 m • temperature: 740.7 m • combined: 777.8 m	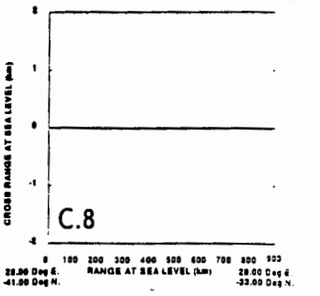

Table 6.5: Table Showing The Horizontal Ray Diagrams Produced For The Eddy Experiment, Demonstrating Sound Propagation Through A Warm Core Eddy Feature.

Temperature Structure	Combined Scenario
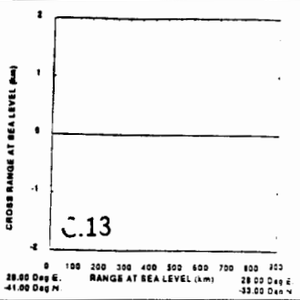 C.13	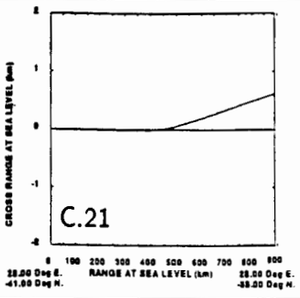 C.21
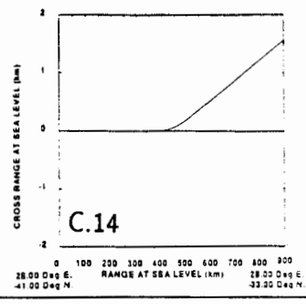 C.14	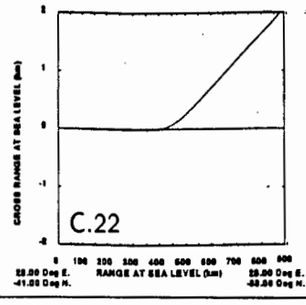 C.22
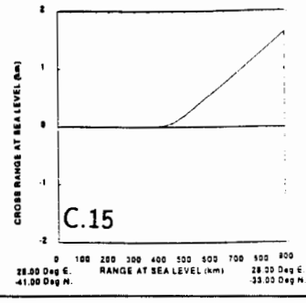 C.15	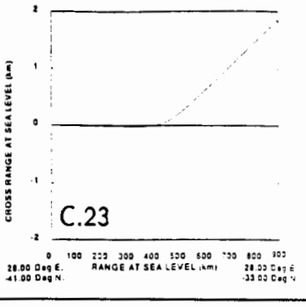 C.23
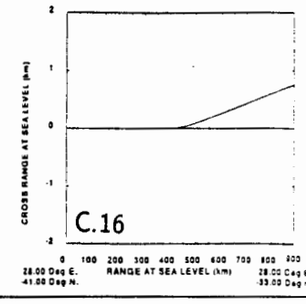 C.16	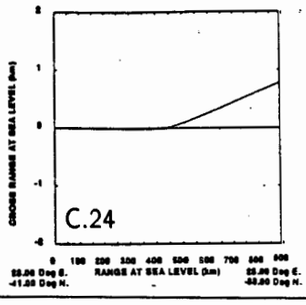 C.24

The maximum refraction, away from the vortex, of approximately $722.2\ m$, was experienced by the ray propagating through the center of the vortex. The ray propagating through the vortex $\frac{1}{2}\ a\ radius$ from the center had refraction of about $518.0\ m$ away from the vortex. For the ray propagating through the vortex $1\ radius$ radius from the center the horizontal refraction was approximately $166.7\ m$. For the ray propagating $1\frac{1}{2}\ radii$ from the vortex center horizontal refraction was observed to be approximately $7.4\ m$. It is interesting to notice that the refraction effects for a relatively low velocity anticyclonic vortex, with a maximum velocity of $1.5\ m.s^{-1}$ were far larger than the refraction effects for a zonal current flowing twice as fast.

Now in the same way that the displacement equations were considered for the agulhas current scenario, the displacement equations derived at the end of section 3.5, with an initial direction of $\underline{k} = (0, k_2, 0)$, were considered:

$$\frac{\partial x_1}{\partial t} = 0 \qquad \frac{\partial x_2}{\partial t} = V_2(x_1, x_2, x_3) + c_o \quad \frac{\partial x_3}{\partial t} = 0$$

And according to the model used, $\mathcal{VVORTX}3$, taken at $1000\ m$:

$$V_2(x_1, x_2, x_3) = V_2(-1, x_2, x_3) = \frac{-734.1584(1000)^2}{|-127-x_2|+|28-x_3|}(1 - e^{\frac{-1.26(|-127-x_2|+|28-x_3|)}{3025^2}})(x_3 - 28)e^1$$
$$V_3(x_1, x_2, x_3) = V_3(-1, x_2, x_3) = \frac{734.1584(1000)^2}{|-127-x_2|+|28-x_3|}(1 - e^{\frac{-1.26(|-127-x_2|+|28-x_3|)}{3025^2}})(x_2 - 127)e^1$$

Also, in the same way that the current was $110\ km$ wide, so the eddy feature was $110\ km$ in diameter, this meant that at the maximum width of the eddy feature:

$$\Delta t = \frac{110000\ m}{1480\ m.s{-}1} \simeq 74.3\ s$$

For the ray propagating through the center of the vortex the predicted ray displacement would be:

$$\int_o^{74.3}[V_2 + c_o]\partial t \; =$$
$$\int_o^{74.3}[\frac{-734.1584(1000)^2}{|37.2-t|}(1 - e^{\frac{-1.26(|37.2-t|)}{3025^2}})(t - 37.2)e^1 + 1480]\partial t$$

As the eddy traveled towards the east so the time spent, for the ray, within the feature would reduce. The amount of refraction would become:

$$\int_o^t[V_2 + c_o]\partial t = [V_2]_o^t + 1480\Delta t$$
$$\int_o^t[V_3]\partial t = [V_3]_o^t$$

In the temperature only scenario the ray traveling through the center of the sound speed perturbation intersected the perturbation orthogonally and therefore was not affected by the sound speed structure. However as the ray traveled towards the east so the ray intersected the perturbation more obliquely and large amounts of refraction away from the sound speed perturbation were observed. This corresponds to the range-dependent ray tracing theory that was introduced in the vertical plane in section 3.4. While the theory was introduced in the vertical plane it was equally applicable in the horizontal plane and this scenario provided an example of the fact that an increase sound speed would result in refraction away from the perturbation.

A large horizontal refraction, of approximately $1555.6\ m$, was observed for the ray traveling through the perturbation $\frac{1}{2}\ a\ radius$ from the center. For the ray which grazed the perturbation, $1\ radius$ from the perturbation center, the horizontal refraction was the most for this scenario, approximately $1629.6\ m$. Finally the ray propagating $1\frac{1}{2}\ radii$ from the perturbation center experienced only approximately $740.7\ m$ of horizontal refraction away from the eddy, this

reduction in horizontal refraction was expected since the ray was no longer close to the intense sound speed perturbation.

In the combined scenario the velocity structure and the sound perturbation appeared to have complimented each other in terms of the horizontal refraction. The horizontal refraction through the center of the eddy was approximately $611.1\ m$, through $\frac{1}{2}\ a\ radius$ approximately 2074.1 , through $1\ radius$ approximately $1833.3\ m$ and through $1\frac{1}{2}\ radii$ approximately $777.8\ m$.

The horizontal angular deflection of the ray traveling through the center of the eddy was:

$$\arctan(\tfrac{611.1\ m}{505000\ m}) \simeq 0.0693^{o}$$

Where $611.1\ m$ was the horizontal refraction through the center of the eddy, measured at the receiver site, and $505000\ m$ was the horizontal distance from the position where the ray entered the eddy to the receiver site. This means that for this experiment the horizontal angular deflection of the ray path through the center of the eddy was approximately 0.0693^{o} , for an eddy with a fractional variation of 0.02 (or 2%) at the eddy center. Munk (1980) stated that the horizontal angular deflection of the ray path through a circular eddy is approximately double that of the fractional variation in sound speed at the eddy center, in this case the horizontal angular deflection was almost three and a half times that of the fractional variation in sound speed at the eddy center.

Bibliography

[1] Baer R.N. (1980)

Calculations of Sound Propagation Through An Eddy.

Journal of Acoustic Society of America, Vol. 67, No. 4, April, pp1180-1185.

[2] Henrick R.F., Jacobson M.J. and Siegmann W.L. (1980)

General Effects Of Currents And Sound Speed Variations On Short-Range Acoustic Transmission In Cyclonic Eddies.

Journal of Acoustic Society of America, Vol. 67, No. 1, January, pp121-134.

[3] Henrick R.F., Siegmann W.L. and Jacobson M.J. (1977)

General Analysis Of Ocean Eddy Effects For Sound Transmission Applications.

Journal of Acoustic Society of America, Vol. 62, No. 4, October, pp860-870.

[4] Kamenkovich V.M., Koshlyakov M.N and Monin A.S. (editors) (1986)

Synoptic Eddies In The Ocean.

D.Reidel Publishing Company, The Netherlands, pp433.

[5] Munk W.H. (1980)

Horizontal Deflection Of Acoustic Paths By Mesoscale Eddies.

Journal of Physical Oceanography, Vol.10, April, pp596-604.

Chapter 7

SUMMARY AND CONCLUSIONS

7.1 Summary Of The Experiment And Results

An outline of the numerical experiment is presented here as well as a summary of the results previously presented in Chapter Six. The results are displayed in table 7.1 and table 7.2, which contain the vertical and horizontal results respectively. The purpose of these tables was not only to provide a quick reference, but to make the reasoning behind the conclusions easier to follow.

The numerical experiment began by propagating a sound ray through a range-independent environment, this horizontally stratified environment was kept as a background environment throughout the experiment. This scenario demonstrated the basic acoustic property of long range acoustic transmission in a range-independent environment, that is the presence of the SOFAR channel

was clearly demonstrated.

A zonal current and its associated temperature structure were included into the environment. Firstly the ray was transmitted through the sound speed (implied temperature) structure of the feature associated with the Agulhas Current. This was followed by propagating sound through the zonal velocity structure associated with the current. Finally the two components were combined together to provide a realistic range-dependent environment and a sound ray was propagated through it. The results showed the downwards displacement of the ray beneath the warm structure in the sound speed only scenario. Horizontal refraction in the direction of the current flow occurred to the ray propagating through the velocity structure, that was a zonal current. Finally in the realistic combined scenario the downwards displacement to the ray in the vertical plane was the same as that in the temperature only scenario, but the horizontal refraction was reduced.

A natural extension to this scenario was to consider the effects of sound propagation through the Agulhas Return Current. Staying with the current scenario propagation through the sound speed (implied temperature) structure associated with both the Agulhas and Agulhas Return Current was considered, followed by propagation through the zonal velocity structure associated with the Agulhas Return Current. The final experiment in the current scenario was to combine the sound speed structure associated with both the Agulhas and Agulhas Return Currents as well as the velocity structure associated with the Agulhas Return Current. The results for the Agulhas Return Current scenario were consistent with the Agulhas Current results.

Figure	Model Environment	Downwards Displacement
Figure A.1	uniform ocean	0 m
Figure A.3	oblique ray	0 m
Figure B.2	agulhas temperature	200 m
Figure B.3	agulhas combined	200 m
Figure B.6	return temperature	200 m
Figure B.7	return combined	200 m
Figure C.1	eddy velocity - $r = 0$	0 m
Figure C.2	eddy velocity - $r = \frac{1}{2}$	0 m
Figure C.3	eddy velocity - $r = 1$	0 m
Figure C.4	eddy velocity - $r = 1\frac{1}{2}$	0 m
Figure C.9	eddy temperature - $r = 0$	200 m
Figure C.10	eddy temperature - $r = \frac{1}{2}$	150 m
Figure C.11	eddy temperature - $r = 1$	60 m
Figure C.12	eddy temperature - $r = 1\frac{1}{2}$	$\star\star\star$
Figure C.17	eddy combined - $r = 0$	200 m
Figure C.18	eddy combined - $r = \frac{1}{2}$	150 m
Figure C.19	eddy combined - $r = 1$	50 m
Figure C.20	eddy combined - $r = 1\frac{1}{2}$	0 m

Table 7.1: Summary Of Observed Results For All The Ray Diagrams In The Vertical Plane

Figure	Model Environment	Horizontal Refraction
Figure A.2	uniform ocean	0 m
Figure B.1	agulhas velocity	46.3 m
Figure B.4	agulhas combined	35.2 m
Figure B.5	return velocity	55.6 m
Figure B.8	return combined	37.0 m
Figure C.5	eddy velocity - $r = 0$	722.2 m
Figure C.6	eddy velocity - $r = \frac{1}{2}$	518.5 m
Figure C.7	eddy velocity - $r = 1$	166.7 m
Figure C.8	eddy velocity - $r = 1\frac{1}{2}$	7.4 m
Figure C.13	eddy temperature - $r = 0$	0 m
Figure C.14	eddy temperature - $r = \frac{1}{2}$	1555.6 m
Figure C.15	eddy temperature - $r = 1$	1629.6 m
Figure C.16	eddy temperature - $r = 1\frac{1}{2}$	740.7 m
Figure C.21	eddy combined - $r = 0$	611.1 m
Figure C.22	eddy combined - $r = \frac{1}{2}$	2074.1 m
Figure C.23	eddy combined - $r = 1$	1833.3 m
Figure C.24	eddy combined - $r = 1\frac{1}{2}$	777.8 m

Table 7.2: Summary Of Observed Results For All The Ray Diagrams In The Horizontal Plane

Finally sound propagation through a warm core mesoscale eddy was considered. Beginning propagation through the sound speed (implied temperature) structure, followed by propagation through the an anticlockwise vortex current structure, which corresponds to the velocity structure of a warm core eddy feature in the southern hemisphere. Both these components were combined together in order to consider propagation through a more realistic warm core mesoscale eddy, such as those found in the Agulhas Current region. For all the eddy scenarios rays propagating through the center $\frac{1}{2}$ *a radius* , 1 *radius* and $1\frac{1}{2}$ *radii* from the eddy center were considered. The results were again consistent with the current scenario, except the horizontal refraction was away from the eddy center.

7.2 Conclusions

In order to keep the conclusions focused, the objectives for this thesis, which were presented at the end of section 1.1, are restated here. The first objective was to consider the effects of warm core features on long range acoustic propagation through them using $\mathcal{HARPO}$ (Georges, Jones and Lawrence, 1990; Jones, Riley and Georges, 1986)a hamiltonian ray tracing program for the ocean. The next objective was to apply the results of the numerical experiment to features typical of oceanographic features found within the Agulhas Current Region. The final objective was to assess the usefulness of $\mathcal{HARPO}$ as a predictive tool in terms of long range acoustic propagation in the ocean.

The numerical experiments performed for this thesis did not produce the large

refraction and vertical displacement effects that have been presented in a large amount of other acoustic propagation modeling research which mainly considered propagation through exaggerated features in order to determine extreme effects, an exception is Newhall et al (1990). The purpose of studying propagation through exaggerated features seems to be in order to determine refractive and displacement processes, rather than to quantify the amount of refraction and displacement that occurs as a result of sound propagating through them.

The experiments that were performed and that have been described in this thesis used realistic parameters and have clearly demonstrated that the velocity and sound speed (implied temperature) structure of warm core oceanographic features, such as warm zonal currents and warm mesoscale eddies have a far reaching effect on sound propagating through them.

Consider first the results for sound propagating through the warm core zonal currents, which were designed to represent the Agulhas and Agulhas Return Currents. These currents were both discussed in detail in Chapter Four and are considered to have two components, the velocity and sound speed structures, that affect sound propagation through them.

Firstly the warm water associated with the currents causes the sound channel to be depressed in that region, a ray propagating through the feature dives down following the new deeper sound channel. The associated velocity structures resulted in significant amounts of horizontal refraction, in the direction of the current flow, to rays propagating through them. When the velocity and temperature structures were combined together into a more realistic scenario

the ray was still forced downwards by the warm current core and because of this less horizontal refraction occurred to the ray, that was now propagating beneath the current core, than in the velocity only scenario.

Secondly the eddy scenario was considered. As Munk (1980) concluded the horizontal refraction through a warm core feature would be away from the center of the feature, so all the refraction for the eddy feature was directed away from the eddy center. Also for the ray propagating through the center of the eddy the horizontal angular deflection was approximately three and a half times that of the fractional variation in sound speed at the eddy center.

For the ray traveling through the center of the combined eddy scenario the conclusion was the same as that for the current scenario, in that the warm water of the feature forced the sound channel downwards, this resulted in the ray traveling below the current core and therefore less horizontal refraction than in the vortex only scenario.

For the rays traveling through the eddy feature, that entered the feature obliquely the sound speed structure played a strong role in the amount of horizontal refraction which occurred. The most horizontal refraction occurred to the ray traveling through $\frac{1}{2}$ *a radius* from the eddy center and then the amount of horizontal refraction decreased as the eddy traveled towards the east. As the eddy traveled eastwards so the intensity of the sound speed perturbation was reduced and hence the decrease in horizontal refraction.

In conclusion *HARPO* was useful as a modeling tool, in terms of determining

which feature would cause more horizontal refraction or downwards displacement to a particular ray, than another feature. The results have clearly shown that *HARPO* performs well as a predictive tool in determining the effects of oceanic features on sound propagating through them.

7.3 Extension Into Real Environments

A natural extension of this work would be to include real hydrographic data, collected within the area of interest, and incorporated as the model environment. The inability to do this was indeed the primary limitation of the PC version of *HARPO* used for this thesis. Its implementation has to await the extended software, but future work taking advantage of this can be contemplated as future studies.

Real data goes well beyond the idealized geometrics of the model environments of this thesis. Additional measures of the deviation from simple propagation paths are needed so as to gain necessary insights. For example, the horizontal refraction of a ray passing through a region of fully three-dimensional range dependence can be described in terms of the variation of horizontal refraction angle along the propagation path and the change in overall travel time for the new environment.

Repeated propagation studies for changing real environments can be used to investigate the evolution of real oceanographic environments past fixed sources and receivers.

Bibliography

[1] Georges T.M., Jones R.M. and Lawrence R.S. (1990).
A PC version of the HARPO ocean acoustic ray tracing program.
NOAA Report, Wave propagation Laboratory, Boulder CO., pp18.

[2] Jones R.M., Riley J.P. and Georges T.M. (1986).
HARPO - A versatile three dimensional Hamiltonian ray tracing program for acoustic waves in an ocean with irregular bottom.
NOAA Report, Environmental Research Laboratories, Boulder CO., pp455.

[3] Munk W.H. (1980)
Horizontal Deflection Of Acoustic Paths By Mesoscale Eddies.
Journal of Physical Oceanography, Vol.10, April, pp596-604.

[4] Newhall A.E., Lynch J.F., Chiu C.S and Daugherty J.R.(1990)
Improvements in Three Dimensional Ray Tracing Codes for Underwater Acoustics.
In Lee D., Cakmak A. and Vichnevetsky R. (editors).
Computational Acoustics Volume 1. Elsevier Science Publisher, B.V., North Holland, pp169-185.

Appendix A

A UNIFORM OCEAN ENVIRONMENT

Figure:	Model Environment	Plane	Page Number
Figure A.1	uniform ocean	vertical	154
Figure A.2	uniform ocean	horizontal	155
Figure A.3	oblique ray	vertical	156

Table A.1: List Of The Location Of The Ray Diagrams For Sound Propagating Through A Horizontally Stratified Ocean Environment

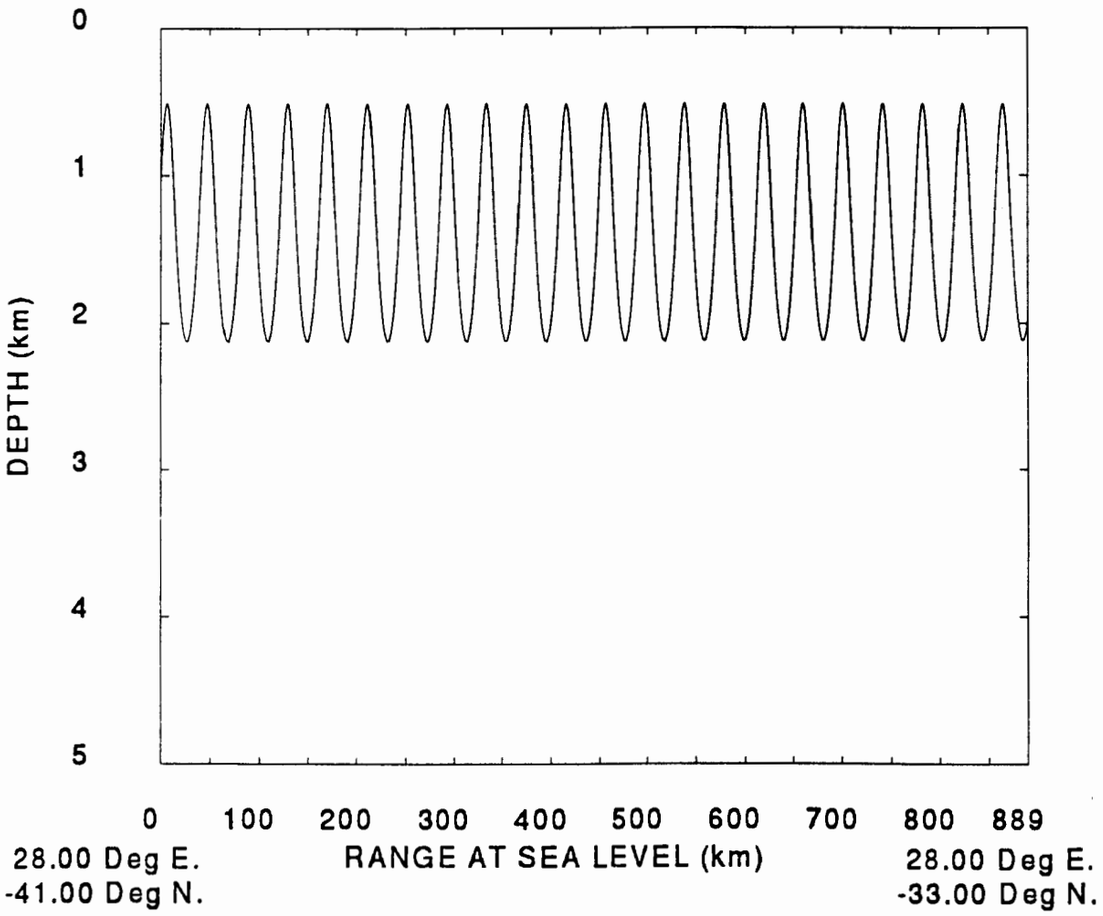

Figure A.1: Uniform Ocean - Vertical Profile

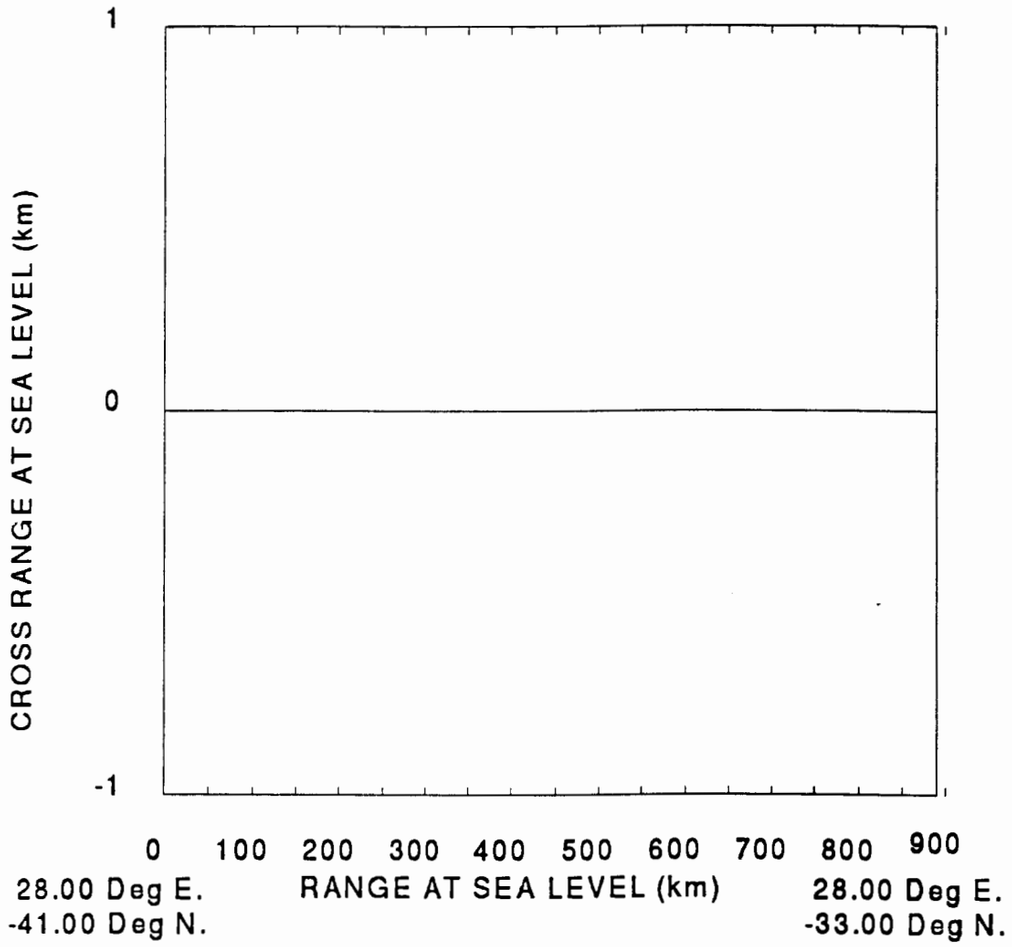

Figure A.2: Uniform Ocean - Horizontal Profile

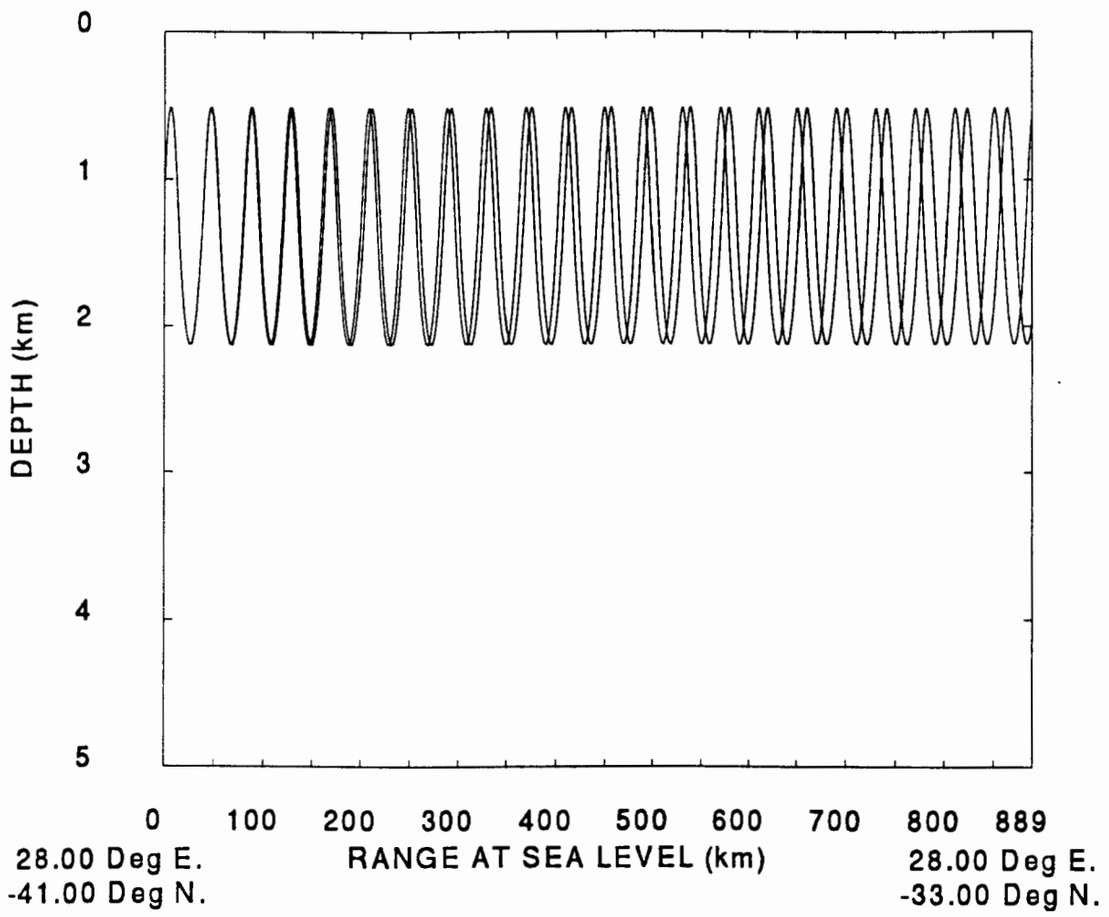

Figure A.3: Uniform Ocean - Oblique - Vertical Profile

Appendix B

A CURRENT ENVIRONMENT

Figure:	Model Environment	Plane	Page Number
Figure B.1	agulhas velocity	horizontal	159
Figure B.2	agulhas temperature	vertical	160
Figure B.3	agulhas combined	vertical	161
Figure B.4	agulhas combined	horizontal	162
Figure B.5	return velocity	horizontal	163
Figure B.6	return temperature	vertical	164
Figure B.7	return combined	vertical	165
Figure B.8	return combined	horizontal	166

Table B.1: List Of The Location Of The Ray Diagrams For Sound Propagating Through A Current Environment

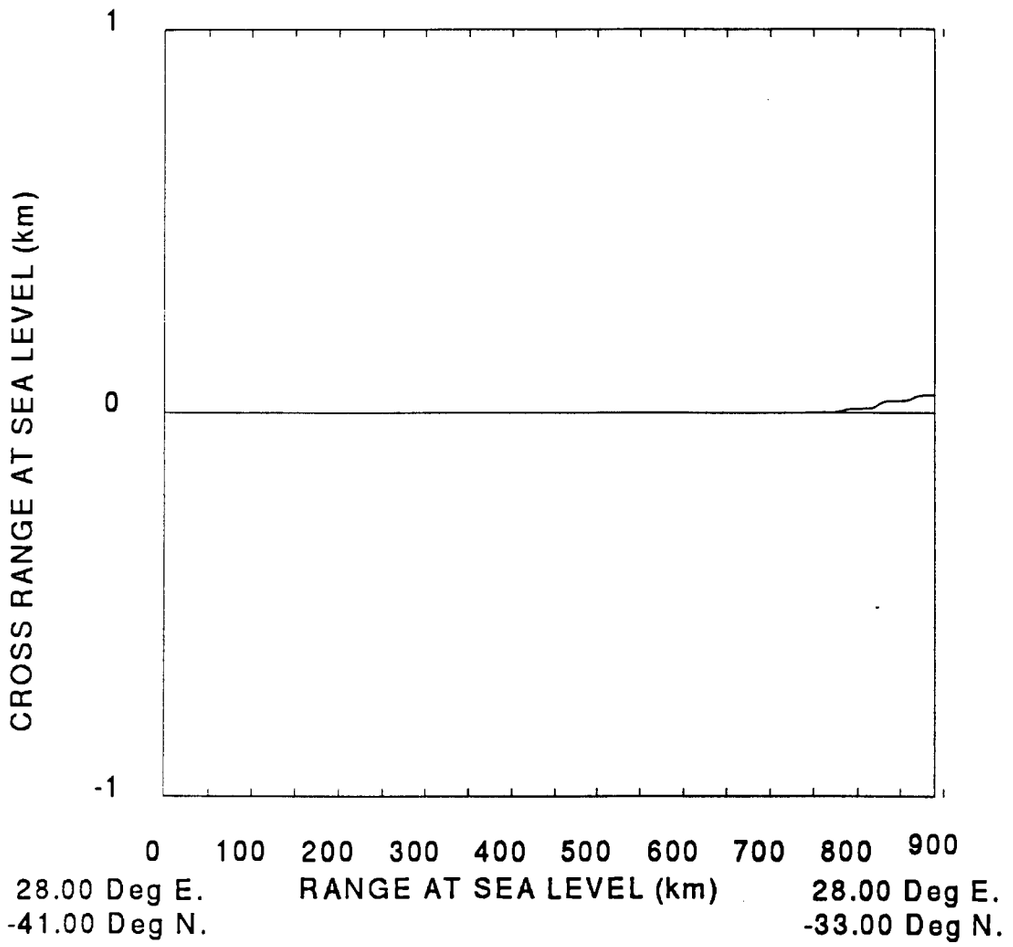

Figure B.1: Agulhas Current Velocity Structure - Horizontal Profile

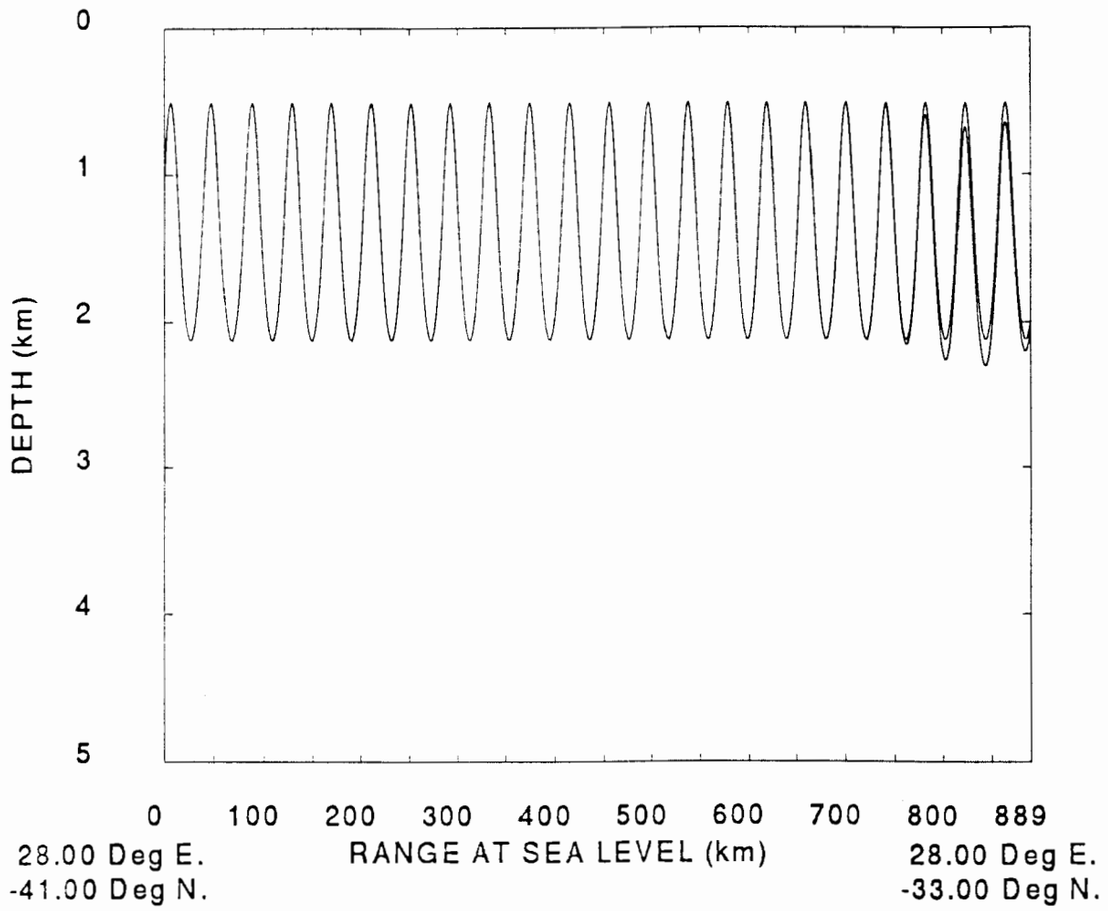

Figure B.2: Agulhas Current Temperature Structure - Vertical Profile

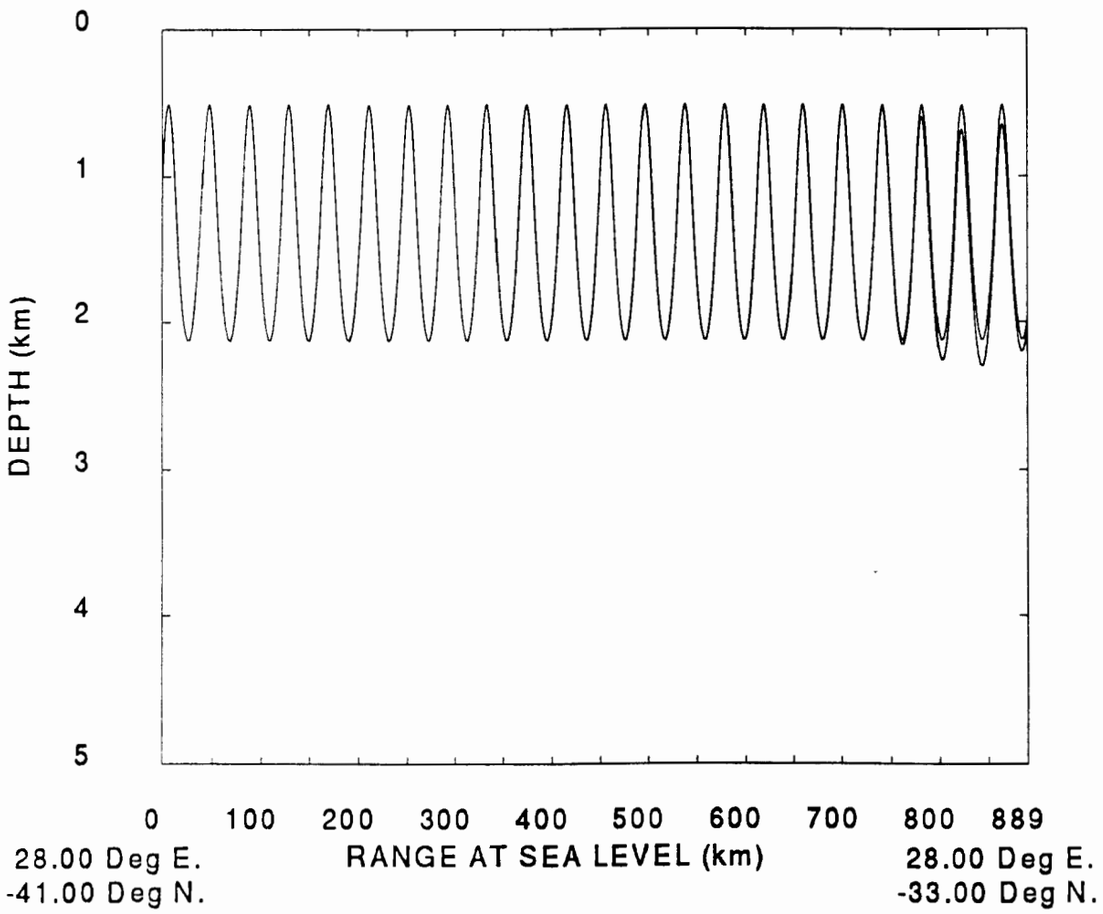

Figure B.3: Agulhas Current Combined Scenario - Vertical Profile

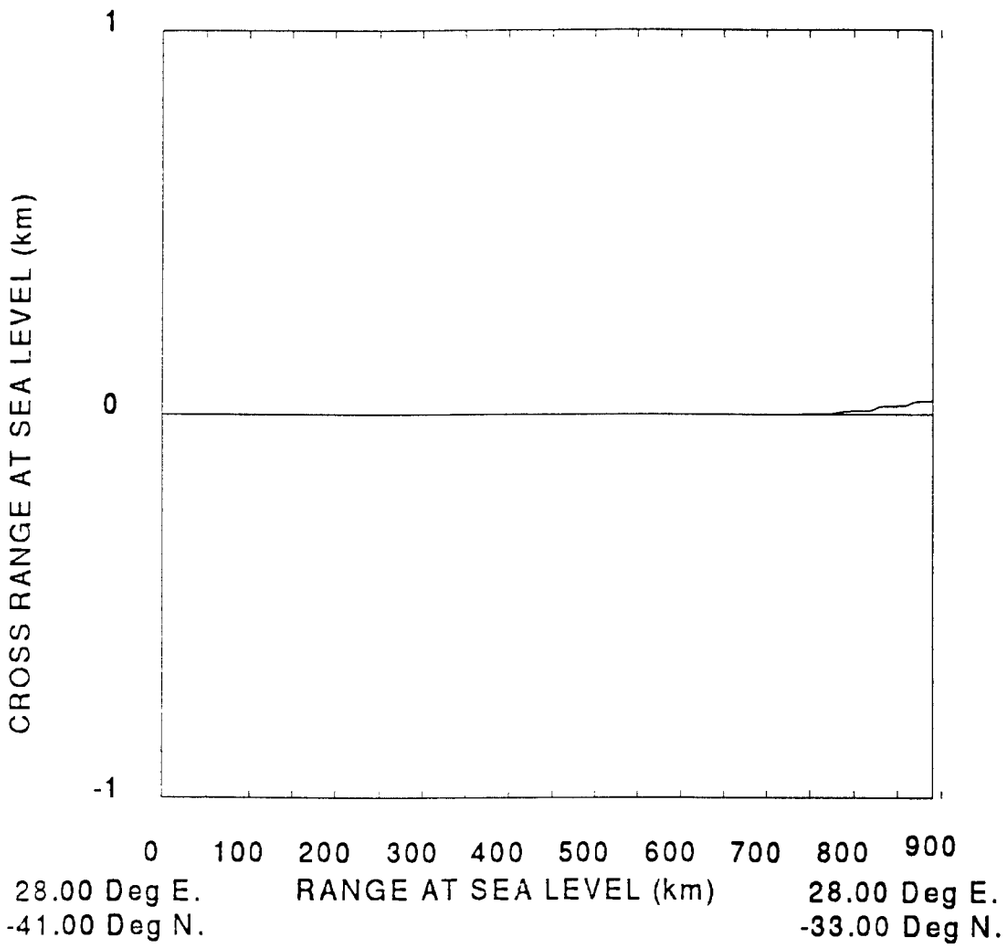

Figure B.4: Agulhas Current Combined Scenario - Horizontal Profile

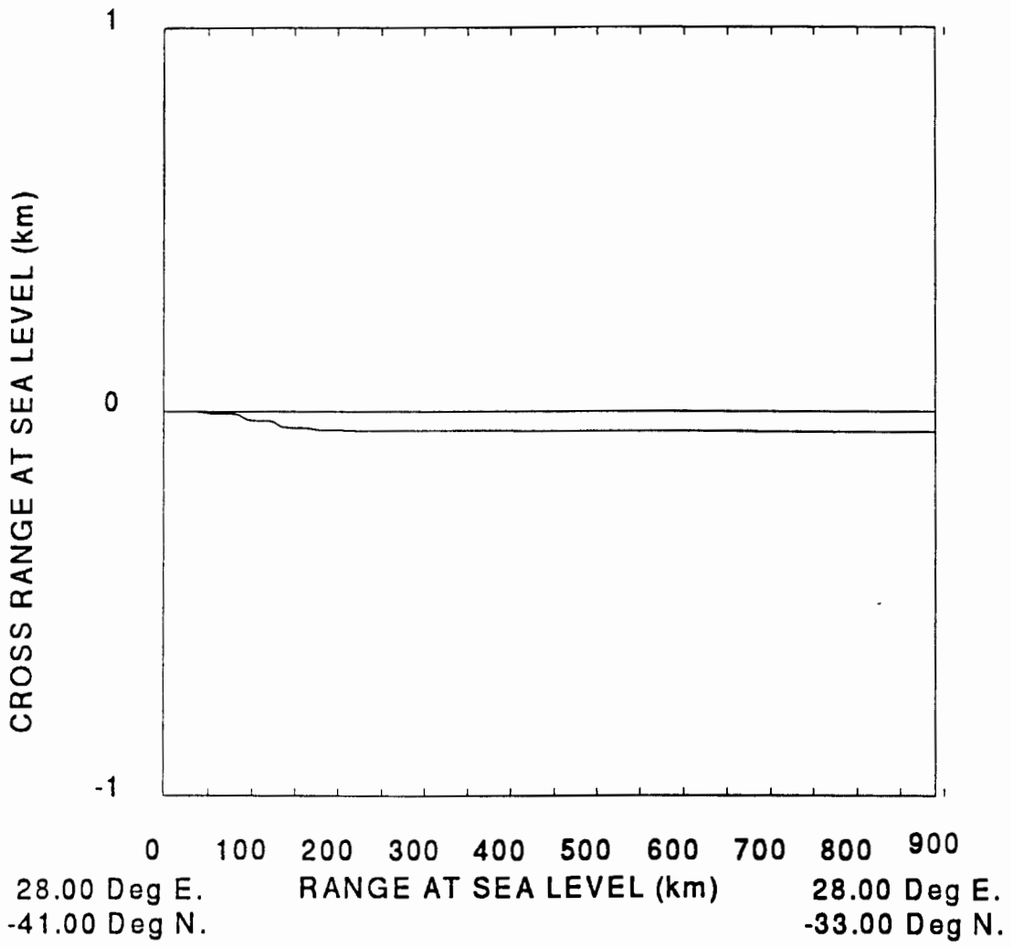

Figure B.5: Return Current Velocity Structure - Horizontal Profile

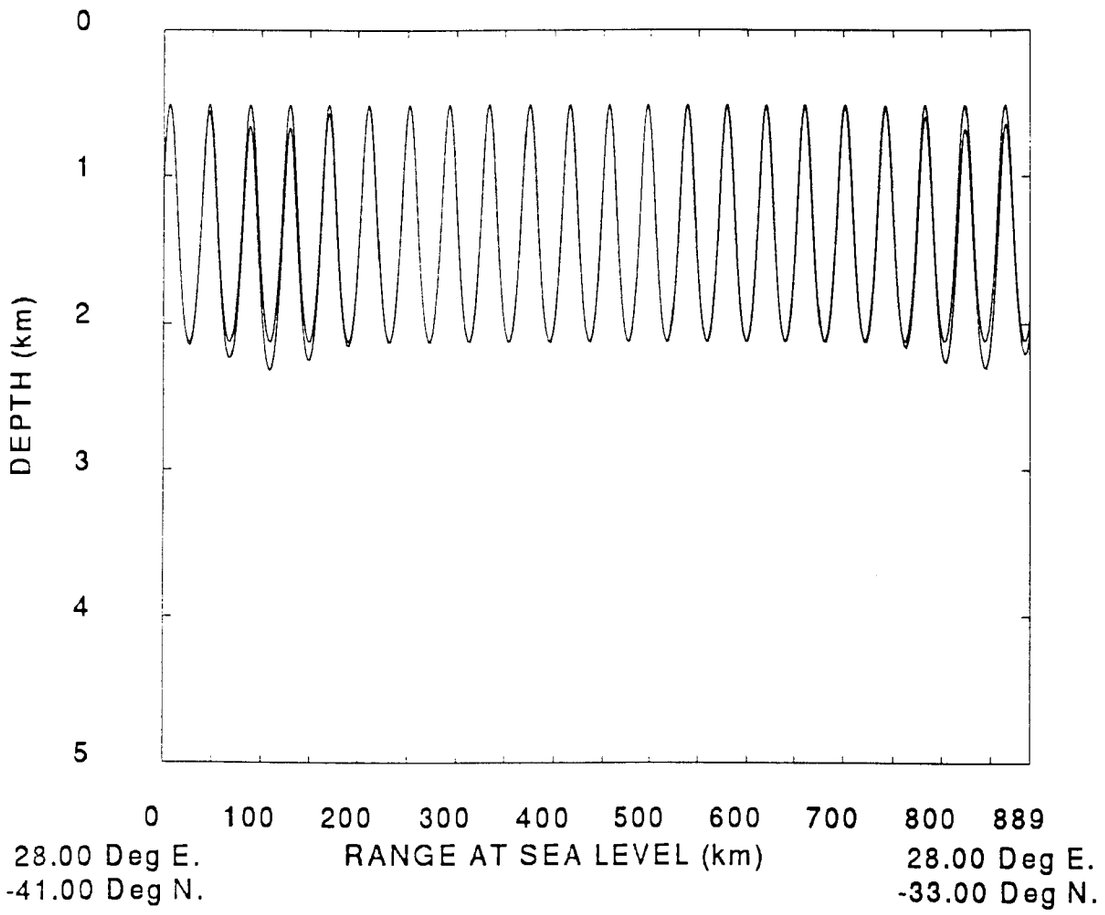

Figure B.6: Return Current Temperature Structure - Vertical Profile

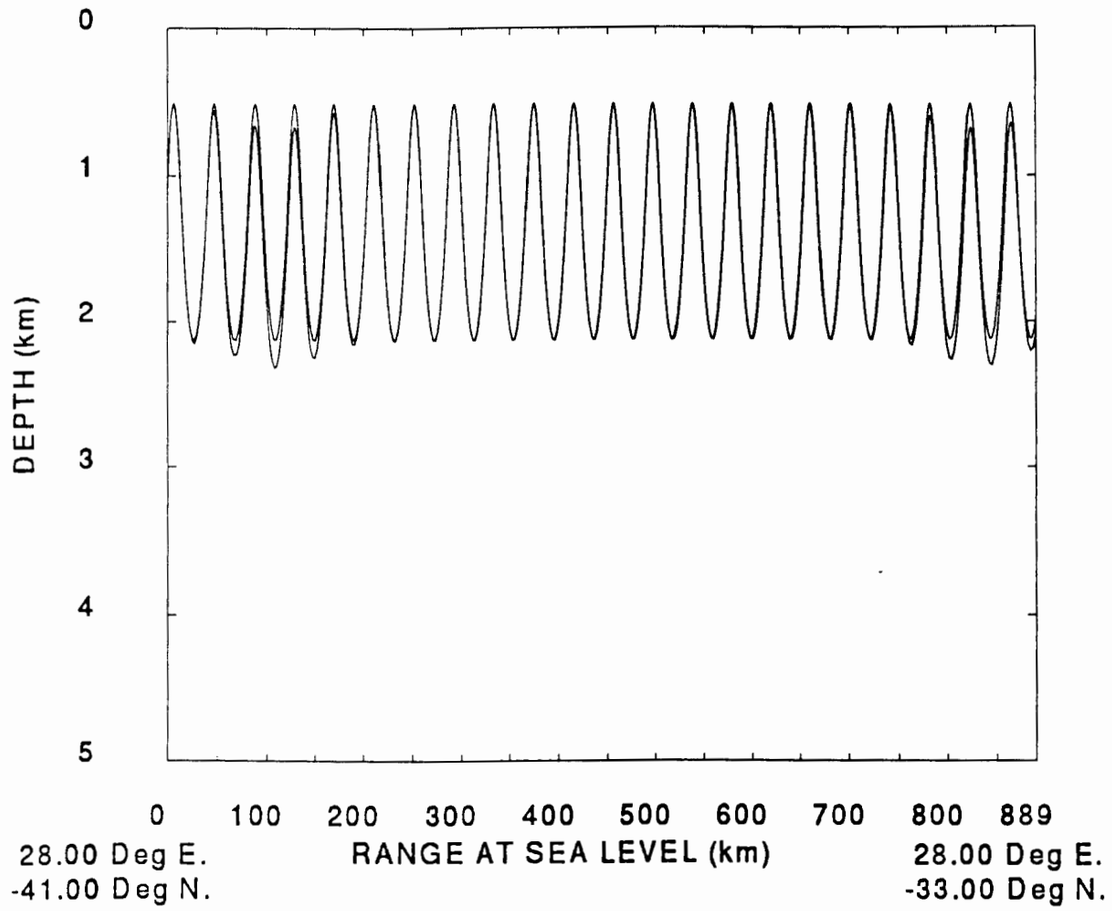

Figure B.7: Return Current Combined Scenario - Vertical Profile

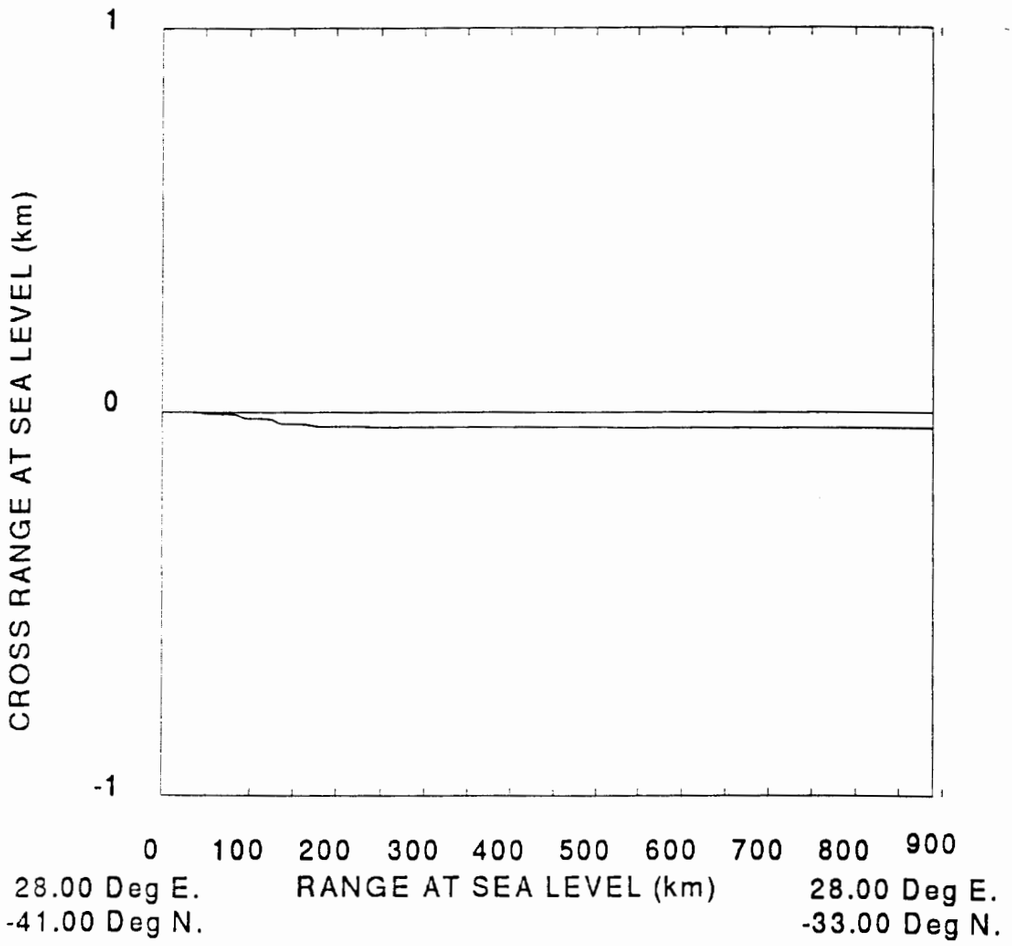

Figure B.8: Return Current Combined Scenario - Horizontal Profile

Appendix C

AN EDDY ENVIRONMENT

Figure:	Model Environment	Plane	Page Number
Figure C.1	eddy velocity - $r = 0$	vertical	169
Figure C.2	eddy velocity - $r = \frac{1}{2}$	vertical	170
Figure C.3	eddy velocity - $r = 1$	vertical	171
Figure C.4	eddy velocity - $r = 1\frac{1}{2}$	vertical	172
Figure C.5	eddy velocity - $r = 0$	horizontal	173
Figure C.6	eddy velocity - $r = \frac{1}{2}$	horizontal	174
Figure C.7	eddy velocity - $r = 1$	horizontal	175
Figure C.8	eddy velocity - $r = 1\frac{1}{2}$	horizontal	176
Figure C.9	eddy temperature - $r = 0$	vertical	177
Figure C.10	eddy temperature - $r = \frac{1}{2}$	vertical	178
Figure C.11	eddy temperature - $r = 1$	vertical	179
Figure C.12	eddy temperature - $r = 1\frac{1}{2}$	vertical	180
Figure C.13	eddy temperature - $r = 0$	horizontal	181
Figure C.14	eddy temperature - $r = \frac{1}{2}$	horizontal	182
Figure C.15	eddy temperature - $r = 1$	horizontal	183
Figure C.16	eddy temperature - $r = 1\frac{1}{2}$	horizontal	184
Figure C.17	eddy combined - $r = 0$	vertical	185
Figure C.18	eddy combined - $r = \frac{1}{2}$	vertical	186
Figure C.19	eddy combined - $r = 1$	vertical	187
Figure C.20	eddy combined - $r = 1\frac{1}{2}$	vertical	188
Figure C.21	eddy combined - $r = 0$	horizontal	189
Figure C.22	eddy combined - $r = \frac{1}{2}$	horizontal	190
Figure C.23	eddy combined - $r = 1$	horizontal	191
Figure C.24	eddy combined - $r = 1\frac{1}{2}$	horizontal	192

Table C.1: List Of The Location Of The Ray Diagrams For Sound Propagating Through An Eddy Environment

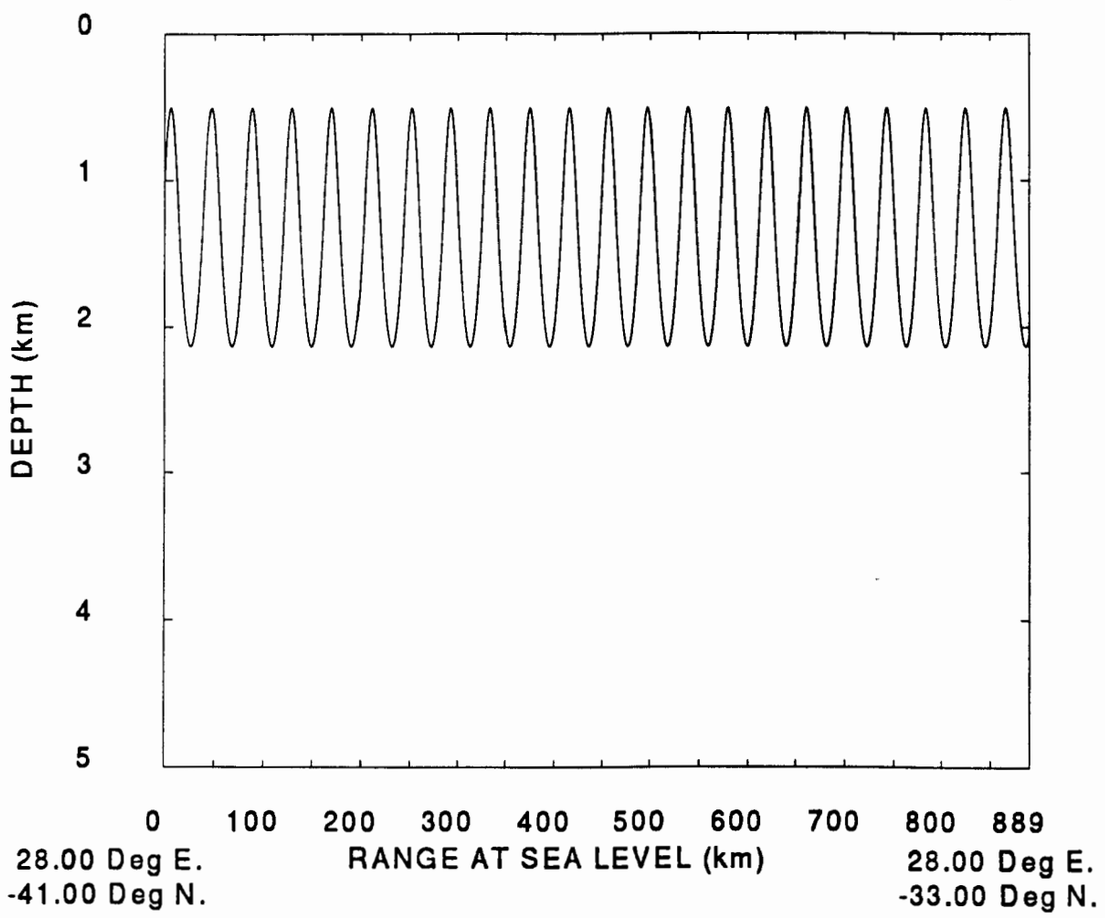

Figure C.1: Anticlockwise Vortex - $R = 0$ - Vertical Profile

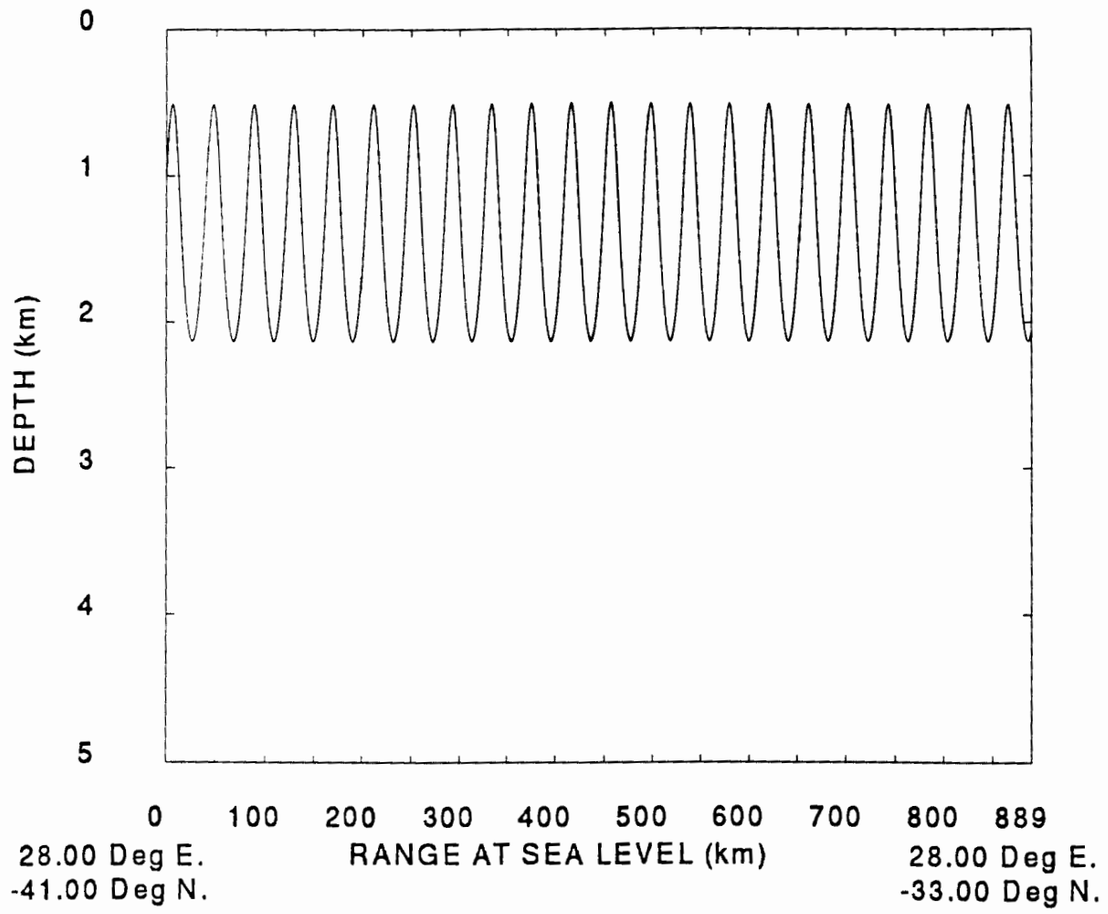

Figure C.2: Anticlockwise Vortex - $R = \frac{1}{2}$ - Vertical Profile

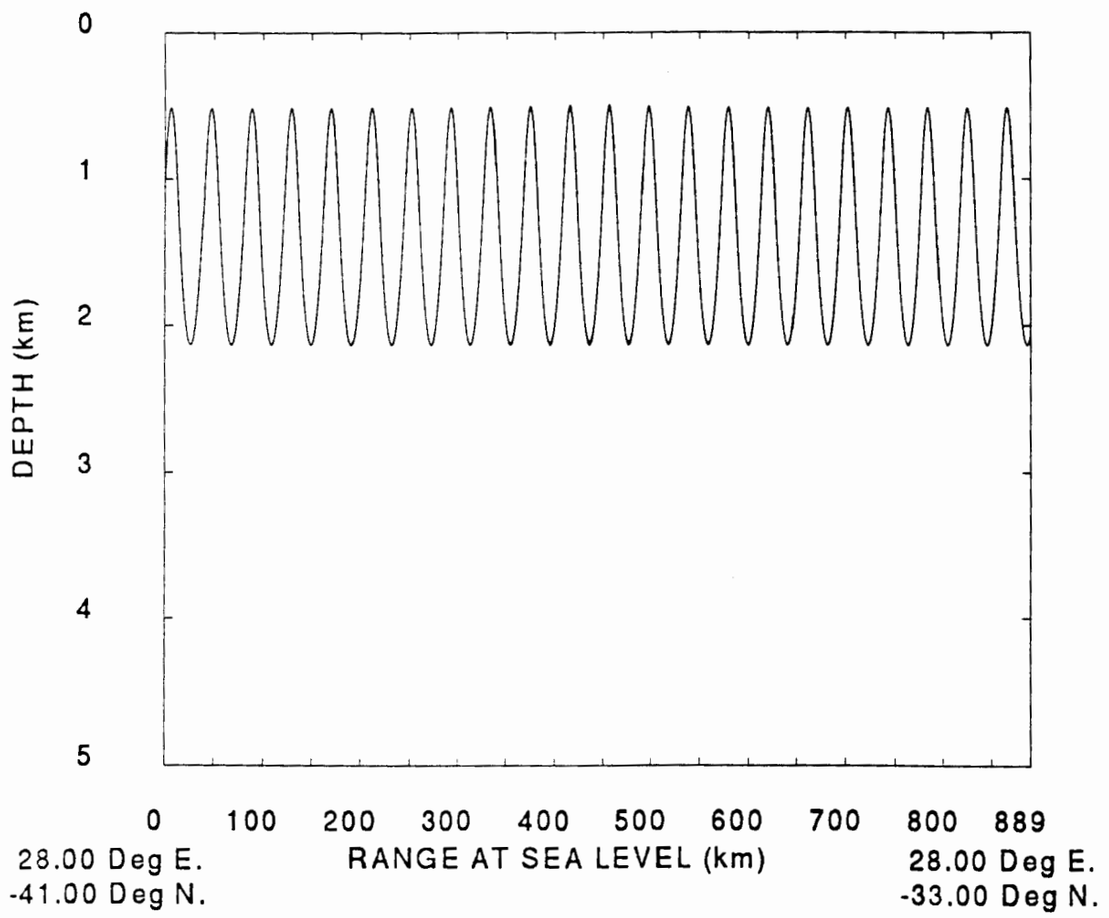

Figure C.3: Anticlockwise Vortex - $R = 1$ - Vertical Profile

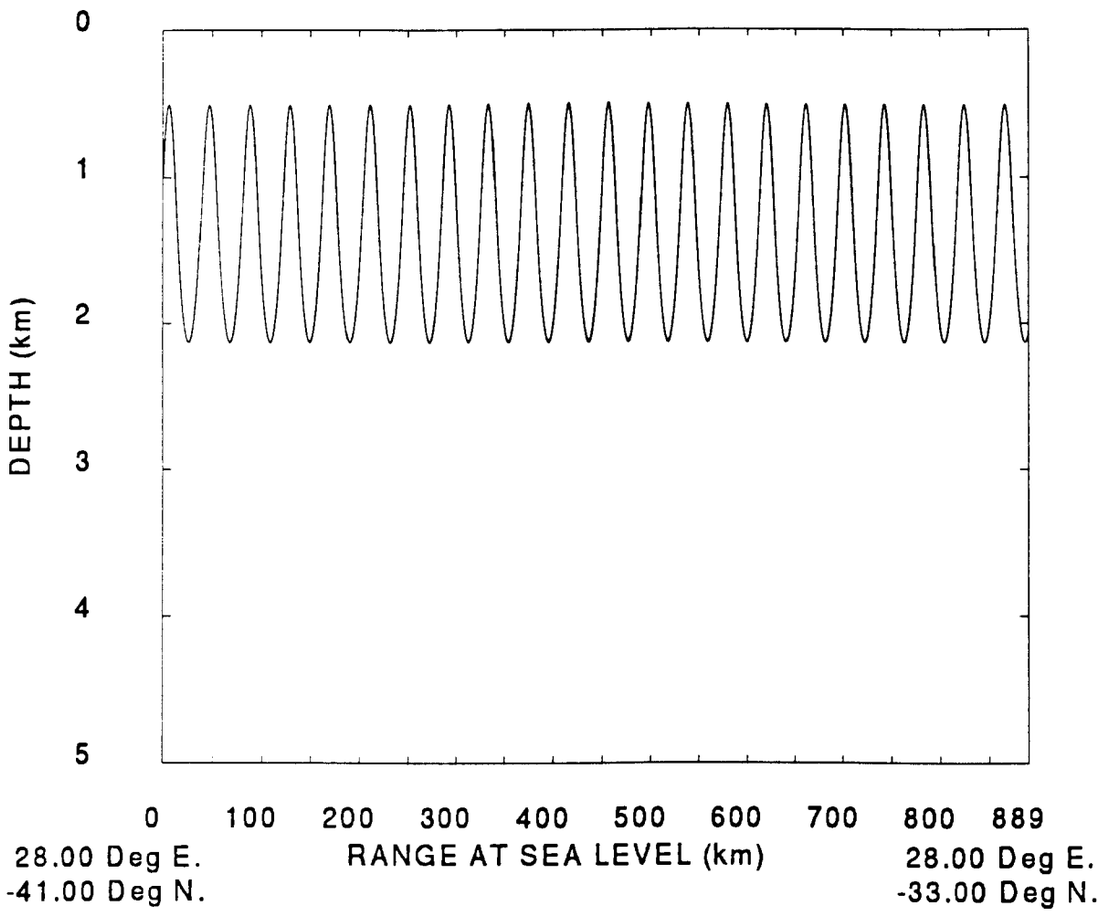

Figure C.4: Anticlockwise Vortex - $R = 1\frac{1}{2}$ - Vertical Profile

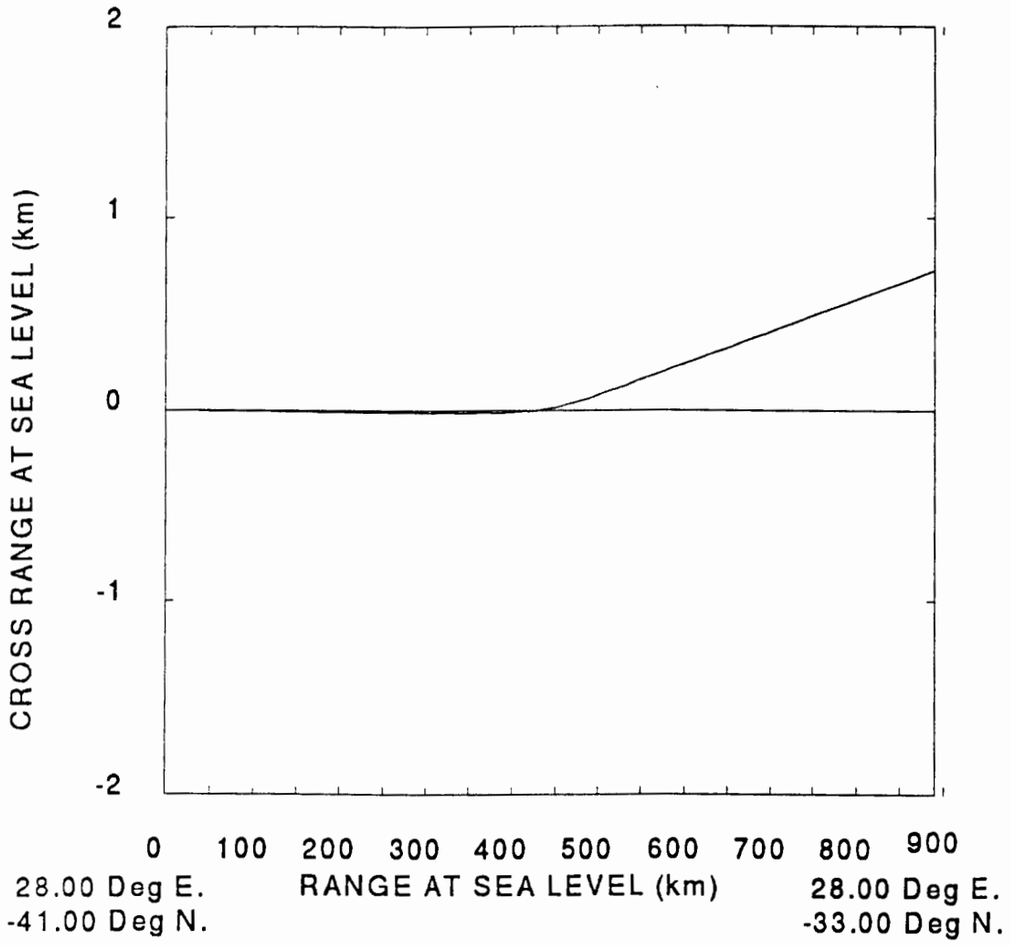

Figure C.5: Anticlockwise Vortex - $R = 0$ - Horizontal Profile

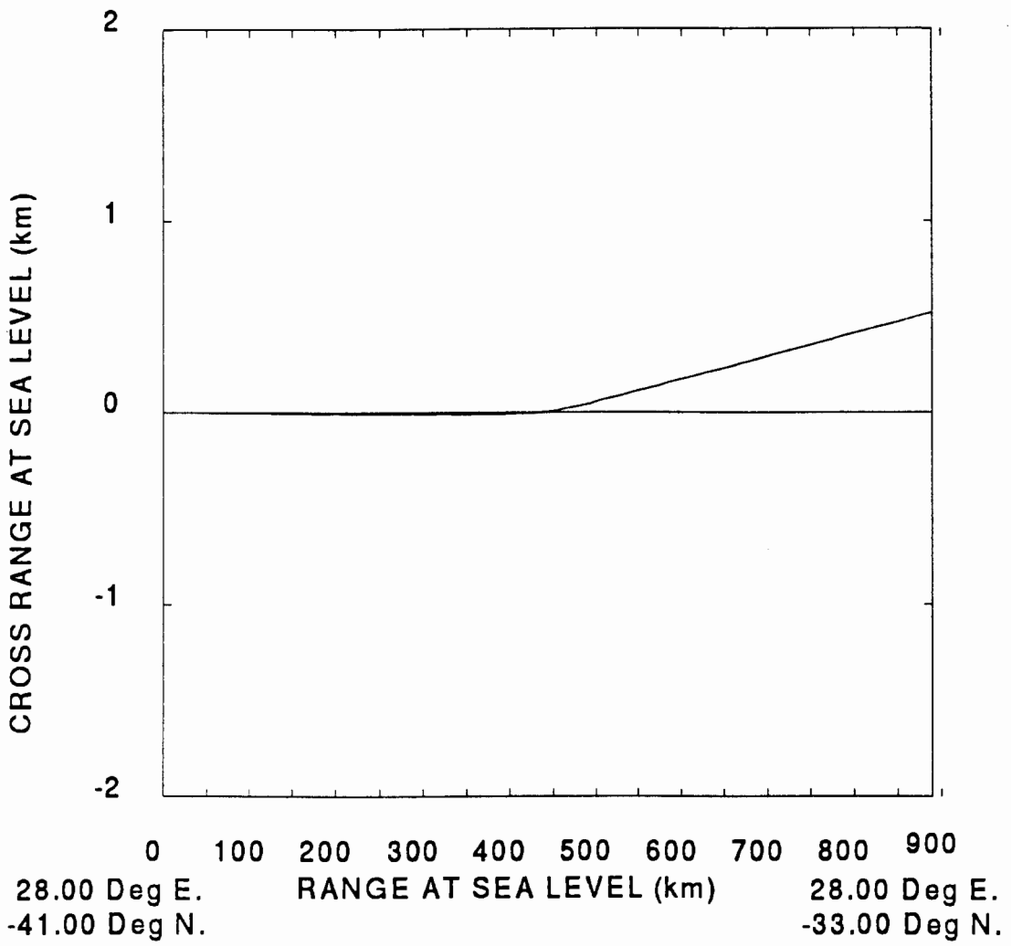

Figure C.6: Anticlockwise Vortex - $R = \frac{1}{2}$ - Horizontal Profile

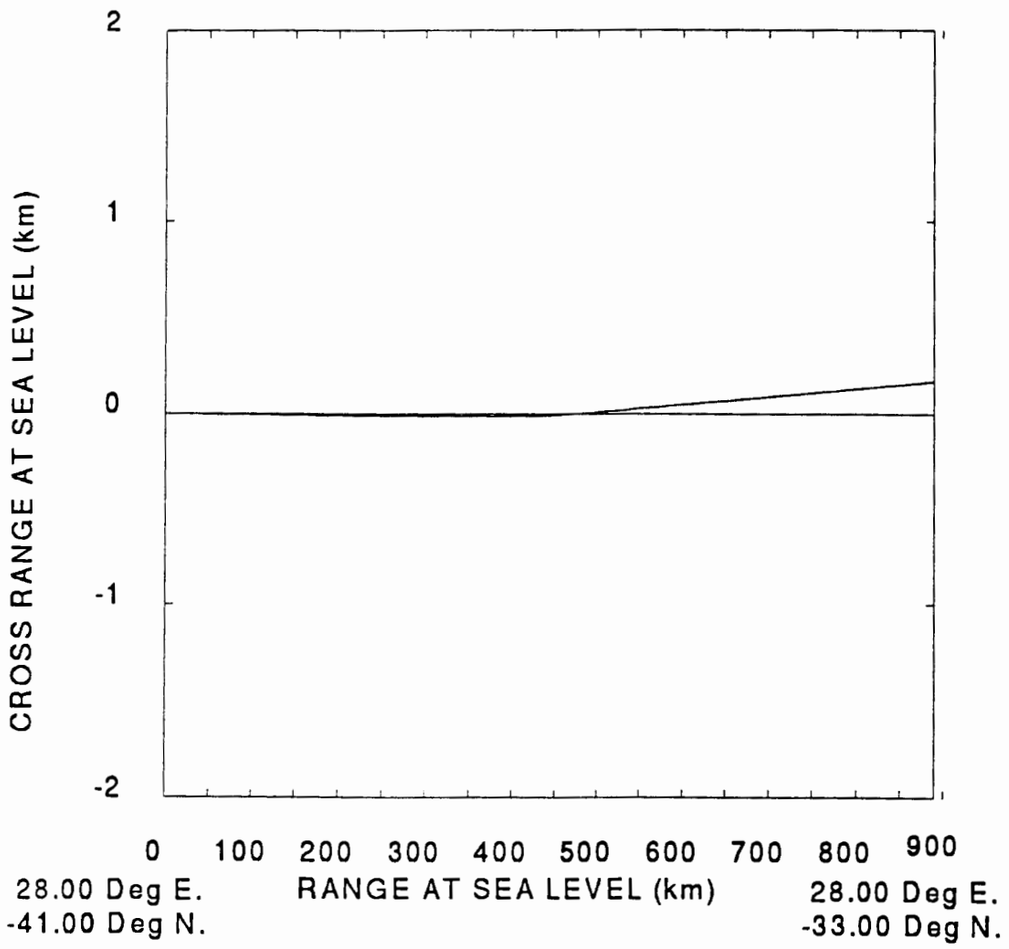

Figure C.7: Anticlockwise Vortex - $R = 1$ - Horizontal Profile

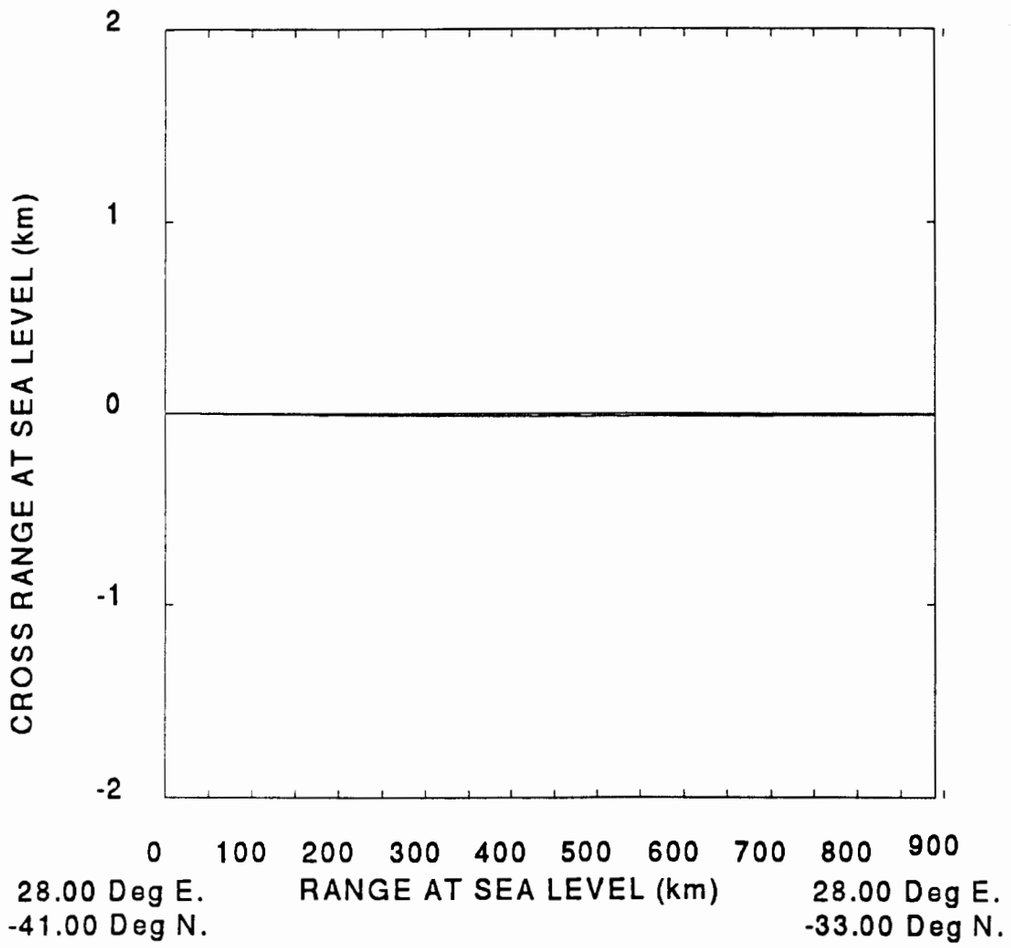

Figure C.8: Anticlockwise Vortex - $R = 1\frac{1}{2}$ - Horizontal Profile

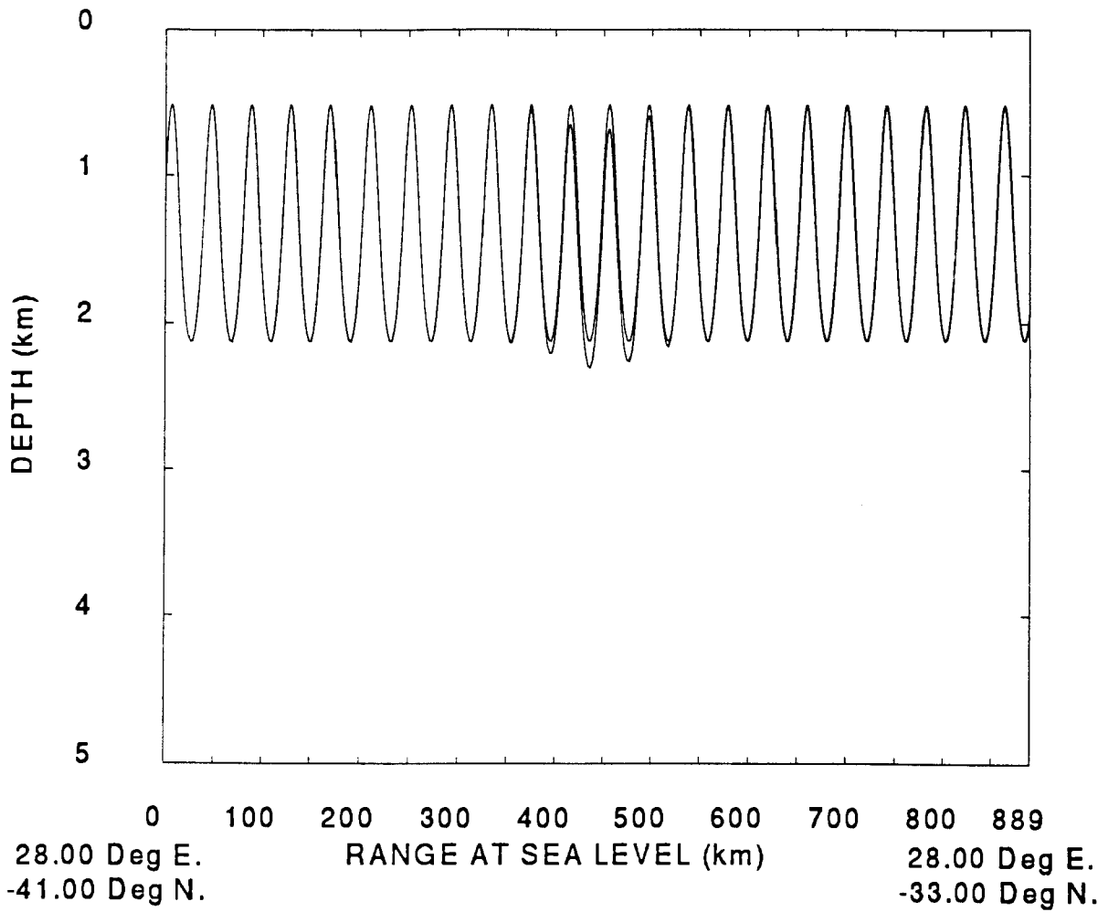

Figure C.9: Warm Core Perturbation - $R = 0$ - Vertical Profile

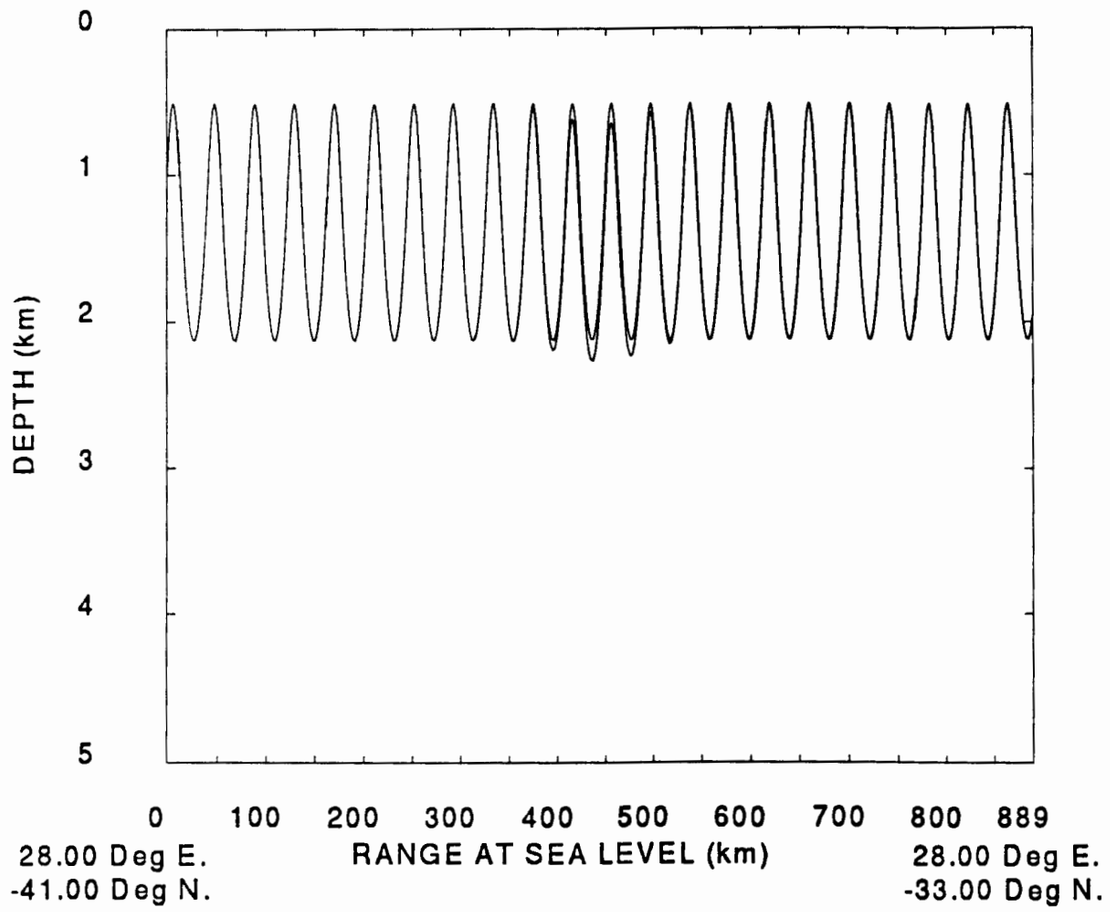

Figure C.10: Warm Core Perturbation - $R = \frac{1}{2}$ - Vertical Profile

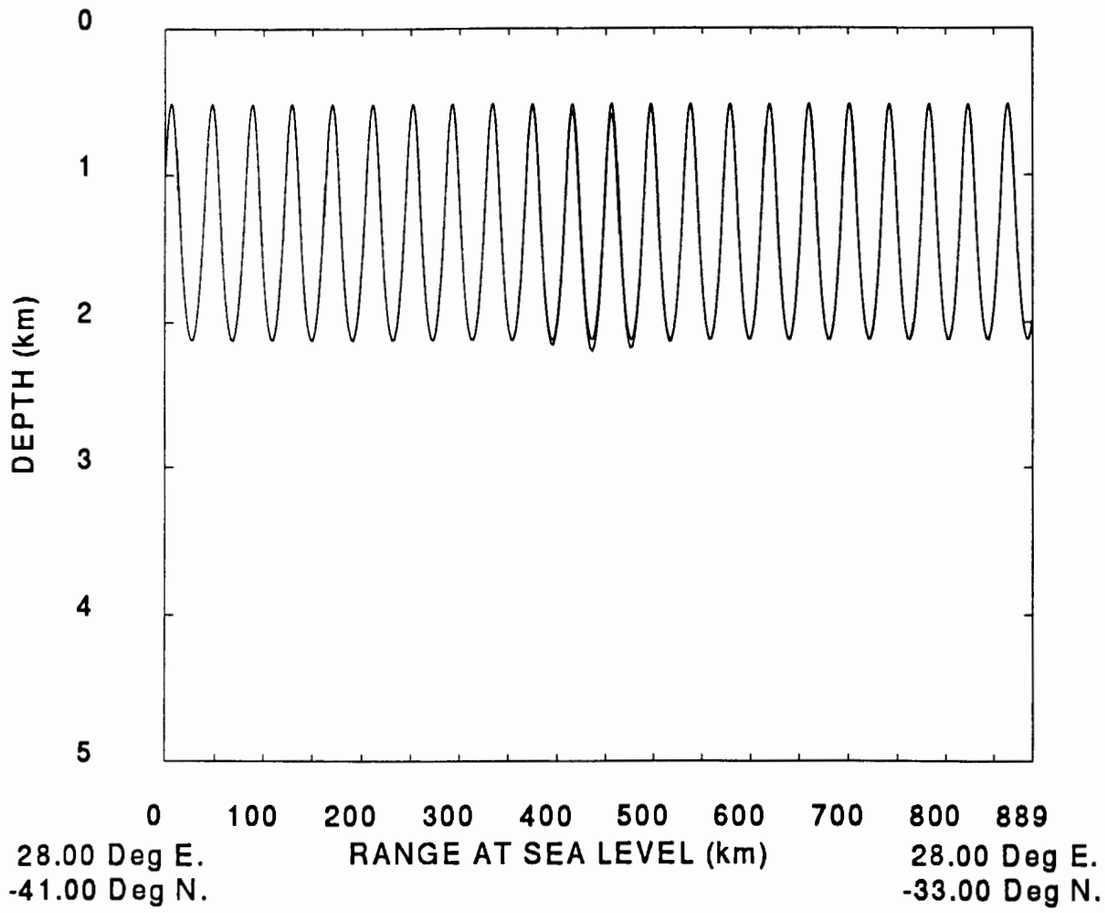

Figure C.11: Warm Core Perturbation - $R = 1$ - Vertical Profile

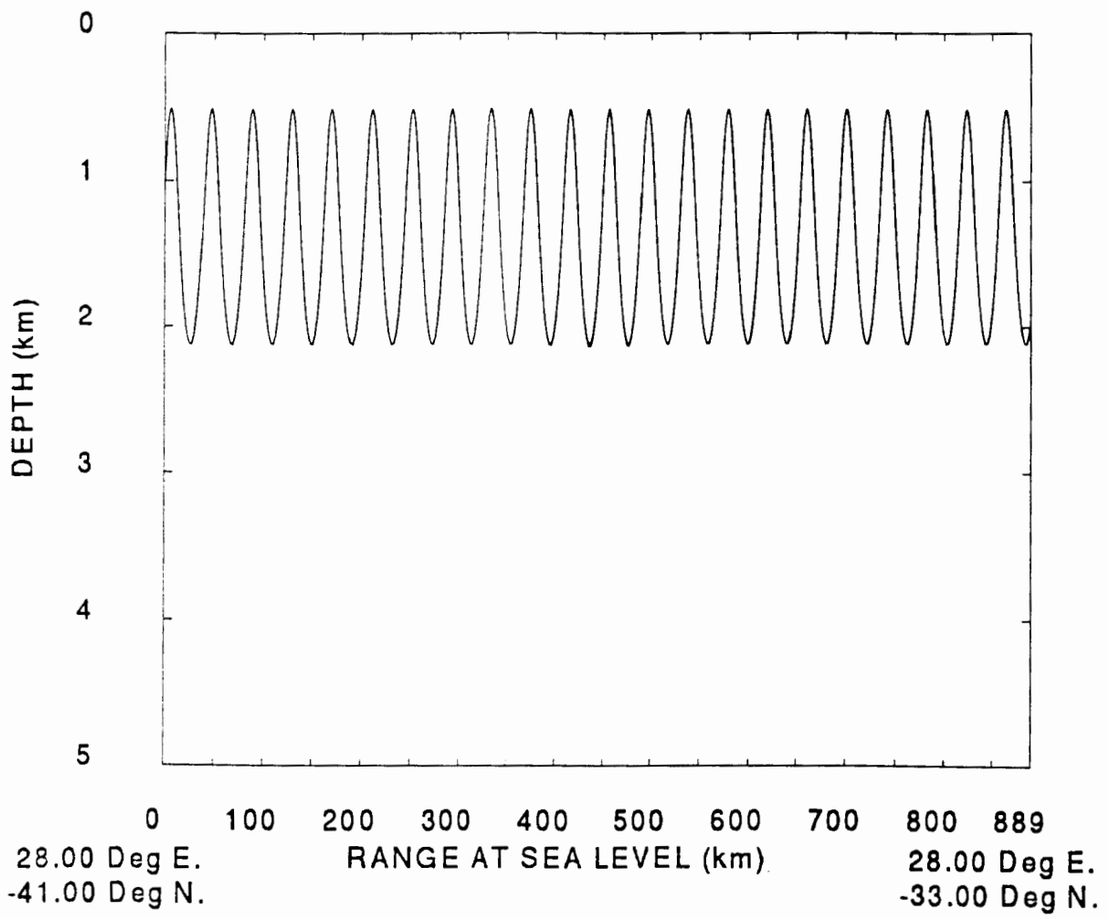

Figure C.12: Warm Core Perturbation - $R = 1\frac{1}{2}$ - Vertical Profile

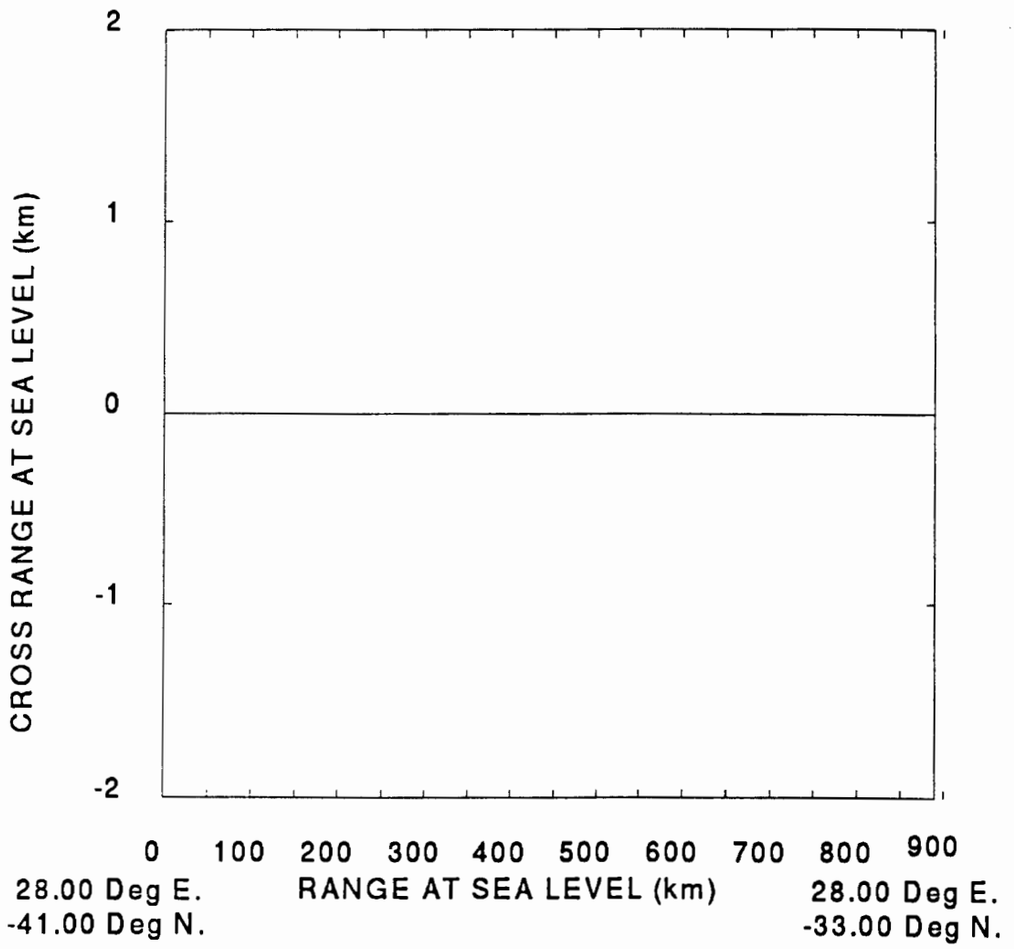

Figure C.13: Warm Core Perturbation - $R = 0$ - Horizontal Profile

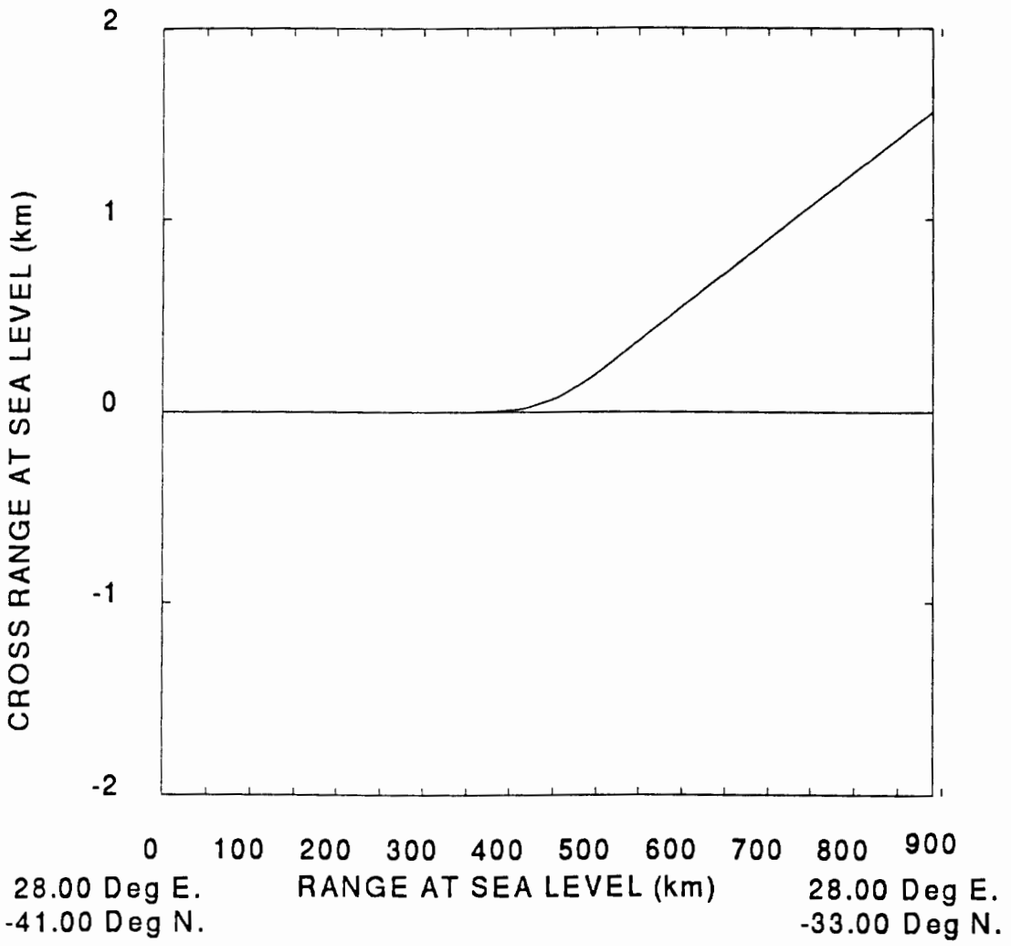

Figure C.14: Warm Core Perturbation - $R = \frac{1}{2}$ - Horizontal Profile

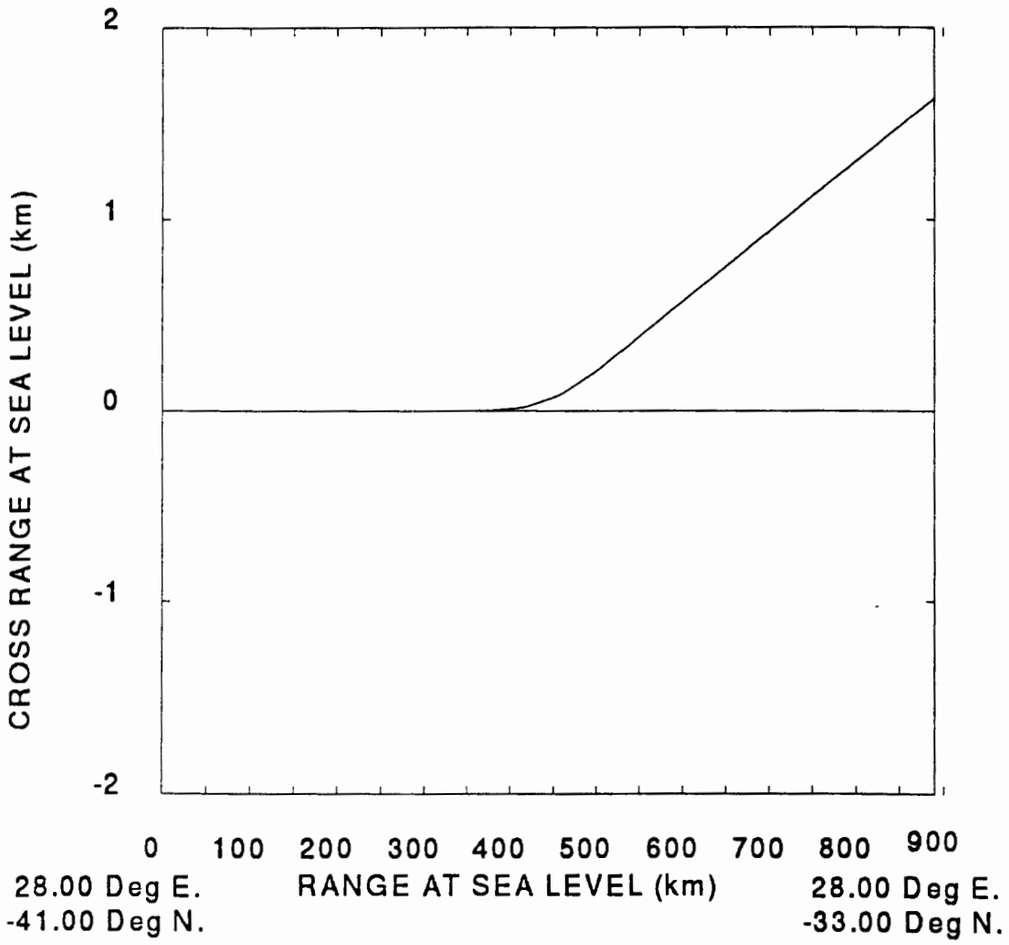

Figure C.15: Warm Core Perturbation - $R = 1$ - Horizontal Profile

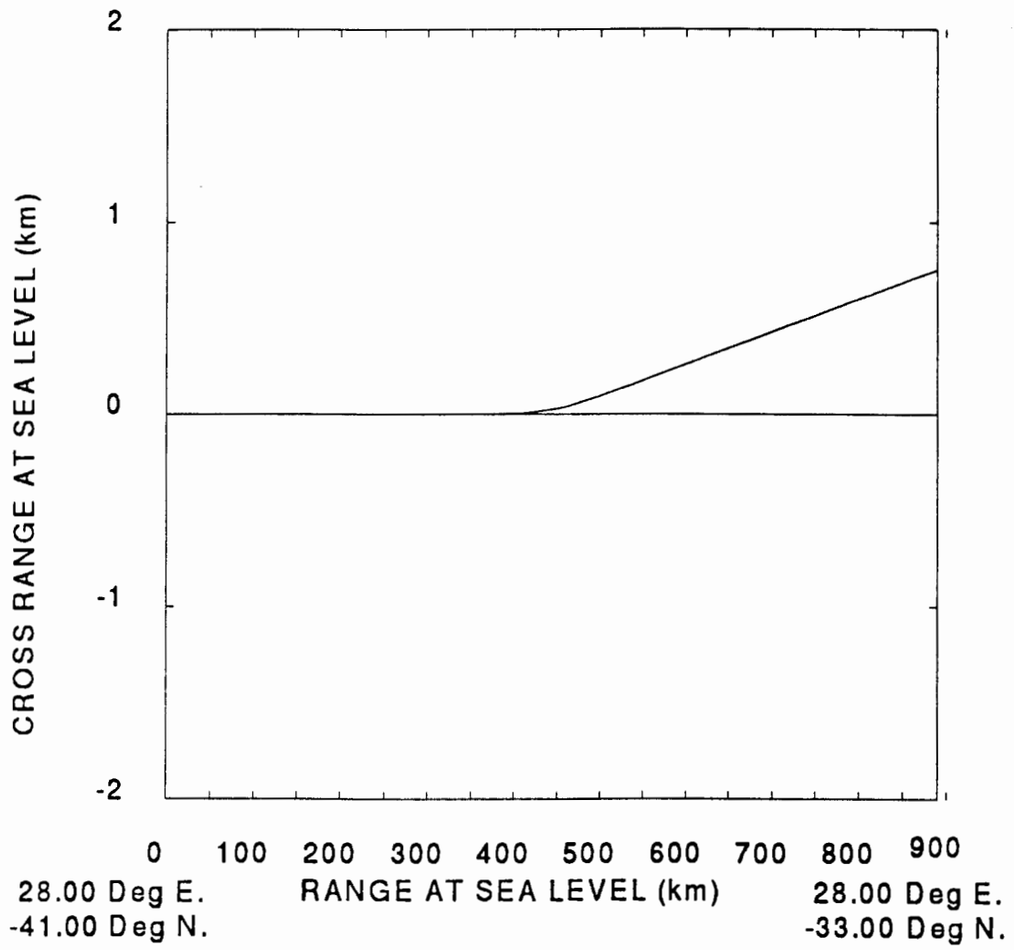

Figure C.16: Warm Core Perturbation - $R = 1\frac{1}{2}$ - Horizontal Profile

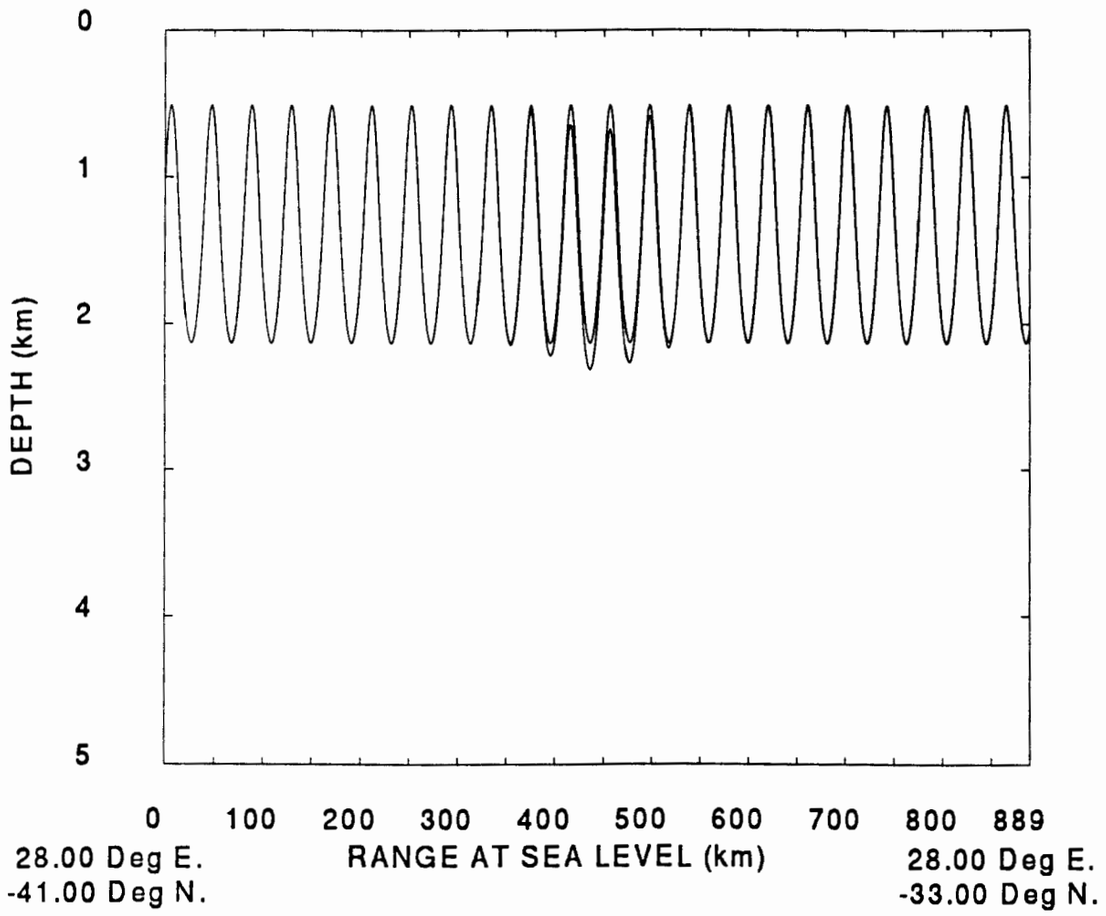

Figure C.17: Anticlockwise Warm Core Eddy - $R = 0$ - Vertical Profile

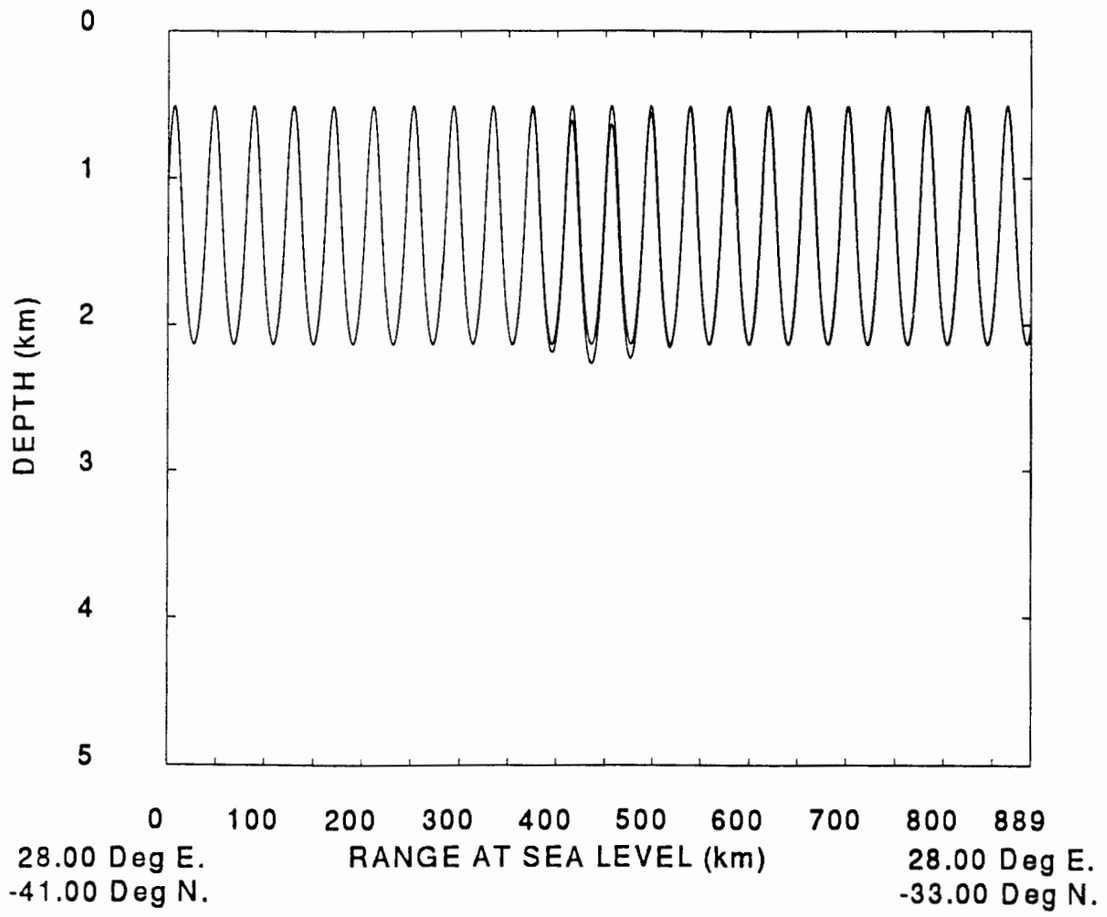

Figure C.18: Anticlockwise Warm Core Eddy - $R = \frac{1}{2}$ - Vertical Profile

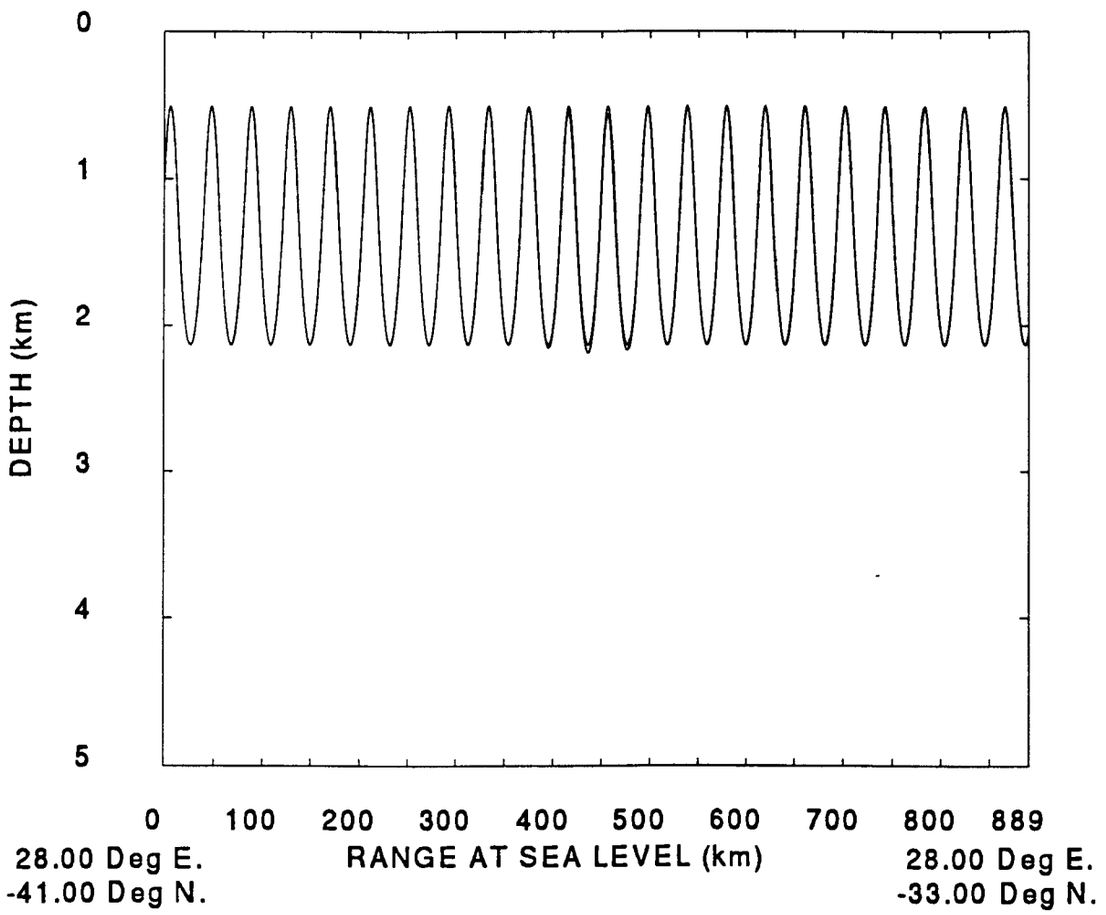

Figure C.19: Anticlockwise Warm Core Eddy - $R = 1$ - Vertical Profile

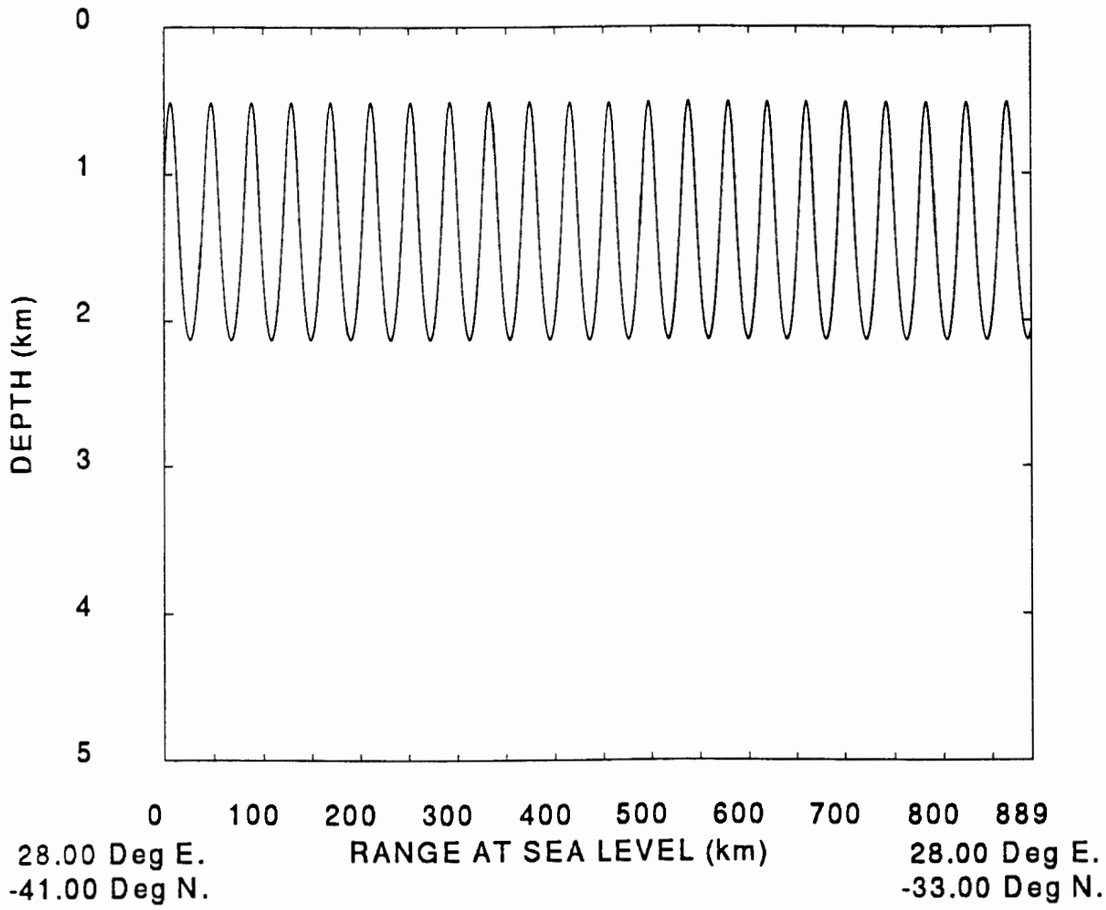

Figure C.20: Anticlockwise Warm Core Eddy - $R = 1\frac{1}{2}$ - Vertical Profile

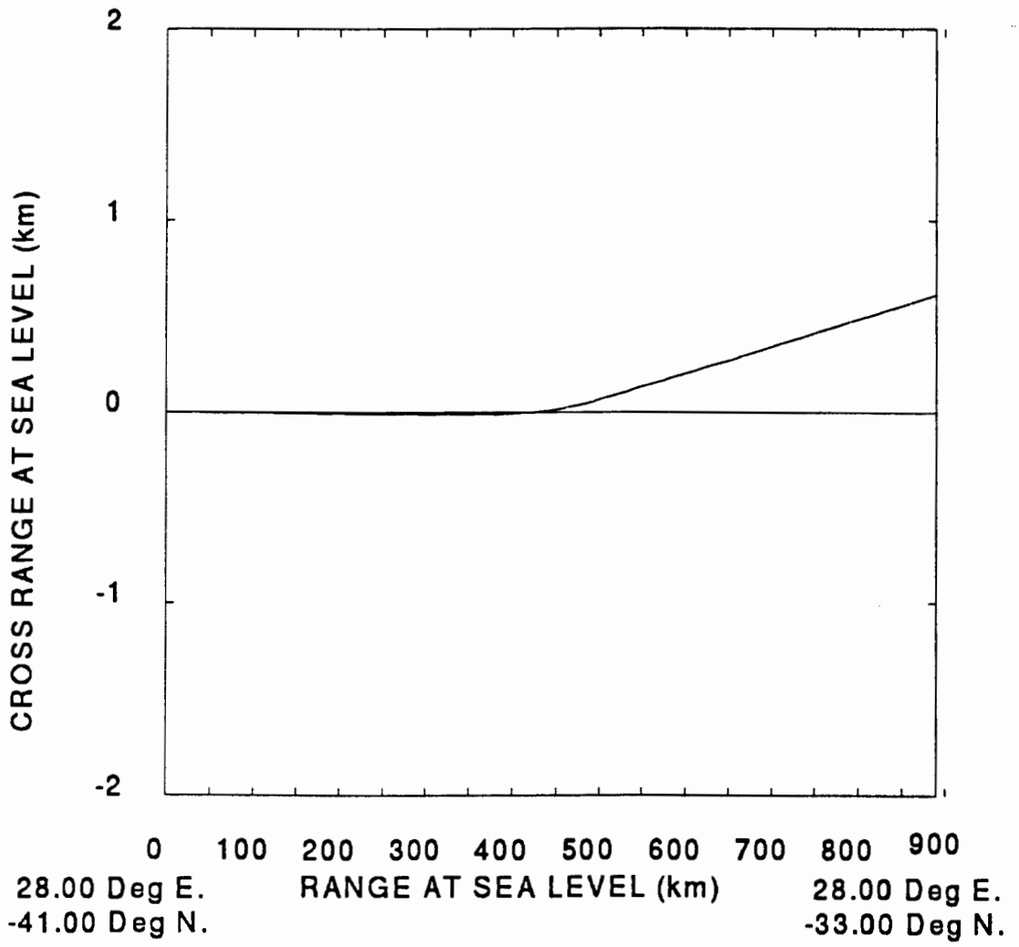

Figure C.21: Anticlockwise Warm Core Eddy - $R = 0$ - Horizontal Profile

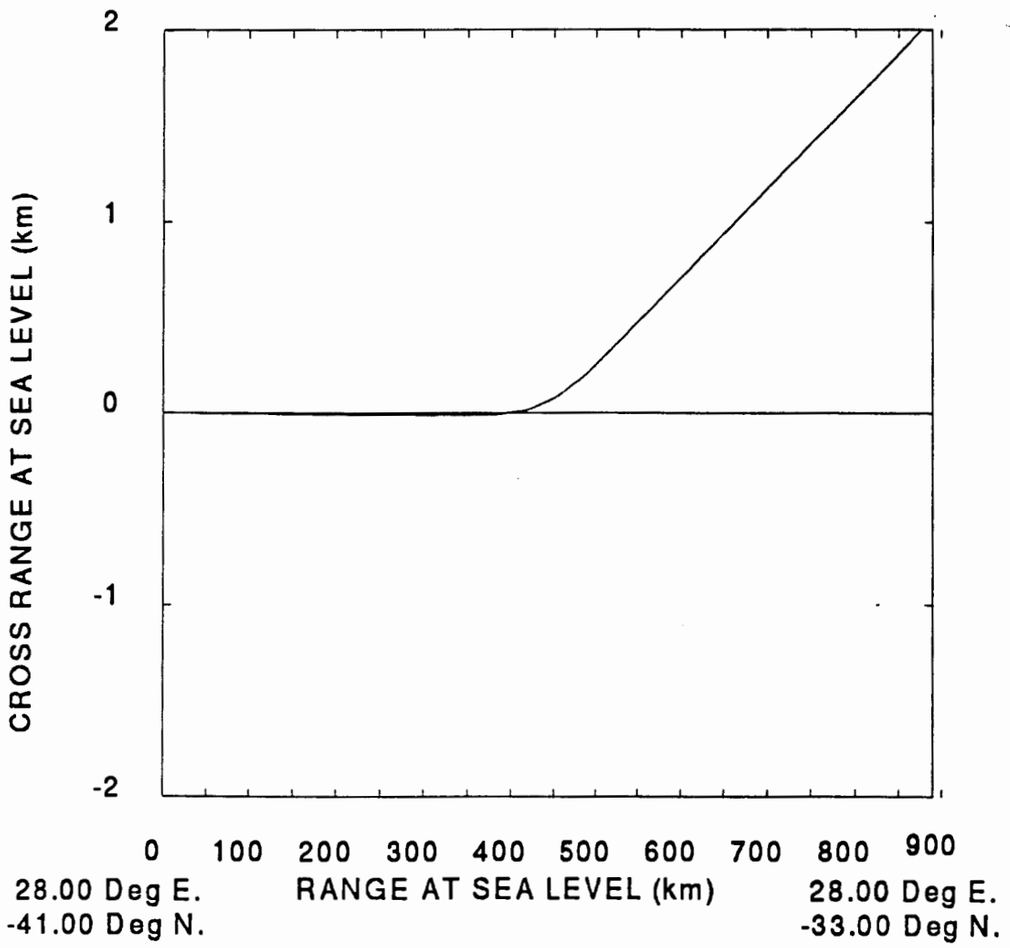

Figure C.22: Anticlockwise Warm Core Eddy - $R = \frac{1}{2}$ - Horizontal Profile

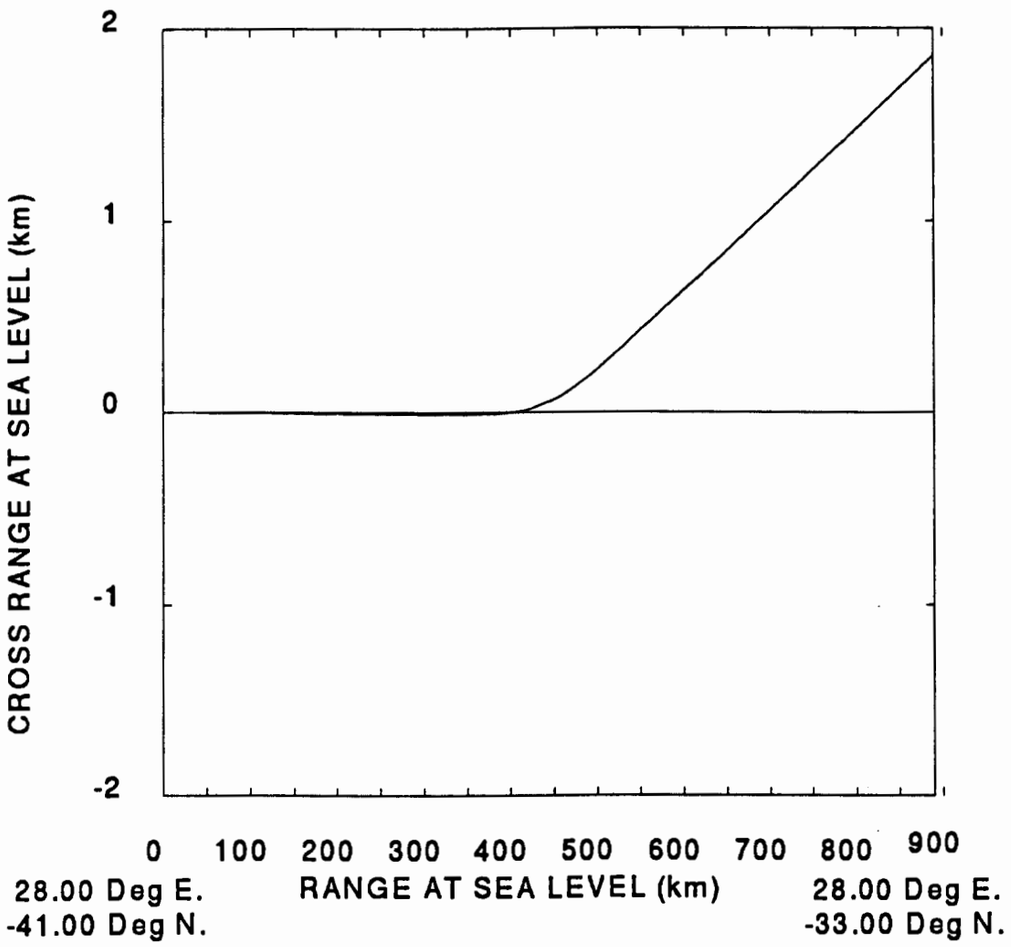

Figure C.23: Anticlockwise Warm Core Eddy - $R = 1$ - Horizontal Profile

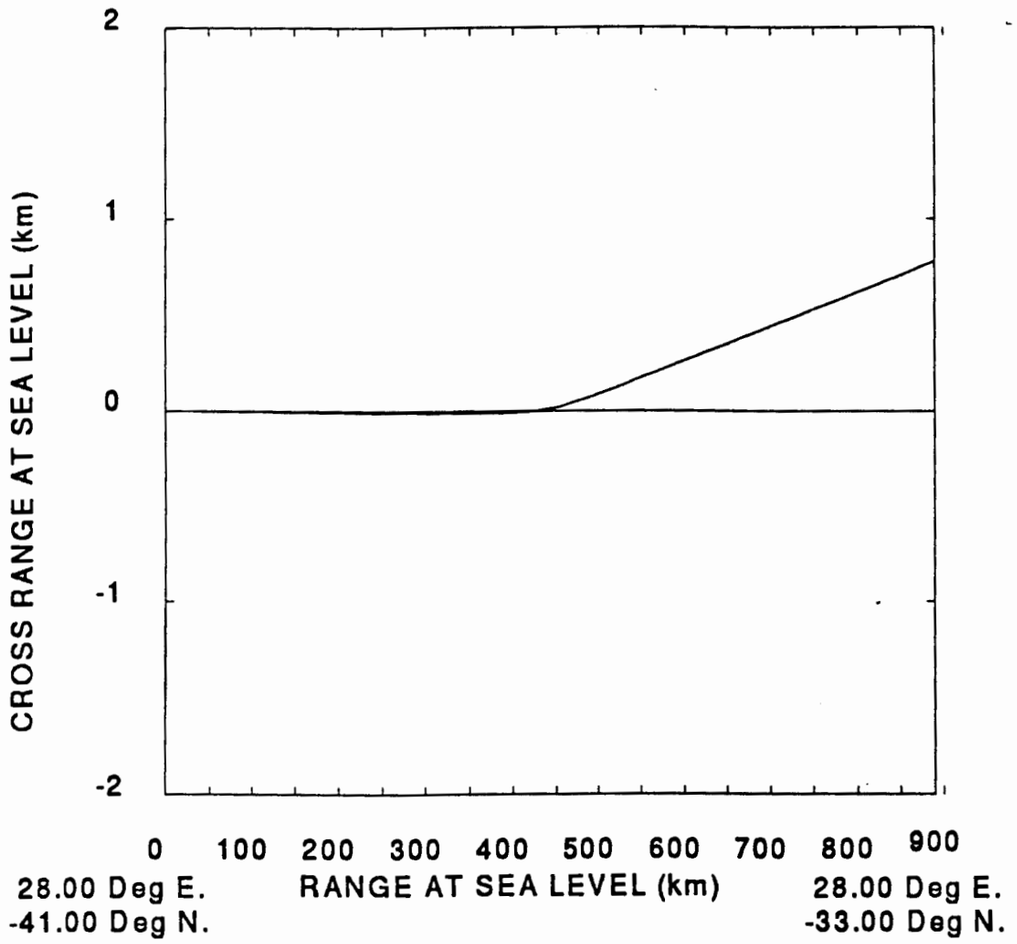

Figure C.24: Anticlockwise Warm Core Eddy - $R = 1\frac{1}{2}$ - Horizontal Profile